

### Modeling Mitral Valve Dynamics: From Experimental Validation to Patient-Specific **Simulations**

Christierson, Lea

2025

Document Version: Publisher's PDF, also known as Version of record

Link to publication

Citation for published version (APA):

Christierson, L. (2025). Modeling Mitral Valve Dynamics: From Experimental Validation to Patient-Specific Simulations. [Doctoral Thesis (compilation), Department of Biomedical Engineering]. Department of Biomedical Engineering, Lund university.

Total number of authors:

Creative Commons License: CC BY-SA

Unless other specific re-use rights are stated the following general rights apply: Copyright and moral rights for the publications made accessible in the public portal are retained by the authors and/or other copyright owners and it is a condition of accessing publications that users recognise and abide by the legal requirements associated with these rights.

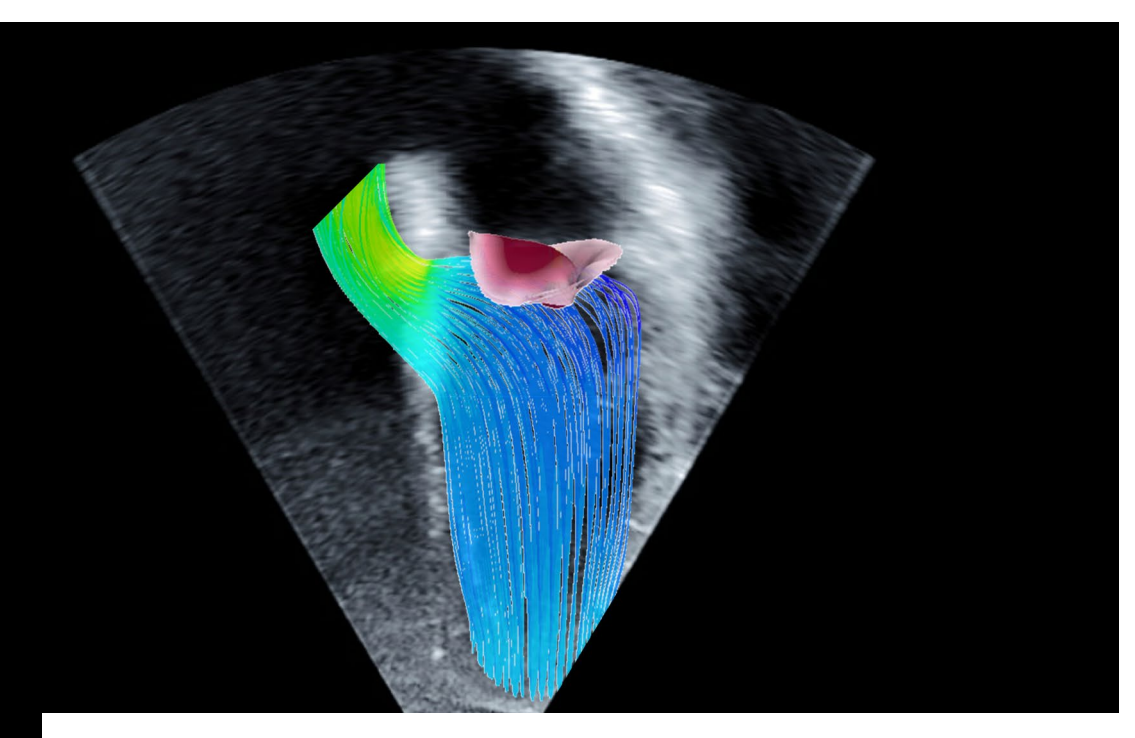
• Users may download and print one copy of any publication from the public portal for the purpose of private study

- or research.
- You may not further distribute the material or use it for any profit-making activity or commercial gain
   You may freely distribute the URL identifying the publication in the public portal

Read more about Creative commons licenses: https://creativecommons.org/licenses/

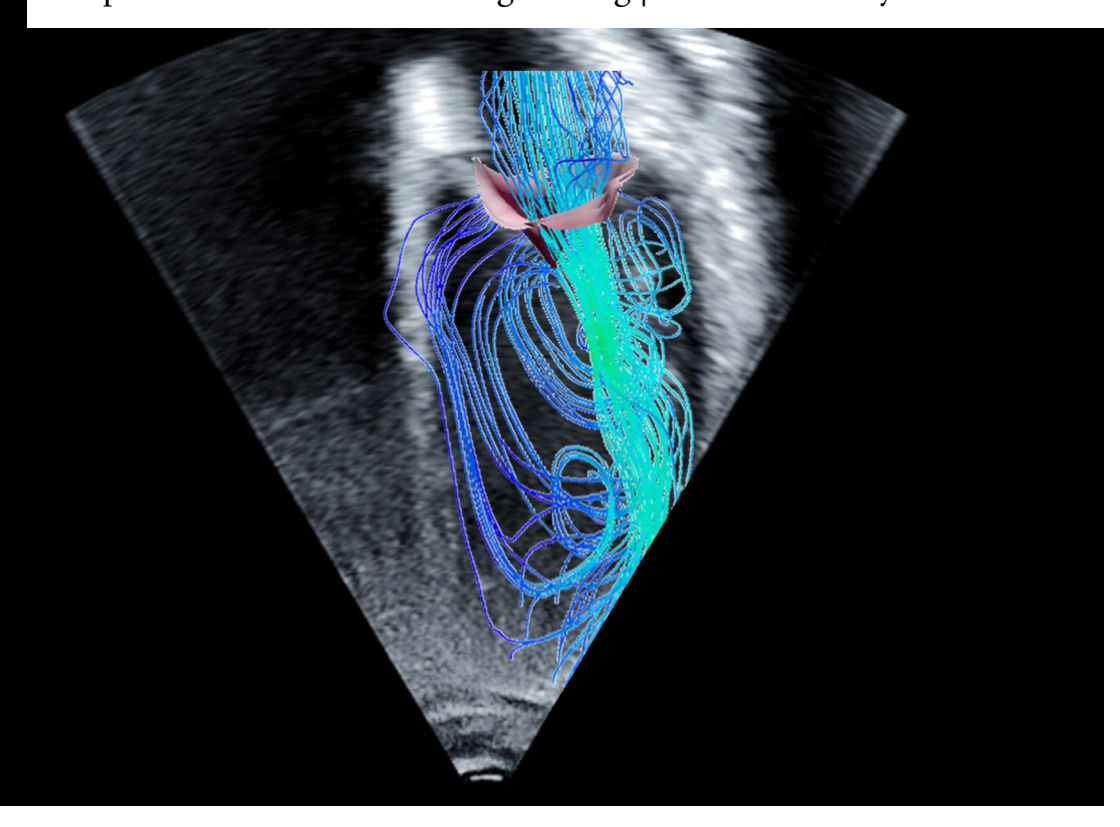
If you believe that this document breaches copyright please contact us providing details, and we will remove access to the work immediately and investigate your claim.

Download date: 26. Nov. 2025



# Modeling Mitral Valve Dynamics: From Experimental Validation to Patient-Specific Simulations

Lea Christierson Department of Biomedical Engineering | Lund University



# Modeling Mitral Valve Dynamics: From Experimental Validation to Patient-Specific Simulations

Lea Christierson



#### DOCTORAL DISSERTATION

by due permission of the Faculty of Engineering, Lund University, Sweden. To be defended in lecture hall *E:1406*, *E-building*, *Ole Römers väg 3*, *Lund*, *Sweden*Friday November 14<sup>th</sup>, 2025 at 9.00

Faculty opponent

Assoc. Prof. Emiliano Votta

Department of Electronics, Information and Bioengineering, Politecnico di Milano, Milan, Italy

#### Public defence

November 14<sup>th</sup> 2025, at 9.00 a.m. in E:1406, E-huset Lund University, Ole römers väg 3, 223 63 Lund, Sweden

#### Supervisors

Assoc. Prof. Nina Hakacova

Pediatric Heart Center, Skåne University Hospital, Lund University, Lund, Sweden

Prof. Hanna Isaksson

Department of Biomedical Engineering, Lund University, Lund, Sweden

Prof. Johan Revstedt

Department of Energy Sciences, Lund University, Lund, Sweden

Prof. Petru Liuba

Pediatric Heart Center, Skåne University Hospital, Lund University, Lund, Sweden

#### Faculty opponent

Assoc. Prof. Emiliano Votta

Department of Electronics, Information and Bioengineering, Politecnico di Milano, Milan, Italy

#### Board of examination

Prof. Tino Ebbers

Department of Health, Medicine and Caring Sciences, Linköpings Universitet, Linköping, Sweden

Assoc. Prof. Marie Sand Traberg

Health technology, Technical University of Denmark, Copenhagen, Denmark. Employed as Advanced Quality Assurance Professional at Novo Nordisk.

Prof. Johan Hoffman

Division of Computational Science and Technology, KTH Royal Institute of Technology, Stockholm, Sweden

Docent Sandra Lindstedt

Department of Clinical Sciences, Lund University, Lund, Sweden

**Cover Illustration:** Fluid-structure interaction of a mitral valve in systolic and diastolic configurations, with patient-specific hemodynamics overlaid on the corresponding echocardiographic images.

Department of Biomedical Engineering

Lund University

P.O. Box 118, SE-221 00 Lund, Sweden

ISBN: 978-91-8104-677-9 (printed) ISBN: 978-91-8104-678-6 (electronic) ISRN-nr: LUTEDX/TEEM-1147-SE

Report No. 8/25

© 2025 Lea Christierson

Printed in October 2025 by Tryckeriet i E-huset, Lund, Sweden

# Populärvetenskaplig sammanfattning

Hjärtat består av fyra hålrum; två kammare och två förmak, som separeras av fyra hjärtklaffar. Dessa säkerställer att blodet enbart flödar åt ett håll och ger därmed hjärtat förutsättningarna för effektiv pumpning av blodet. Mitralisklaffen är en av dessa fyra hjärtklaffar och separerar vänster förmak från vänster kammare, vilket gör att den utsätts för det högsta trycket i hjärtat. För att mitralisklaffen ska kunna motstå detta höga tryck finns rep-liknande strukturer som kallas chordae tendineae, vilka stabiliserar klaffen. Sjukdomar som påverkar mitralisklaffen kan därför ha ödesdigra konsekvenser. Ungefär 1% av alla barn föds med hjärtfel, där vissa patienter även drabbas av sjukdomar som påverkar just mitralisklaffen. Detta kan yttra sig i form av en stenos, vilket innebär att klaffen öppnas restriktivt och utövar en obstruktion för blodflödet, eller i form av en regurgitation, som innebär att den läcker blod tillbaka till förmaket. Båda tillstånden behöver oftast åtgärdas kirurgiskt, s.k. klaffplastik. Detta innebär ett komplext ingrepp och det är ibland svårt att förutspå operationsresultatet. Patient-specifika datormodeller hade därför i framtiden kunnat användas för att komplettera dagens ultraljud och magnetröntgen för att få en bättre förståelse av klaffunktionen och hemodynamiken. Dessa typer av modeller skulle också kunna möjliggöra virtuell testning av olika ingrepp innan operation, för att bättre kunna avgöra vilket ingrepp som är bäst för patienten.

I den här avhandlingen har en sådan datormodell utvecklats och validerats, med syfte att kunna prediktera klaffunktion och hemodynamiken efter klaffplastik. Datormodellen är baserat på fluid-struktur interaktion, vilket innebär att man matematiskt med hjälp av hållfasthetslära och flödesmekanik kan modellera hur blodet påverkar klaffen och hur klaffen i sin tur påverkar blodflödet.

I den första delstudien byggdes en experimentell uppsättning av en förenklad hjärtmodell, där noggranna mätningar av parametrar relevanta för utvärderingen av klaffunktion utfördes. I delstudie två utvecklades sedan datormodellen för att simulera den experimentella uppställningen från delstudie ett, där simuleringsresultaten jämfördes mot de experimentella mätningarna. Detta möjliggjorde en välkontrollerad validering där parametrar viktiga för utvärderingen av klaffunktionen kunde undersökas. Valideringen visade att datormodellen i detta tillrättalagda fall kan uppskatta trycket över klaffen och flödets hastighet genom klaffen med hög noggrannhet.

I den tredje delstudien vidareutvecklades datormodellen för att simulera mänskliga mitralisklaffar hos friska frivilliga. Baserat på 3D ultraljudsbilderna av klaffen kunde patient-specifika datormodeller utvecklas. Simuleringsresultaten utvärderades mot mätningar på klaffunktion och visade åter igen att vi kan uppskatta hastigheten genom klaffen med en felmarginal liten nog för kliniskt användande. Dessutom är simuleringarna baserade på ultraljudsbilder, som tas på alla patienter som utreds för hjärtfel, vilket ökar den kliniska impelementerbarheten.

I den fjärde delstudien applicerades datormodellen på klaffar från barn med hjärtfel. Mitralisklaffen simulerades både i sitt preoperativa tillstånd och i sitt postoperativa tillstånd baserat på ultraljudsbilder. Klaffens funktion och hemodynamiken jämfördes sedan mot uppmätta ultraljudsdata tagen före och efter operationen för utvärdering av modellen. Utvärderingen gjordes baserat på parametrar man i kliniken använder för att utvärdera och gradera klaffsjukdom, för att visa på potentialen för kliniskt användande. Detta lade grunden för den sista och femte delstudien där klaffens töjningar (som är ett mått på klaffens deformation) och krafterna i chodrae jämfördes mellan friska och sjuka mitralisklaffar. Det undersöktes huruvida dessa numeriska mått har potentialen att användas som diagnostiska parametrar för att identifiera klaffsjukdom.

I den här avhandlingen har en datormodell för patientspecifika simuleringar av mitralisklaffen före och efter operation stegvis utvecklats och validerats. Den har visat sig ha potential för framtida klinisk implementation och har potentialen att i framtiden bistå som verktyg för att möjliggöra både en bättre förestående av klaffunktionen samt förberedelse inför en klaffplastik och därmed öka chanserna för ett lyckat ingrepp.

# **Abstract**

The heart consists of four chambers, two atria and two ventricles, separated by four valves that ensure unidirectional blood flow and efficient cardiac function. Among these, the mitral valve regulates blood flow between the left atrium and left ventricle and is one of the most mechanically loaded structures in the heart, stabilized by the chordae tendineae, which are connective structures. Consequently, mitral valve disease can have severe consequences. Approximately 1% of children are born with congenital heart defects, some of which involve mitral valve abnormalities such as stenosis (restricted opening) or regurgitation (leakage). Both conditions can be lifethreatening and often require surgical repair. However, predicting post-surgical valve function remains challenging. Patient-specific computational modeling could, in the future, complement imaging modalities such as echocardiography and magnetic resonance imaging (MRI) by providing additional insights into valve function and hemodynamics. Such models may also allow virtual testing of surgical strategies, supporting pre-operative planning and personalized treatment.

This thesis represents an initial step toward developing and validating a computational model capable of predicting mitral valve function and flow dynamics following surgical intervention. The model is based on fluid-structure interaction (FSI), which couples solid and fluid mechanics to capture the interplay between blood flow and valve motion.

In **Study I**, a simplified left heart phantom was developed to provide experimental data for model validation. The setup was exposed to pulsatile flow under physiological conditions, while valve opening, velocity, and pressure were measured using echocardiography, MRI, and pressure probes. The system demonstrated minimal cycle-to-cycle variation. The resulting dataset was made publicly available to support future validation efforts of cardiac-inspired FSI models. In **Study II**, the

same geometry and flow conditions were used in computational simulations to validate the developed FSI framework. The simulated transmitral velocities and pressure differences showed good agreement with the experimental data, with clinically acceptable error margins. Qualitative comparisons of flow streamlines further confirmed the model's ability to reproduce realistic hemodynamic patterns.

Building on this, Study III extended the framework to simulate mitral valve function in healthy humans. Echocardiographic data from ten volunteers were used to generate patient-specific valve geometries and derive individualized flow boundary conditions from left ventricular volume measurements. The simulated results matched echocardiographic observations throughout the cardiac cycle, confirming that the model captured valvular motion and hemodynamics in the atrium and ventricle. With a validated pipeline for patient-specific simulations, Study IV applied the model to pediatric patients with mitral regurgitation. Pre- and post-operative echocardiograms were used to reconstruct valve geometries before and after surgery. and valve function Simulated hemodynamics were compared echocardiographic data, demonstrating the model's ability to reproduce clinically relevant parameters used to grade regurgitation. Finally, Study V explored biomechanical parameters, specifically valve strain and chordal forces, as potential diagnostic indicators. Significant differences in leaflet strain were found between healthy and regurgitant valves, while regurgitant valves exhibited higher diastolic chordal forces, suggesting leaflet tethering and altered loading conditions.

In summary, the overarching aim of this thesis was to develop and validate a clinically feasible FSI framework for patient-specific modeling of mitral valve function and hemodynamics. The work demonstrates both the challenges and potential of modeling the complex interaction between blood flow and valve motion. It also illustrates the value of simulation-based approaches for improving understanding of valve mechanics and evaluating surgical repair strategies. This framework represents an important step toward a computational tool that could assist clinicians in planning and optimizing mitral valve repair.

# List of appended papers

This thesis presents a review of the author's contributions to the field of biomedical engineering and pediatric cardiology. The selected publications are referenced by their roman numerals throughout the text, with Papers I–V appended at the end, reproduced with permission from the copyright holders. In these works, the studies were designed by the supervisors together with the author of this thesis. For all included papers, the author of this thesis was primarily responsible for developing the numerical method, analyzing the results, and was the main writer of the manuscripts. She also contributed to the study design and specified the research question for each study, together with the co-authors.

I. L. Christierson, P. Frieberg, T. Lala, J. Töger, P. Liuba, J. Revstedt, H. Isaksson, and N. Hakacova. Multi-Modal in Vitro Experiments Mimicking the Flow Through a Mitral Heart Valve Phantom. Cardiovascular Engineering and Technology, 2024, 1-12

The author of this thesis (LC) constructed the experimental setup together with TL and JT, and conducted all experimental tests together with other co-authors; echocardiography measurements were conducted with NH, MRI scans with TL and JT, and the pressure measurements were conducted with PF. LC did all data analysis, statistics, and visualization of the results. LC drafted the manuscript as well as the answers to the reviewer comments.

II. L. Christierson, P. Frieberg, T. Lala, J. Töger, P. Liuba, J. Revstedt, H. Isaksson, and N. Hakacova. Validation of fluid-structure interaction simulations of the opening phase of phantom mitral heart valves under physiologically inspired conditions. Computers in Biology and Medicine, 2024, 171: 108033

LC developed the computational model and performed all measurements, data analysis, and comparisons. LC drafted the manuscript and the answers to the reviewers' comments.

III. L. Christierson, P. Frieberg, P. Liuba, E. Hedström, J. Revstedt, H. Isaksson, and N. Hakacova. Prediction of healthy mitral valve hemodynamics in children and adults: validation of fluid-structure interaction simulations to echocardiography and magnetic resonance imaging. Computers in Biology and Medicine, 2025, 194:110455

LC developed the computational model and pipeline for patient-specific modeling, recruited the healthy volunteers, and coordinated their examinations. LC attended all echocardiography examinations performed by NH and all MRI examinations performed by EH. LC conducted all sensitivity analyses, valve and ventricle segmentations, and drafted the manuscript and the answers to the reviewers' comments.

IV. L. Christierson, J. Revstedt, A. Pozza, A. Dragulescu, C. Morgan, O. Honjo, L. Mertens, H. Isaksson, and N. Hakacova. Toward Precision in Prediction of Pediatric Mitral Valve Repair Using Patient-Specific Fluid-Structure Interaction Modeling. (Submitted)

LC developed the computational model and recruited the patients together with NH. LC performed a majority of the segmentations together with NH, who also did all the segmentations. Further, LC did all simulations and measurements for analysis and validation purposes. LC drafted the manuscript.

V. L. Christierson, J. Revstedt, L. Mertens, A. Dragulescu, M. Karlsson, H. Isaksson, and N. Hakacova. Mitral valve strain and chordal forces as potential diagnostic parameters in pediatric mitral valve disease. *Manuscript under preparation (to be submitted in 2025)* 

LC collected all the data, performed the data analysis, and prepared the results reported in the paper. LC drafted the first version of the manuscript.

# Acknowledgements

Taking a step back and realizing that I have actually finished this project and completed my PhD is so crazy. There have been so many times when I have doubted myself and thought that I would never manage to create what I actually did. This has been such a journey for me, where I have learnt so much about myself and made wonderful friends along the way. The computational model I developed during these four years will forever be my baby, and I feel immensely proud of what I have achieved. However, this work would have been impossible to complete without the support of many colleagues, friends, and family.

I want to start by thanking my main supervisor. Nina, I would never have experienced one of the most challenging and rewarding adventures in my life if it weren't for you. Thank you for giving me the privilege of becoming a PhD candidate. I am so grateful for your mentorship, for all that you've taught me, and for the endless joy and excitement you bring into all you do. Our tight collaboration and together figuring my PhD out as we went has been such a journey. Thank you for always seeing the solutions instead of the problems, for always having time for me in your busy clinical schedule, and for giving me so many opportunities to advance and develop in my career and as a person. Thank you for the great time in Toronto, for letting me visit your lab there, and for inviting me into your home. Our weeks together there were so inspiring and so much fun, both during and after work hours.

I would also like to thank my co-supervisors Hanna, Johan, and Petru. Hanna, thank you for always giving the most meticulous feedback, your eye for high-quality research, and guidance in strategic choices throughout my PhD. Johan, you have always seen the positive sides in my work and been so encouraging. Thank you for always finding these little details in my work (that I didn't ask for help with!) that I could improve, but hadn't seen before. It always made the model better and led to

new, cool ideas. Petru, you are an endless idea-machine, and I am so grateful for your infinite trust from the beginning. I really wish that your dream of having an engineering team at the Pediatric Heart Center will be fulfilled, to accommodate all your innovative (and sometimes crazy) ideas.

To all my current and former colleagues at the Lund Biomechanics group: thank you for taking me in as one of your own. Isabella, Gustavo, and Hector for making the beginning of my PhD such a blast with beers, sauna, and afterworks. Viktor, for all your guidance on every kind of software, input, and patience with debugging, and all the kladdkaka. Thank you for always coming to my office for a break and random chit chat, it always made my day a bit better. Kunal, you always bring such a fun mood into the office, thank you for all the long conversations about life and thesis writing. Lorenzo, thank you for all the time you took to solve all kinds of issues I ran into and for all the nice corridor conversations. Thank you to all the other members of the Biomechanics group for the lunch runs, fika-breaks, and great afterworks. I would also like to thank my other colleagues at the Department of Biomedical Engineering for the Friday-fikas and PhD student events. Ulrika, thank you for listening to my worries and helping me with all practicalities regarding my employment. Megan, Franzi, and Felix, thank you for all the board game nights and lunches.

To my dear colleagues at the Pediatric Heart Center. Thank you for all the nice company at conferences and for believing in my work. Thank you for always inviting me to your meetings, where I got to learn so much about the clinical practice, patient care, and waffles. The work you do is so important, and your passion for what you do has always inspired me.

Thank you to all my colleagues and collaborators at the cardiac MR group. To Petter, for your infinite wisdom, wit, limericks, and patience. You were the one who made my PhD project possible, and you have been like a mentor to me during my PhD, for which I will always be so grateful. Tania, thank you for all those endless hours in the basement, sharing pure frustration and excitement about the pump setup. I am so happy to have found such a wonderful friend in you. Thank you for all the wine evenings, yapping, and parties at the base.

To my Lunda-family. Thank you for all the fun nights together, the summers at Berra's, the ski trips, and now, all the weddings. We always have so much fun when we are together, thank you for all those great memories. Olivia, tack för att du är min bästa vän som finns där för mig i vått och torrt. Du har alltid dem bästa råden, den vildaste matlagningen och de mest underbara pysselprojekten. Jag är så tacksam för att allid kunna vända mig till dig för allt mellan himmel och jord. Carro och Erik

"Ayvar", några av få som är kvar i Skåne, tack för alla fina stunder i torpet och på stan med en öl, alla härliga promenader och trevliga middagar.

Rania och Minh; ni adopterade in mig i ert maskingäng och sedan dess har vi hängt ihop. Tack för all stöttning, alla samtal och alla skratt tillsammans. Utan allt ert underbara sällskap och drama hade mitt liv varit lite färglösare.

To AcroYoga Syd in Malmö, thank you for providing a space where I can forget about work and lose track of time. Thank you for all the great acroyoga moments, the fails, the successes, and all the fun trips to festivals.

To my family, my parents, Susanne and Patrik, and my siblings, Jana and Clemens. Danke, dass ihr immer für mich da seid. Es ist immer so schön nach Rydebäck nach Hause zu kommen, ein Bier zu trinken und von den Hunden attackiert zu werden. Ich bin so froh, euch nah zu haben, ohne euch hätte ich es nicht geschafft. Ich hab euch alle so lieb. Mattias, min klippa, min cheerleader och min bästa vän. Du får alltid tuffa dagar att kännas lättare. Tack för att du alltid finns där för mig och går med på mina tokiga idéer, livet är så mycket roligare med dig.

Lea Christierson Lund, October 2025

1 (hin

# List of abbreviations

2D Two-Dimensional

3D Three-Dimensional

ALE Arbitrary Lagrangian-Eulerian

CFD Computational Fluid Dynamics

CT Computed Tomography

FE Finite Element

FEM Finite Element Method

FSI Fluid-Structure Interaction

FWHF Full Width Half Maximum

MRI Magnetic Resonance Imaging

PC-MRI Phase-Contrast Magnetic Resonance Imaging

RANS Reynolds-Averaged Navier Stokes

SPH Smooth Particle Hydrodynamics

# **Table of Contents**

Populä	rvete	enskapli	g sammanfattning	ii
Abstrac	ct	•••••		iv
List of a	appe	nded paj	pers	vi
Acknov	vledg	gements .		viii
List of a	abbro	eviations	Ş	xii
Table o	of Co	ntents		xiv
1 I	ntro	duction .		2
2 A	Aim a	and desig	gn of thesis	4
	2.1		nesis outline	
3 E	Backę	ground		8
3	3.1	The h	uman heart	8
		3.1.1	The mitral apparatus	
		3.1.2	Mitral valve disease	
3	3.2	Presur	gical planning	12
		3.2.1	Echocardiography	13
		3.2.2	Magnetic resonance imaging	13
3	3.3	Comp	utational modeling of heart valves	14
		3.3.1	Computational solid mechanics	
		3.3.2	Computational fluid dynamics	
		3.3.3	Fluid-Structure Interaction	22

4	Met	hods		30		
	4.1	The s	simplified heart model	30		
		4.1.1	In vitro phantom experiments (Study I)	31		
		4.1.2	Validation of the FSI model (Study II)	33		
	4.2	Patie	nt-specific modeling	35		
		4.2.1	Validation in healthy volunteers (Study III)	35		
		4.2.2	Modeling mitral regurgitation (Study IV)			
		4.2.3	Valve strain and chordal forces (Study V)	40		
5	Resi	Results				
	5.1	The s	simplified left heart model	42		
		5.1.1	In vitro phantom experiments (Study I)	42		
		5.1.2	Validation of the FSI model (Study II)	44		
	5.2	Patie	nt-specific modeling	45		
		5.2.1	Validation in healthy volunteers (Study III)			
		5.2.2	Modeling mitral regurgitation (Study IV)			
		5.2.3	Valve strain and chordal forces (Study V)	48		
6	Disc	Discussion				
	6.1	5.1 Developing the patient-specific model				
		6.1.1	Patient-specific valve geometries			
		6.1.2	The left heart model	54		
		6.1.3	Patient-specific hemodynamics	55		
	6.2	Mode	55			
	6.3	Novel parameters with diagnostic potential				
	6.4					
		6.4.1	Next steps in the model development			
		6.4.2	Toward clinical implementation	60		
7	Sun	ımary an	nd conclusions	62		
8	Refe	erences		64		
9	Apn	ended n	apers	84		

# 1 Introduction

The heart is a central organ in the circulatory system, responsible for maintaining pulsatile blood flow throughout the body. To ensure efficient pumping, the heart valves play a critical role by regulating unidirectional blood flow. As passive tissues, heart valves are guided solely by the inertial forces of blood flow, which in a healthy heart maximizes inflow, minimizes flow resistance, and prevents backflow during the cardiac cycle. Failure of the heart valves can have severe, even fatal, consequences. Cardiovascular disease remains one of the leading causes of death globally 1. Although acquired mitral valve disease is rare, it remains a serious pediatric condition often linked to congenital heart defects, which affect approximately 9 in 1000 children annually and substantially impact morbidity and mortality 2. Given the complexity of surgical or interventional treatment for heart valve disease, predicting post-surgical outcomes can be challenging. Due to the high risks associated with heart valve repair, achieving successful repair in both adult and pediatric patients has long been a priority, as prosthetic valves and repeated valve replacements carry significant risks and complications. Improved presurgical planning and a deeper understanding of valve anatomy and function prior to repair are therefore essential for enhancing personalized treatment and improving patient outcomes.

Today, echocardiography, magnetic resonance imaging (MRI), and occasionally computed tomography (CT) are used to assess valve anatomy and function for surgical planning. Patient-specific computer models using fluid-structure interaction (FSI) could, in the future complement these traditional imaging modalities by visualizing the valve anatomy and simulating its function before and after surgery. This allows for a more detailed understanding of valve function and provides insights into how different surgical approaches may impact valvular dynamics. Thus, patient-specific simulations have the potential to enhance presurgical planning by offering

additional information on valve function, ultimately increasing the likelihood of improved surgical outcomes.

The reason why these models are not yet implemented in clinical settings is due to several factors. First, such simulations are highly complex, requiring substantial computational resources and time. Additionally, there is a lack of comprehensive validation against clinically relevant parameters <sup>3</sup>. Assessing the accuracy and reliability of FSI simulations is challenging, as they involve both fluid and structural domains <sup>4</sup>, particularly in a clinical context where their influence on diagnosis must be carefully evaluated. Ensuring the accuracy of FSI simulations in a clinical setting is crucial for providing reliable results that support, rather than hinder, medical decision-making. To achieve this, validation against established gold-standard reference modalities is essential to guarantee results that are both trustworthy and clinically useful <sup>5</sup>.

This thesis has been conducted within a translational research environment at the intersection of engineering and medicine, giving me the role of a translator between the two disciplines. A central objective of this work has been to bridge the gap between the disciplines by presenting the complex challenge of modeling mitral valve dynamics and left-heart hemodynamics in a way that is both technically rigorous for engineers and clinically meaningful for medical doctors. The intention of the work presented in this thesis has therefore been to contribute to the dialogue between the fields of medicine and engineering by presenting a framework that is accessible to both communities, thereby enabling a shared understanding that can be applied, evaluated, and advanced within both fields.

# 2 Aim and design of thesis

The goal of this thesis was to contribute knowledge within fluid-structure interaction modeling of soft tissues submerged in blood, a fluid of similar density, and to shed light on which factors affect the heart valve function and hemodynamics to gain an understanding of the mechanisms behind mitral valve disease.

The aim of this thesis was to develop a computational framework for pre-operative simulations using standard clinical assessment data from echocardiography for diseased mitral valves to predict the post-operative hemodynamics and valve function in children with heart disease. To reach this aim, a simplified left heart model was first developed and validated against phantom experiments. This pipeline was further developed to model healthy patient-specific mitral valves and, finally, diseased mitral valves. The model was evaluated against echocardiography and was further employed to evaluate numerical parameters as novel diagnostic markers for mitral valve disease.

The specific objectives of the individual studies in this thesis were:

- I. To create an experimental benchmarking data set for FSI simulation models with an *in vitro* setup mimicking the left heart, including a deforming mitral valve. The data was publicly published for use by the research community (Paper I).
- II. To validate FSI simulations of a simplified left heart model, including the mitral valve, during diastolic physiological-inspired conditions, against the *in vitro* experimental data (Paper II).
- III. To propose a framework using 2D and 3D echocardiography to provide patient-specific mitral valve FSI models and to validate the framework against *in vivo* echocardiography and MRI data from multiple healthy volunteers (Paper III).

- IV. To extend the developed framework to pediatric mitral regurgitation, modeling pre- and post-operative valve function and hemodynamics for comparison with echocardiography data (Paper IV).
- V. To compare the valve strain and chordal forces in healthy and regurgitant mitral valves to elucidate if they can be used as potential diagnostic parameters to identify mitral valve disease (Paper V).

The different objectives described above were addressed in five scientific studies (I–V) depicted in Figure 2.1.

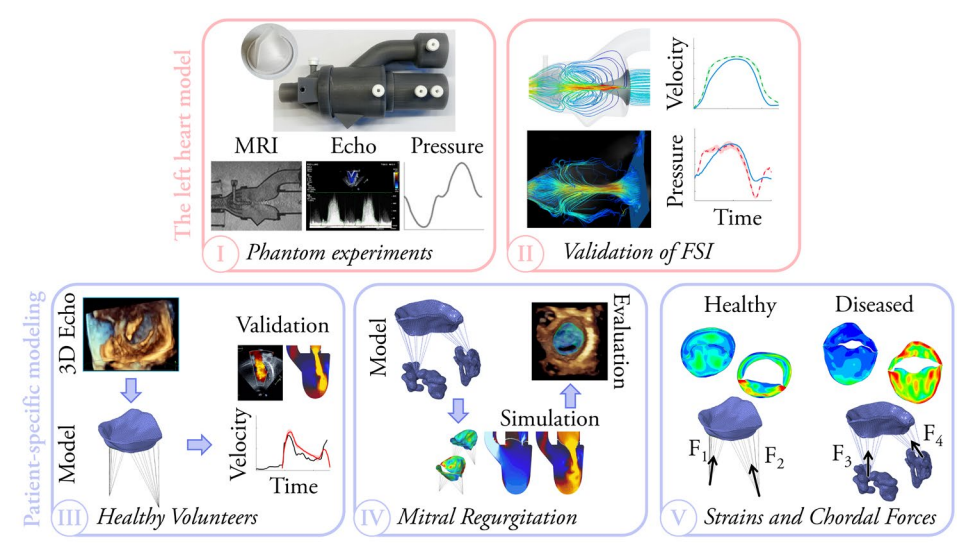


Figure 2.1. Overview of the study design. The roman numerals I-V refer to the papers appended in the thesis and are linked to the objectives. The specific methodologies for each study used are indicated: the *in vitro* test setup (I), which was used for validation of the FSI model (II), which was then further developed for patient-specific healthy and diseased mitral valves (III-V).

# 2.1 The thesis outline

In this thesis, the relevant theoretical background and context for each study are presented in **Chapter 3**, which establishes the foundation for understanding the current state of research in the field as well as the included papers. **Chapter 4** describes the methods employed throughout the thesis, organized by study. The main results and key findings are further presented in **Chapter 5** and analyzed in

**Chapter 6**, where the studies are discussed in relation to one another and to the state of the art research. **Chapter 6** also addresses the main limitations and future opportunities identified across the studies. **Chapter 7** provides the final summary and conclusions, followed by the appended papers included in the thesis.

# 3 Background

This chapter provides the theoretical background and context for the studies included in this thesis. Developing a computational framework for pre-operative simulations of diseased mitral valves requires a solid understanding of the human heart, the clinical imaging modalities used to assess it, and how these can be translated into computational models. Accordingly, this chapter first presents the fundamentals of cardiac anatomy (Section 3.1), followed by an overview of imaging techniques (Section 3.2). Finally, Section 3.3 discusses computational approaches for modeling mitral valve function and left heart hemodynamics.

# 3.1 The human heart

The heart is a central organ in the human circulatory system, responsible for maintaining the pulsatile flow of blood throughout the body and lungs, adjusting quickly to sudden workload changes, and adapting to long-term demands <sup>6</sup>. Structurally, the heart consists of a left and right side, each consisting of a ventricle and atrium (Fig. 3.1A). The right side manages the pulmonary circulation, while the left handles the systemic circulation. Deoxygenated blood enters the right atrium, passes through the tricuspid valve to the right ventricle, and is pumped through the pulmonary valve to the lungs for oxygenation. The oxygenated blood returns to the left atrium, flows through the mitral valve to the left ventricle, and is further pumped to the body via the aorta <sup>7</sup>. Thus, during contraction, called systole, the heart ejects blood from the right ventricle to the pulmonary artery and from the left ventricle to the aorta <sup>8</sup> (Fig. 3.1A). During relaxation, called diastole, the ventricles are filled with blood coming back from the lungs and the body to the left and right ventricles, respectively <sup>9</sup>. The four valves in the heart play a vital role in maintaining a

unidirectional flow of blood and preventing backflow, ensuring efficient pumping, maintaining proper pressure dynamics, and preventing cardiac inefficiencies.

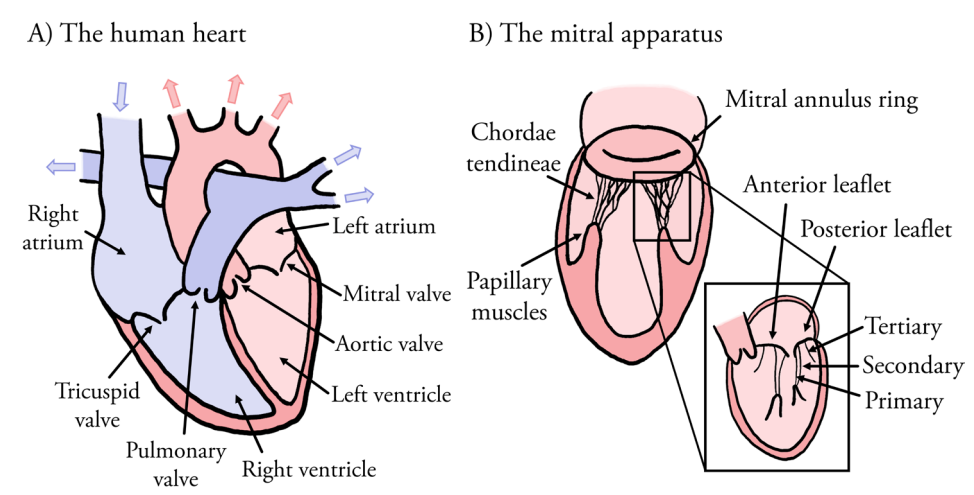


Figure 3.1. The human heart anatomy. A) The human heart consists of four chambers separated by four heart valves, which ensure unidirectional flow of the deoxygenated (blue arrows) and oxygenated (red arrows) blood. B) The mitral valve apparatus, located on the left side of the heart, including the chordae tendineae, which attach to the papillary muscles, emerging from the endocardial wall.

# 3.1.1 The mitral apparatus

The mitral valve, located between the left atrium and left ventricle, is composed of several functional and supporting components (Fig. 3.1B). It includes the anterior and posterior leaflets, which are attached basally to the mitral annulus and supported by the chordae tendineae. The chordae attach at the leaflet free edges (primary chords) and along the ventricular surface (secondary and tertiary chords) <sup>10</sup>. These tendinous structures branch from the papillary muscles, which arise from the ventricular wall, forming a complex web that stabilizes the leaflets. Together, they ensure proper valve closure during systole and prevent leaflet prolapse <sup>11</sup>. The mitral leaflets are composed of four tissue layers: the atrialis, spongiosa, fibrosa, and ventricularis, each with a different thickness and characteristic cells contributing to the valve function. At the sites of chordal insertion, the tissue transitions from a planar collagen structure to a cylindrical collagenous chord, enabling a gradual transition of forces between the leaflets and chordae <sup>12</sup>. Positioned on the left side of the heart, the mitral valve is subjected to some of the highest loads in the human body <sup>13</sup>. In mitral valve disease, it is common for multiple components of the valve

to be affected simultaneously. With disease progression or the presence of comorbidities, additional anatomical components may therefore also become compromised <sup>14</sup>, creating a complex condition. Thus, it is essential to understand the mechanics of the healthy mitral valve apparatus to understand the physiology and correctly interpret the pathophysiology of heart valve disease.

### 3.1.2 Mitral valve disease

Studies have shown that 10% of the general population is affected by mitral valve disease 15, and 9 in 1000 children are born with congenital heart disease, which entails a lifelong chronic condition and has a high impact on the mortality and morbidity of the patient <sup>2</sup>. The mitral valve is affected in approximately 0.5% of all congenital heart disease cases 16 and typically fails in two ways: mitral regurgitation, where the valve leaks during systole, or mitral stenosis, where the valve obstructs the blood flow and creates resistance during diastole. These dysfunctions can result from primary issues related to the valve's anatomy and function or may occur secondary to other cardiac conditions, causing the valve to malfunction despite a healthy anatomy. Mitral valve treatment typically involves surgical repair or replacement with a prosthetic valve via open-heart surgery, or repair using interventional techniques <sup>2</sup>. Both approaches carry significant risks, making successful outcomes a long-standing goal in adult and pediatric cardiology. In children, treatment is more complex as their hearts and valves continue to grow, making them unsuitable for valve prosthesis, posing challenges compared to adults <sup>17</sup>. Additionally, congenital heart disease often presents with a wide range of anatomical anomalies, varying significantly from patient to patient <sup>17</sup>. This variability complicates planning and timing for patient-specific interventions, especially since many techniques are adapted from adult valve repair procedures <sup>18</sup>. Consequently, postoperative success rates are higher in adults than in pediatric patients <sup>17,19,20</sup>.

# Mitral regurgitation

Mitral regurgitation occurs when the mitral valve leaks during systole, leading to volume overload in the left atrium and ventricle. In acute mitral regurgitation, the sudden increase in preload (atrial blood volume) elevates the pressure in the pulmonary circulation. Chronic mitral regurgitation, which often is the case for congenital conditions, can cause irreversible left ventricular remodeling and left atrial enlargement, increasing the risk of atrial arrhythmias <sup>21</sup>. In pediatric cases, primary mitral regurgitation (Fig. 3.2) is often due to mitral valve prolapse, and/or due to congenital abnormalities, such as clefts and flails, or as part of conditions like

atrioventricular septal defects <sup>22</sup>. This can be the cause of secondary ventricular dilatation, resulting in a combination of two pathologies. Pediatric mitral regurgitation can also develop secondary to ventricular dilatation, as the resulting annular enlargement prevents the valve leaflets from reaching and coaptating properly (Fig. 3.2). Historically, mitral regurgitation was primarily treated by surgical valve replacement. However, valve repair techniques have since advanced to preserve native tissue by removing excess tissue, replacing ruptured chordae, or augmenting leaflets with pericardial patches. Minimally invasive transcatheter treatments, such as suturing or using clips to restrict the leaking valve, have also been developed, offering reduced side effects and improved patient outcomes <sup>23,24</sup>.

In the clinical assessment of mitral regurgitation, both the mitral valve structure and the subvalvular apparatus are evaluated, the severity of the regurgitant flow is graded, and the site of the coaptation defect is identified. Together, these assessments provide insight into the underlying mechanism of regurgitation and serve as the foundation for determining whether surgical valve repair is required.

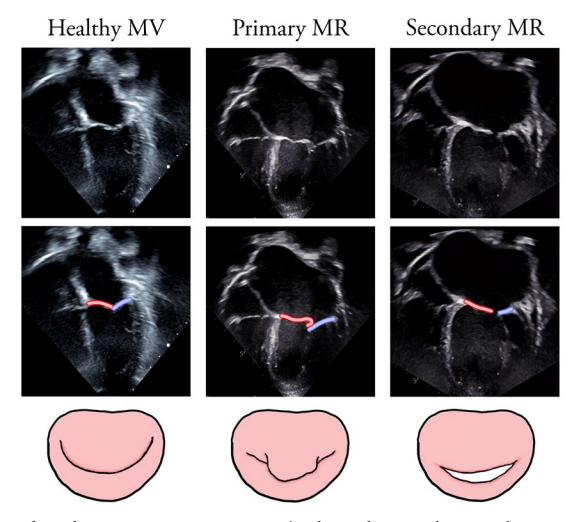


Figure 3.2. Mitral valve regurgitation. 4-chamber echocardiography views of the healthy mitral valve (left), primary regurgitation (middle) that caused secondary ventricular dilatation, and secondary regurgitation (right) due to primary ventricular dilatation. The anterior leaflet is highlighted in pink, and the posterior leaflet is highlighted in blue. The echocardiography images are accompanied by sketches of the arterial view of the mitral valve. MV = mitral valve, MR = mitral regurgitation.

# 3.2 Presurgical planning

Today, surgical planning is primarily based on echocardiographic and MRI findings <sup>25</sup> (Fig. 3.3), occasionally supplemented by CT scans in adult cases <sup>26</sup>, to assess mitral valve mobility, papillary muscle anatomy, chordal distribution, and attachments. Properly understanding the mitral valve apparatus and function is essential when selecting the treatment option. This assessment, combined with the severity of the symptoms <sup>27</sup>, guides the surgical strategy to improve valve mobility, increase the opening orifice, and reduce regurgitation. However, these images are confined to two-dimensional (2D) visualization, which might limit the understanding of the complex valve anatomy. While three-dimensional (3D) echocardiography has become the clinical standard for presurgical planning in pediatric patients <sup>28</sup>, emerging techniques such as virtual reality <sup>29</sup> and 3D printing of patient-specific heart models 30 have gained traction in research-focused centers, to complement traditional 2D imaging. These developments underscore the need for enhanced visualization techniques to better understand mitral valve pathophysiology. Given the complexity of mitral valve repair, particularly in pediatric cases, robust preoperative planning is essential to optimize surgical outcomes 27.

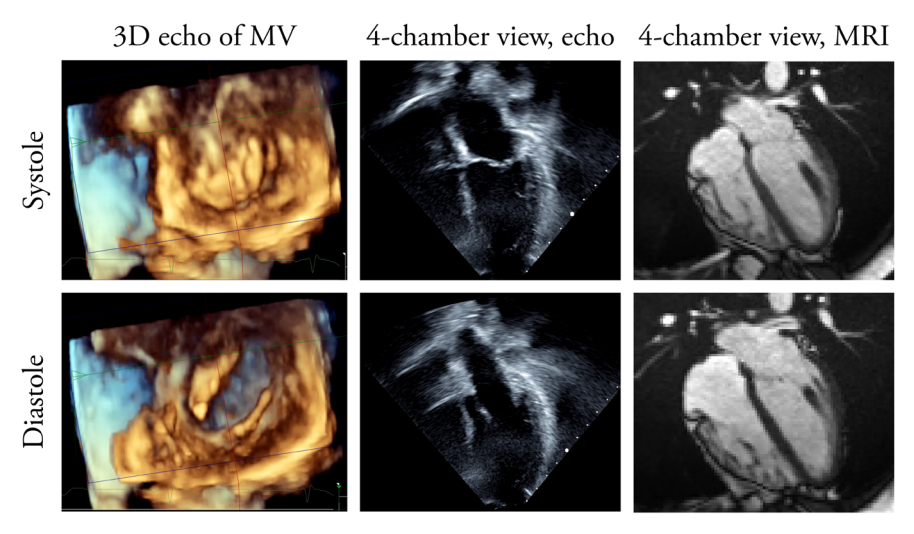


Figure 3.3. Clinical images of the heart. The mitral valve in its systolic and diastolic configuration imaged in 3D with echocardiography (echo) (left), a 4-chamber view with echocardiography (middle) and MRI (right) to exemplify how the different modalities can capture the different heart structures.

In this thesis, echocardiography and MRI are the primary modalities employed to gain information on the mitral valve and left ventricle; therefore, a more detailed description of each modality is provided in the following sections.

### 3.2.1 Echocardiography

Echocardiography was first introduced by Edler and Hertz in Lund, Sweden, in 1954, who used ultrasound to visualize cardiac structures within the body <sup>31</sup>. Sound waves (1.5–7 MHz) emitted by a piezoelectric transducer are reflected at tissue interfaces, with the time delay of returning signals used to reconstruct images <sup>32</sup>. Today, echocardiography is an essential tool for acquiring knowledge of cardiac morphology and function based on 2D and 3D images. With the Doppler effect, ultrasound can determine flow velocities and directionality. This provides information on the hemodynamics in the heart <sup>33</sup>, such as pressure gradient estimations with the simplified Bernoulli equation <sup>34</sup>, which today is the standard diagnostic tool for valvular heart disease <sup>35</sup>.

A high temporal and spatial resolution are essential to capture heart valve dynamics. In ultrasound, spatial resolution depends on frequency: higher frequencies yield better resolution due to shorter wavelengths, but penetrate tissue less effectively, reducing image quality at depth <sup>36</sup>. Axial resolution, which is constant along the beam, is approximately half the ultrasound wavelength, giving ~1 mm at 5 MHz <sup>37</sup>. Lateral resolution, determined by the beam width, decreases with distance due to divergence <sup>37</sup>. Temporal resolution (frame rate) depends on the time needed to reconstruct images from reflected signals; shallower depths and fewer scan lines improve it, as signals travel shorter distances and are emitted from fewer sources <sup>36</sup>.

Due to its noninvasive nature, low cost, accessibility, and high temporal and spatial resolution, echocardiography is the clinical gold standard for heart valve evaluation, as recommended by the European Society of Cardiology <sup>38</sup> and the American Heart Association/American College of Cardiology <sup>35</sup>.

### 3.2.2 Magnetic resonance imaging

MRI is based on the concept that protons (the positively charged particles in the nucleus of an atom) have a spin that varies when subjected to a magnetic field, similar to that of a compass needle. The precession frequency of the spin scales linearly with the magnetic field strength, and thus, by inducing a spatially varied magnetic field gradient over an object, the spin frequency also varies spatially <sup>39</sup>. These signals can

be detected, separated, and interpreted, and the object can thus be reconstructed as an image, which has laid the foundation of spatially encoded MR imaging <sup>40,41</sup>. Given its sensitivity to proton density, MRI can differentiate materials and tissue heterogeneity <sup>39</sup>, offering a non-ionizing, noninvasive imaging modality ideal for detailed internal visualization of the different soft tissues in the human body.

Cardiac MR is the reference standard for quantifying ventricular volumes and blood flow, most commonly using 2D phase-contrast (PC) MRI <sup>42,43</sup>. Beyond anatomical imaging, it is frequently applied to confirm valvular stenosis or regurgitation initially suspected by echocardiography <sup>44,45</sup>, and is particularly valuable in patients with poor acoustic windows, where high-quality echocardiograms are challenging to obtain <sup>46</sup>. More recently, 4D flow MRI (3D + time) has expanded cardiac MR capabilities by encoding blood flow in all spatial directions throughout the cardiac cycle. This enables comprehensive retrospective analysis, in contrast to 2D PC-MRI, which is limited to pre-defined imaging planes <sup>42</sup>.

# 3.3 Computational modeling of heart valves

Computational modeling may be employed to virtually simulate and assess the valve function prior to valve repair. Further, a computational model has the potential to predict the valve function in case of successful repair, enabling different techniques to be tested virtually. This would enable a more well-informed decision on the valve repair method, thus increasing the possibility of a positive surgical or interventional outcome and improving patient-specific care <sup>47</sup>. For this, different approaches such as solid mechanics, fluid dynamics, and fluid-structure interaction can be used, which are presented in the following sections.

### 3.3.1 Computational solid mechanics

Computational solid mechanics is important in modeling the mitral valve function, as it provides insight into the deformations and internal forces of the heart valve, thereby enhancing our understanding of the valve function and remodeling when subjected to normal and pathological loading conditions <sup>48</sup>.

In computational solid mechanics, the behavior of a solid subjected to an inner or outer agent is described by a set of force equilibrium equations. The finite element method (FEM) is most commonly employed, where the solid domain is spatially discretized into finite elements, for which the force equilibrium equations are numerically solved. The force equilibrium equations, derived from Newton's second

law, are usually non-linear and thus described as a set of partial differential equations (Eq. 3.1) linking the stress tensor,  $\sigma$ , to the acceleration, i.e., the second time derivative of the displacement  $\boldsymbol{u}$ , and the density  $\rho$ .

$$\nabla \cdot \boldsymbol{\sigma} - \rho \frac{\partial^2 \boldsymbol{u}}{\partial t^2} = 0$$
 Equation 3.1

Early FEM-based heart valve models appeared in the 1970s, where blood flow was represented as a pressure distribution acting on the leaflets, yielding preliminary insights into valve dynamics <sup>49–51</sup>. The following sections detail different approaches for modeling the geometric description and material behavior of the mitral valve.

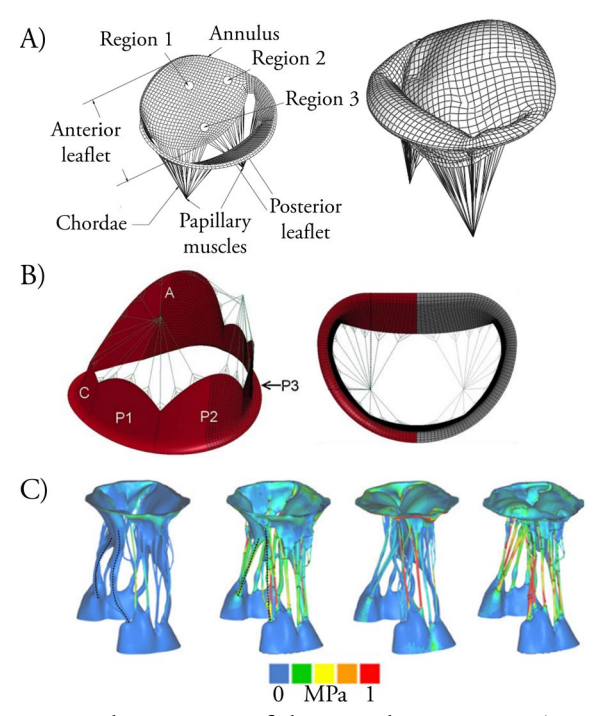
#### Geometric description

Early finite element (FE) models of the mitral valve relied on idealized and simplified geometries <sup>51,52</sup> (Fig. 3.4A-B). These models showed the effect of the chosen material model and gave information on different modeling aspects. However, they could not represent patient-specific variations. Later advancements introduced parametric idealized geometries, which adapted generic valve shapes to *in vivo* measurements, improving the geometric representation while maintaining computational efficiency <sup>53</sup>. These models could simulate conditions like mitral regurgitation due to left ventricular dilation <sup>54</sup>. However, understanding the mitral valve in the context of anatomical malformations requires patient-specific geometries, which can be acquired from clinical imaging through segmentation.

Since echocardiography provides high-resolution images of the heart valve, it forms a solid basis for valve segmentation. Several approaches exist, including commercial tools that extract valve geometries from 3D echocardiographic data <sup>55</sup>, in-house segmentation pipelines <sup>56</sup>, and deep learning-based methods <sup>57–59</sup> developed for healthy and regurgitant valves. Segmentation from cardiac MRI is less common as the leaflet edges are difficult to delineate <sup>42,60</sup>. To overcome this limitation, researchers have combined MRI-based ventricular geometries with simplified or echocardiography- or CT-derived valve geometries <sup>61–63</sup>. In instances where MRI was directly used for valve segmentation, manual approaches were employed to delineate the mitral <sup>64</sup> and aortic valve geometries <sup>65</sup>, since manual segmentation is still considered the gold standard, as it offers control over which cardiac structures are included in the valve apparatus. However, this process is time-consuming, motivating the development of various automated segmentation methods <sup>57,66</sup>. FE models based on echocardiography <sup>67,68</sup> and CT <sup>69,70</sup> to segment the valves, have enabled detailed reconstruction of patient-specific geometries <sup>71</sup>, supporting the

simulation of heart valve diseases such as mitral regurgitation <sup>72</sup>, and interventions like undersized ring annuloplasties <sup>73</sup> and MitraClip placement <sup>74</sup>. A challenge remains in obtaining mitral valve segmentations that accurately capture the patient-specific geometry <sup>47,64</sup>.

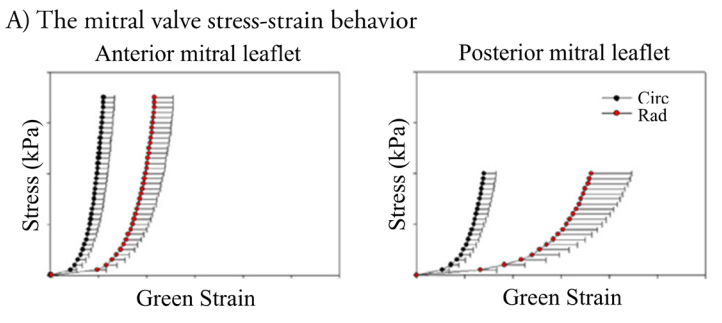
Resolving the chordae tendineae also remains challenging using echocardiography and MRI. Therefore, many patient-specific mitral valve models rely on anatomical descriptions to approximate the chordal structure <sup>47,62,63,70,75</sup>. Various pipelines have been developed to construct chordal structures, demonstrating good agreement with CT data <sup>71,76</sup>. With FE models based on CT data, Toma et al. showed that the chordal structure affects the blood flow <sup>77</sup>, and Feng et al. concluded that the patient-specific chordal configuration obtained from CT imaging was superior to simplified chordae structures when investigating the leaflet coaptation <sup>69</sup> (Fig. 3.4C).

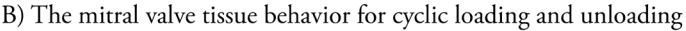


**Figure 3.4. Geometric descriptions of the mitral apparatus**. A) One of the earliest FEM-models of the mitral valve, reprinted from <sup>51</sup> with permission from Springer Nature. B) A generic description of the mitral valve for comparing FSI and FEM, reproduced from <sup>52</sup> according to the Creative Commons CC-BY license. C) The mitral apparatus discretized based on CT data, figure reprinted from <sup>77</sup> with permission from John Wiley and Sons.

#### Constitutive models

Proper material modeling is crucial for capturing mitral valve mechanics. In early studies, isotropic, linear elastic behavior was often assumed <sup>54,63,64</sup> or using a resistive method. These resistive methods model leaflet motion as fully driven by blood flow, omitting elastic resistance and therefore the need for a constitutive model <sup>62,78,79</sup>. Histological staining shows that the mitral valve leaflets are fibrous <sup>80</sup>, and tensile tests (Fig. 3.5) reveal a non-linear, anisotropic behavior <sup>81–83</sup> with minimal viscosity <sup>84,85</sup>. To account for these properties, the mitral leaflets can be modeled using fiber-reinforced materials with hyperelastic fibers embedded in a linear elastic matrix <sup>86</sup>. Since no viscoelastic behavior is observed by the leaflet tissue, omitting the time dependence is a fair approximation <sup>87,88</sup>. To describe the hyperelasticity of the fiber inclusions, a strain energy function is required, and the two most used in literature are the Fung-type strain energy function <sup>89,90</sup> and the invariant-based fiber-reinforced strain energy function <sup>47,69,70,81,82</sup>. There is still no definitive consensus on which strain energy function should be used, and uniaxial and biaxial tensile tests





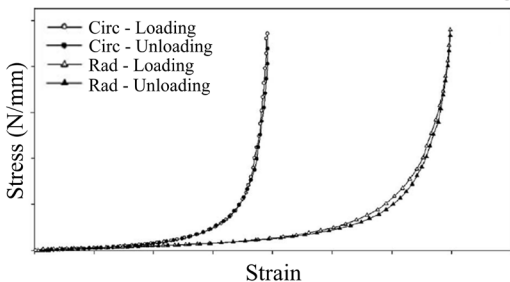


Figure 3.5. The material behavior of mitral valve tissue. A) Biaxial testing of the anterior and posterior mitral valve showing the average circumferential (circ.) and the radial (rad) material behavior for 11 samples, reprinted from <sup>183</sup> with permission from Elsevier. B) Cyclic loading and unloading of the anterior mitral valve leaflet showing negligible hysteresis for the circumferential direction and a small amount for the radial direction, reprinted from <sup>87</sup> with permission from Springer Nature.

show a discrepancy between material properties measured *in vivo* and *ex vivo*, due to pre-strain, making accurate material modeling challenging <sup>80,91</sup>. Emerging neural network models show promise in learning anisotropic responses directly from experimental data, which might be a future method to overcome these modeling challenges <sup>92</sup>. A foundation to this complex problem of modeling mitral valve tissue is the significant variability in data on human mitral valve tissue tests <sup>93,94</sup>, and the lack of data for the pediatric cohorts. Thus, adult tissue material behavior is often assumed for pediatric mitral valves <sup>75</sup>.

To fully capture the complete behavior of the mitral valve, accurate modeling of the chordae tendineae is required as well. The chordae material model is equally important as the geometrical representation to capture the dynamics of the mitral valve <sup>69</sup>. Linear elastic modeling approaches have been investigated <sup>52,64</sup>, subsequently followed by non-linear modeling approaches using Neo-Hookean <sup>80,82,95</sup> or Ogden formulations <sup>70,84</sup>, successful in capturing the non-linear stress-stretch responses exhibited by the chordae tendineae. More complex modeling approaches entail an elastic fiber-reinforced material, with one family of fibers oriented along the longitudinal direction of the chordae <sup>69,96,97</sup>.

### 3.3.2 Computational fluid dynamics

Computational fluid dynamics (CFD) is a crucial component in modeling mitral valve dynamics, as it provides valuable insight into the left heart hemodynamics, which are fundamental for assessing heart valve function <sup>99</sup>. Mathematically, fluid motion is described by the conservation of mass, momentum, and energy.

The mass conservation equation (Eq. 3.2) states that the rate of change of mass within a fluid system equals the net rate of mass flow into the system, expressed in terms of the velocity vector,  $\boldsymbol{u}$ , and the fluid density,  $\boldsymbol{\rho}$ . The momentum equation (Eq. 3.3), derived from Newton's second law, states that the rate of change of momentum equals the sum of the forces on a fluid particle. These forces include the pressure (a normal stress),  $\boldsymbol{p}$ , the viscous stresses,  $\boldsymbol{\tau}$ , and a general body force,  $F_M$ . Finally, the energy equation (Eq. 3.4), based on the first law of thermodynamics, states that the rate of change of energy,  $\boldsymbol{E}$ , equals the combined contributions of heat addition, described by Fourier's law through the thermal heat conductivity k and the temperature gradient  $\nabla T$ , the work done on a fluid particle, and the effects of potential energy changes are represented as the source term  $S_E$ . In CFD, these governing equations are discretized on a mesh covering the geometry and solved numerically.

$$\frac{\partial \rho}{\partial t} + \nabla \cdot (\rho \mathbf{u}) = 0$$
 Equation 3.2

$$\frac{\partial(\rho u)}{\partial t} + u \cdot \nabla(\rho u) = -\nabla p + \nabla \tau + F_M$$
 Equation 3.3

$$\rho \frac{\partial \mathbf{E}}{\partial t} + \rho \mathbf{E} \cdot \nabla = \nabla \cdot (-p\mathbf{u} + \mathbf{\tau} \cdot \mathbf{u}) + \nabla \cdot (k\nabla T) + S_E \quad \text{Equation 3.4}$$

Because the flow-induced pressure distribution across the mitral valve leaflet varies spatially and temporally throughout the cardiac cycle, it cannot be fully captured by FE simulations alone. As this pressure field contributes to the onset and progression of valvular disease <sup>98</sup>, incorporating blood flow is essential for assessing the strains and stresses in the valve leaflets <sup>52,99</sup>. Therefore, the following sections outline the fundamental principles of modeling left heart hemodynamics using CFD, including numerical approaches to modeling the behavior of blood flow and turbulent flows.

#### Constitutive models

The material properties of blood are equally important as those of the mitral apparatus when simulating heart valve dynamics. Since the mitral leaflets passively interact with the blood flow and simultaneously exert forces on the fluid, the choice of material parameters for the fluid significantly influences the leaflet motion <sup>100</sup>. Blood consists primarily of plasma (a Newtonian fluid) and red blood cells. These give it non-Newtonian properties, i.e., a non-linear relationship between viscosity and shear rate, due to the red blood cells' tendency to cluster, deform, and aggregation <sup>101</sup>, which causes shear-thinning. Thus, blood is a complex fluid suspension of cellular elements in plasma <sup>101</sup> and is therefore considered non-Newtonian <sup>102</sup>.

Most heart valve studies assume Newtonian fluid behavior, which is appropriate for high Reynolds numbers, where non-Newtonian effects like granularity are negligible <sup>100</sup>. However, in low shear rate conditions, such as blood passing through small gaps, the blood viscosity no longer remains constant <sup>103</sup>. This can be described by the Carreau-Yasuda model <sup>104–107</sup> (Fig. 3.6), which takes on almost constant viscosity values for high and low shear rates, with an exponential decrease in the transitional region. The Casson model <sup>105,108</sup> (Fig. 3.6) which is a power law, taking on high viscosity values for low shear rates and low viscosity values for high shear rates, has also been used, or the Quemada model <sup>109</sup> (Fig. 3.6) which models a plateau of high viscosities at low shear rates and a plateau of lower viscosities for high shear rates. Although these models reproduce the shear rate-viscosity relation, they cannot

represent elastic stresses or viscoelastic effects that blood has been shown to have <sup>110</sup>. Further, a challenge lies in capturing the patient-specific plasma composition, hematocrit, and red blood cell clustering, which all affect the blood properties as well, introducing high complexity into the computational models <sup>111</sup>.

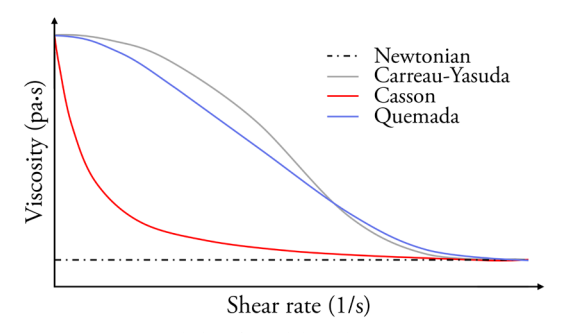


**Figure 3.6. Constitutive models for blood.** A representative sketch of the viscosity/shear rate-dependence in blood modeled with the Newtonian, Carreau-Yasuda, Casson, and Quemada models. The graph was inspired by <sup>107</sup>.

### Modeling turbulence

The Reynolds number is a dimensionless parameter defined by the ratio of the viscous and inertial forces, which predicts whether a flow is laminar or turbulent. Flow is considered laminar when the ratio of fluid velocity and viscosity is low, i.e., when the Reynolds number is below a critical threshold. In this regime, fluid particles follow smooth paths with little or no mixing, and the flow can be fully described by the continuity and Navier-Stokes equations. For higher Reynolds numbers, once the critical Reynolds number is exceeded, however, even small perturbations may trigger transition to turbulence, characterized by chaotic motion, enhanced mixing, and increased flow resistance <sup>112</sup>. Turbulence is often quantified using the Reynolds stress tensor, which considers the turbulent velocity fluctuations as apparent stresses <sup>113</sup>. Since this tensor appears when averaging the governing equations, it also forms the basis for turbulence modeling.

In the left heart, blood velocity and the valve opening (i.e., opening diameter of the flow domain) vary throughout the cardiac cycle, leading to a large span of Reynolds numbers during mitral inflow <sup>63,114</sup>. As a result, intracardiac blood flow often resides within a transitional regime, neither fully laminar nor fully turbulent <sup>115</sup>. This presents a challenge for computational modeling, as neither a laminar nor a turbulence model can fully represent the flow behavior. The most widely used turbulence models are based on the Reynolds-Averaged Navier-Stokes (RANS)

equations, such as the k- $\varepsilon$  <sup>116,117</sup> and the k- $\omega$  <sup>118</sup>, models, which rely on the Boussinesq hypothesis to approximate a linear relationship between the Reynolds stress tensor and the mean strain rate <sup>119</sup>. However, the averaging procedure intrinsic to RANS smooths out transient fluctuations such as swirls and vortices, limiting accuracy in transitional regimes where temporal dynamics are crucial.

Turbulence has a significant impact on cardiac flow dynamics, contributing to vortex formation downstream of the mitral valve that influences valve closure <sup>61,70,78</sup>, as well as altering wall shear stresses <sup>120</sup> (Fig. 3.7). Nevertheless, many studies approximate blood flow as laminar <sup>63,65,114</sup>, arguing that turbulence has only a marginal effect on clinical outcomes <sup>65,118</sup>.

As an alternative to RANS, higher-fidelity approaches directly compute turbulent fluctuations rather than modeling them. Large Eddy Simulation <sup>115,121</sup> and Direct Numerical Simulations <sup>122</sup> resolve turbulent structures with much greater detail, providing valuable insights into cardiac hemodynamics (Fig. 3.7). However, due to their substantially higher computational cost, RANS-based models remain the most commonly used in practice. A key challenge, however, is the lack of consensus in the literature regarding which modeling approach most accurately captures intracardiac flow behavior.

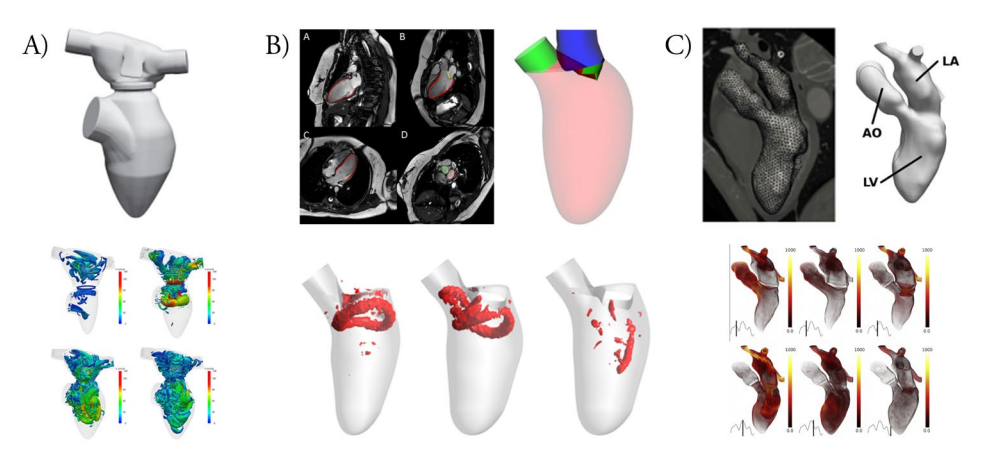


Figure 3.7. Blood flow modeling in the left heart. A) Characterization of the blood flow in an idealized heart model using Large Eddie Simulation (LES), reprinted from <sup>121</sup> with permission from John Wiley and Sons. B) Investigation of the vortex formation in the left heart under laminar flow conditions, reprinted from <sup>61</sup> with permission from Elsevier. C) Patient-specific left heart simulations based on MRI imaging were performed using LES to investigate the left heart hemodynamics, reprinted from <sup>115</sup> with permission from Elsevier.

#### 3.3.3 Fluid-Structure Interaction

The principles of computational solid mechanics and computational fluid dynamics can be coupled to capture the interaction between a deformable solid and a surrounding fluid, an approach known as fluid-structure interaction (FSI). In modeling the mitral valve, FSI is essential, as neither fluid nor solid mechanics alone can reproduce the complex coupling between the leaflet motion and the blood flow. Therefore, FSI enables detailed analysis of the effects of how spatially and temporally varying pressure distributions affect the leaflet deformation and provides insights into intracardiac flow patterns, such as ventricular vortex formation, that are critical for mitral valve closure <sup>98</sup>. Numerically, FSI coupling can be understood based on two principles:

- 1. The motion of the fluid  $(\boldsymbol{u}_f)$  induces a corresponding motion of the solid, defined by the time derivative of the solid displacement  $\frac{\partial \boldsymbol{d}_S}{\partial t}$ , under the assumption of continuous contact between the fluid and solid, without penetration.
- 2. As the fluid moves, it exerts a fluctuating pressure on the solid surface  $t_f$ , generating fluctuating stresses at the interface  $t_s$ , which induces a corresponding movement of the solid, as these must remain in equilibrium.

This can be translated into two coupling constraints at the fluid-solid interface used to couple the governing equations of fluid and solid domains (Eq. 3.5-3.6). Here, the indices f and s denote the fluid and solid domains, and n is the normal vector.

$$u_f = \frac{\partial d_s}{\partial t}$$
 Equation 3.5

$$m{t}_f = m{t}_S$$
 , where  $m{t}_f = -p m{n}_f + m{ au}_f$  and  $m{t}_S = m{\sigma} m{n}_S$  Equation 3.6

Despite its potential, the clinical use of FSI remains limited, largely due to the complexity inherent to these models, the high computational costs, and the challenges of rigorous validation <sup>3</sup>. Balancing the model accuracy and computational efficiency is therefore critical <sup>3,123</sup>. A major numerical challenge lies in coupling the Eulerian fluid domain (where the coordinate system follows the particle in motion) with the Lagrangian solid mesh (where the coordinate system is static in relation to the particle in motion). The large deformations characteristic of valve motion further complicates this process, often requiring adaptive meshing strategies to maintain numerical stability.

Two main approaches exist for solving FSI problems. In the monolithic approach, the equations governing both flow and structural domains are solved simultaneously within a single solver, providing strong coupling at the cost of high computational demand. In contrast, the partitioned (or segregated) approach solves the fluid and structural equations separately using different solvers, typically with independently generated meshes, requiring exchange of information across the interface. Several numerical strategies have been developed to enforce coupling across this interface, either through boundary-conforming methods or boundary non-conforming methods (Fig. 3.8).

The following sections explore these coupling strategies in greater detail, describe different approaches to modeling the left heart, and review the evolution of mitral valve FSI simulations. Finally, FSI models of other cardiac valves are discussed to provide a broader context for current developments in heart valve FSI modeling.

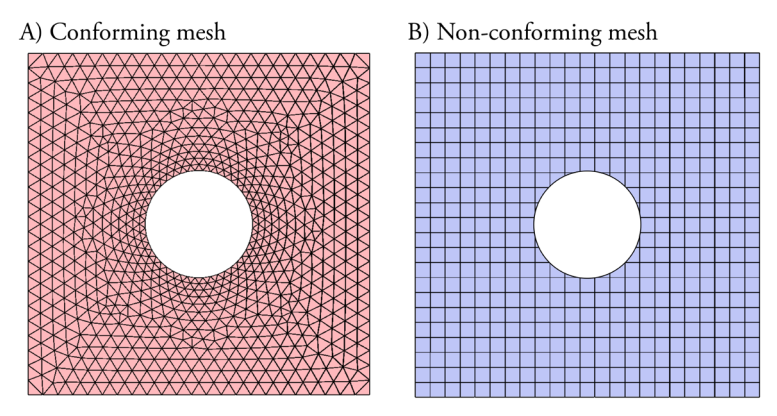


**Figure 3.8. Meshing methods**. Illustrative examples of a boundary A) conforming mesh and a B) non-conforming mesh.

## **Boundary-conforming methods**

Boundary-conforming FSI methods use separate, non-overlapping meshes for fluid and solid domains (Fig. 3.8A). Interaction is managed via the Arbitrary Lagrangian-Eulerian (ALE) method, which incorporates Eulerian and Lagrangian formulations to allow proper coupling. However, large deformations often require frequent remeshing to preserve mesh quality, increasing computational cost <sup>86,124</sup>.

ALE has been employed to model valve dynamics for an idealized aortic valve <sup>99</sup>, a bileaflet mechanical valve <sup>116</sup>, and for a mitral valve prosthesis validated against *ex vivo* data <sup>125</sup>. Khodaei et al. used dynamic meshing within an ALE framework to

simulate left-heart flow, showing good agreement with *in vivo* mitral valve velocities <sup>126</sup>.

To reduce re-meshing demands, the overset (Chimera) method can be used. It allows independently meshed domains to deform using ALE while handling large displacements via mesh-to-mesh interpolation <sup>127,128</sup>. Ge et al. applied this to simulate complex flow in bileaflet valves <sup>114,129</sup>, while Le and Sotiropoulos used it in a simplified left heart model <sup>130,131</sup>. More recently, the overset method has been used for modeling flow in left ventricular assist devices <sup>107</sup>.

### Nonconforming boundary methods

In nonconforming boundary FSI methods, fluid and solid domains use overlapping grids (Fig. 3.8B), allowing for large deformations without re-meshing <sup>86</sup>. The two main approaches are the immersed boundary method and the fictitious domain method. The immersed boundary method, widely used in heart valve modeling, enforces the no-slip condition by solving only the fluid momentum equation <sup>132–134</sup>, while the fictitious domain method solves both fluid and solid equations, but has seen limited application since 2006 <sup>135–139</sup>.

Gao et al. applied an immersed boundary/FE method to simulate the mitral valve, later expanding it to include the left ventricle, with good agreement to *in vivo* data <sup>47,140</sup>. Feng et al. built on this to study chordae structure effects <sup>69</sup>, atrial coupling <sup>96</sup>, and the full left heart and pulmonary circulation <sup>97</sup>. Other studies explored constitutive laws <sup>82</sup> and mitral regurgitation <sup>78</sup> using the immersed boundary/FE framework.

A recent development, immersogeometric FSI, combines ALE and immersed boundary methods. It uses a non-conforming solid mesh immersed in a boundary-fitted fluid grid, maintaining accuracy at the fluid-structure interface without remeshing <sup>141,142</sup>. Applied to bioprosthetic valve modeling, it enables patient-specific simulations and shape optimization <sup>143,144</sup>. Further developments include anisotropic materials <sup>145</sup> and left ventricular modeling <sup>90,146</sup>.

## Left heart modeling

Modeling the human heart presents substantial challenges, particularly when simplifying its intricate structure for FSI simulations while retaining clinical relevance. In recent years, mitral valve simulations have evolved beyond isolated valve models to incorporate larger portions of the cardiac anatomy, offering deeper insights into the upstream and downstream flow behavior and its influence on valve

dynamics. Early approaches employed generic mitral valve geometries embedded within idealized tubular fluid domains to investigate valve function <sup>52,147</sup>. These studies reported that tubular models produced faster fluid velocities during both valve opening and closure, along with reduced vorticity, when compared to ventricular configurations. More anatomically representative models, such as those by Khodaei et al. <sup>148</sup> and Khalafvand et al. <sup>149</sup>, introduced patient-specific left ventricular geometries combined with simplified mitral valve models to examine valvular stress and intraventricular flow patterns, albeit without *in vivo* validation. Notably, the leaflet geometry was shown to influence vortex formation within the ventricle <sup>149</sup>.

Building on this, advanced models by Mao et al. <sup>70</sup> and Gao et al. <sup>47</sup> incorporated both patient-specific left ventricular and mitral valve geometries, enabling predictions of hemodynamic behavior with a dynamically contracting ventricle. These studies demonstrated, for example, that vortex formation within the ventricle contributes to effective mitral valve closure <sup>126,150</sup>. Expanding this approach further, Feng et al. <sup>97</sup> integrated the pulmonary circulation into an already coupled left atrium-left ventricle model, capturing wave propagation through the pulmonary arteries and vortex dynamics within the atrial chamber.

A persistent challenge in FSI modeling lies in determining the balance between model complexity and clinical applicability. No comparison has been made on what effect a contracting ventricle has on the simulation outcome; thus, it is unknown if the accuracy necessary for clinical use is gained or not. Each additional patient-specific cardiac structure increases the numerical complexity, yet potentially improves physiological fidelity. However, acquiring and integrating such detailed anatomical data within feasible time frames remains difficult. To enable clinical translation, these workflows must be streamlined and scalable to larger patient cohorts, as this step is essential for achieving routine clinical implementation.

## Mitral valve modeling

In the field of FSI simulations of the mitral valve and the left heart, several research groups worldwide have advanced the development of complex computational models of mitral valve dynamics, hemodynamics, and valve-ventricle interactions.

Einstein <sup>151</sup> and Kunzelman <sup>152</sup> were the first to report FSI simulations of the mitral valve (Fig. 3.9A). Their studies extended earlier FE models by incorporating blood flow, although the simulations were constrained to a simplified tube-like geometry. Building on this foundation, Toma et al. <sup>153</sup> applied smooth particle hydrodynamics (SPH), which is a mesh-free method in which the fluid is represented by particles

rather than a continuum, to investigate chordal forces in the healthy mitral valve. The same framework was later adapted to study chordal rupture <sup>154</sup> and the modeling of the chordal structure <sup>77</sup>. Subsequent work extended the model to simulate percutaneous transcatheter mitral valve repair techniques in adults, including intravalvular spacers <sup>81</sup> and edge-to-edge repair with varying levels of papillary muscle displacement <sup>155</sup>.

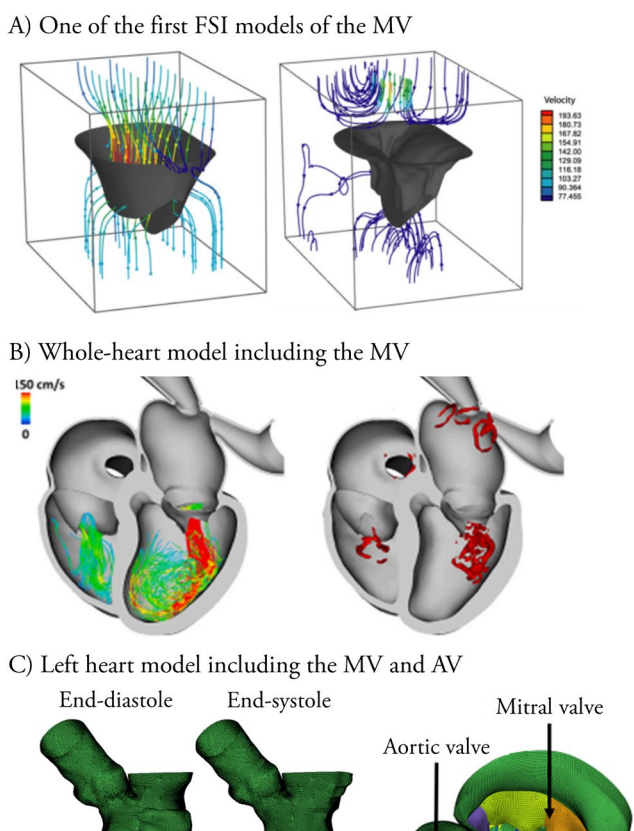


**Figure 3.9. FSI models of the mitral valve.** A) One of the first FSI models of the mitral valve for noninvasive diagnostic evaluation <sup>152</sup>, reproduced with permission through Copyright Clearance Center. B) Whole-heart FSI simulations for evaluating valve annular dynamics and pericardium-heart interactions, reproduced from <sup>158</sup> according to the CC BY license. C) A fully coupled FSI model of the contracting left heart including the mitral and aortic valves, reproduced from <sup>70</sup> according to the CC BY 4.0 license. MV = mitral valve, AV = aortic valve.

A second leading group is that of Luo and colleagues, who initially presented an FSI model of the mitral valve segmented from MRI data <sup>64</sup>. Their research evolved from comparing patient-specific valve models in a tube <sup>156</sup>. They further advanced their model toward increasingly realistic simulations within a contracting left ventricle <sup>47</sup>. Further studies examined the role of chordal architecture <sup>69</sup>, incorporated the left atrium <sup>96</sup> and added pulmonary circulation <sup>97</sup>. This model was used to investigate the left heart hemodynamics and pump function under mitral valve regurgitation, caused by hypertrophic cardiomyopathy and by a calcified mitral valve <sup>157</sup>. Ultimately, their research culminated in a whole-heart FSI model with physiologically realistic valves <sup>158</sup> (Fig. 3.9B).

The third major contribution to the field of mitral valve simulations comes from Sun and colleagues, who first introduced an SPH-based model of bioprosthetic valves <sup>159</sup>. This was subsequently expanded to patient-specific simulations of the left ventricle, mitral valve, and left atrium <sup>70</sup> (Fig. 3.9C). Their model has since been applied to study mitral regurgitation due to chordal rupture <sup>160</sup>, evaluate neochordae repair in mitral valve prolapse <sup>161</sup>, and compare echocardiographic quantification of mitral regurgitation with computational predictions <sup>162</sup>. Their model was also used to evaluate the left heart hemodynamic, structural, and morphologic changes after MitraClip treatments in adults with mitral regurgitation. They showed that although the MitraClip treats regurgitation, it imposed a non-physiological loading on the mitral valve, especially during diastole <sup>163</sup>.

Collectively, these groups have significantly advanced the field by developing sophisticated models that integrate not only the mitral valve but also surrounding cardiac structures. However, their focus has remained primarily on the healthy valve, with limited validation against *in vivo* data. For clinical translation, validation against larger patient cohorts, as well as simulations of pathologic and post-operative conditions with validation against *in vivo* data, is essential. Addressing these gaps is the focus of this thesis, which emphasizes validation against multi-patient echocardiographic data and thus establishes a stronger connection to clinical practice, even without yet incorporating fully patient-specific ventricular and atrial geometries.

## Modeling other cardiac valves

Apart from the mitral valve, FSI models have also been developed for the aortic valve and for mechanical prostheses implanted in the aortic position, offering valuable insights into the broader development of valve simulation methods.

Early work on simplified aortic valve models placed the valve in an idealized straight tube to study hemodynamics <sup>105,108,164,165</sup>. Hsu et al. <sup>144</sup> compared FE and FSI simulations in this setup and showed that their FSI framework provided more physiologically realistic leaflet deformation (Fig. 3.10A). Considerable effort has since gone into refining the numerical approaches for healthy adult aortic valve simulation. For instance, Griffith <sup>166</sup> was among the first to introduce an immersed boundary model of aortic valve dynamics. Shühler et al. <sup>167</sup> developed an open-source FSI model for flow through the aorta, applicable to both native and mechanical valves, although the lack of remeshing limited its performance under large deformations. More recently, Terahara et al. <sup>146</sup> introduced a high-fidelity staggered FSI algorithm for idealized aortic valve geometries.

Pathological conditions have also been explored. FSI has been applied to study the impact of atherosclerotic aortic valves on the coronary hemodynamics <sup>168</sup> and flow patterns in calcified aortic valves <sup>118</sup>. In bicuspid aortic valves, where two of the three

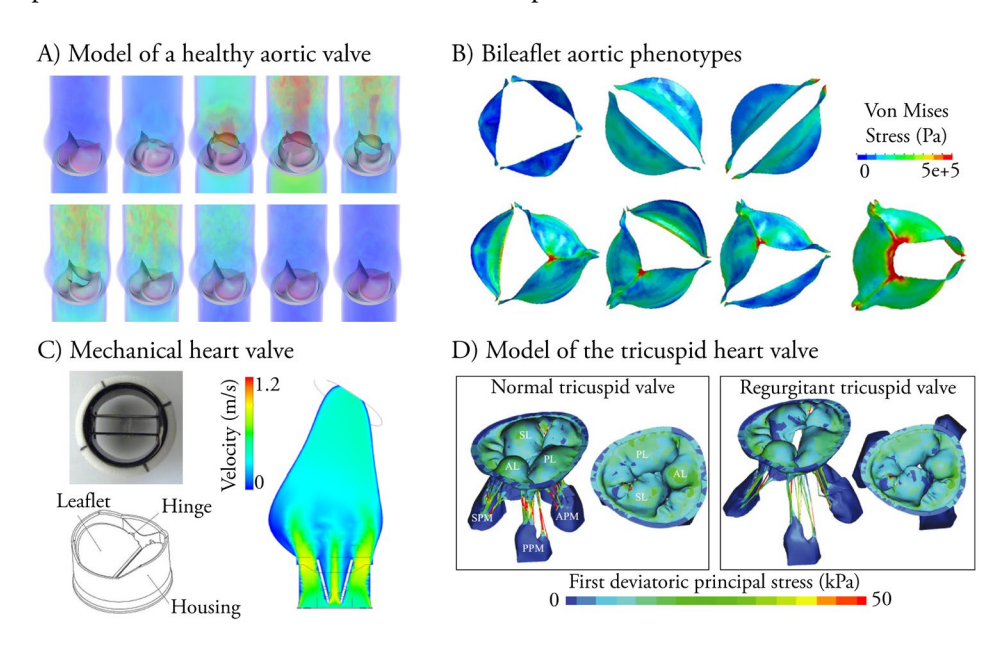


**Figure 3.10. FSI models of other heart valves.** A) FSI model of a healthy aortic valve, reprinted from <sup>144</sup> with permission from Springer Nature. B) Investigation of different bileaflet aortic phenotypes, reprinted from <sup>170</sup> with permission from Springer Nature. C) FSI modeling of a mechanical aortic heart valve prosthesis, reprinted from <sup>117</sup> with permission from Springer Nature. D) FSI simulations of the healthy and regurgitant tricuspid valve, reprinted from <sup>174</sup> with permission from Springer Nature.

cusps are fused, several studies have simulated different phenotypes <sup>169–171</sup> (Fig. 3.10B) and even validated patient-specific models against *in vivo* data <sup>65</sup>.

In adults, valve replacement is commonly employed to address aortic valve malfunction, using bileaflet mechanical valves, surgically implanted bioprosthetic valves, or transcatheter aortic valve replacements. However, prostheses carry risks of hemolysis, platelet activation, and thus thromboembolism, which have been investigated with FSI <sup>117,125</sup> (Fig. 3.10C). Other studies have examined bioprosthetic valves in terms of surrounding flow fields <sup>90,172</sup>, modeled flow through bileaflet mechanical valves to assess annular deformation <sup>116</sup>, coronary hemodynamics <sup>106</sup>, and even coupled valve simulations with contracting left ventricular models. FSI has also been used for transcatheter aortic valve replacements, with some studies validating simulations against *in vitro* experiments <sup>173</sup>.

In contrast, relatively few FSI studies have targeted the right-sided tricuspid and pulmonary valves. Singh-Gryzbon et al. <sup>174</sup> (Fig. 3.10D) studied closure dynamics of a regurgitant tricuspid valve, while Dabiri et al. <sup>175</sup> investigated transcatheter repair strategies for tricuspid regurgitation. For the pulmonary valve, FSI has been used to assess the influence of valve orientation on bioprosthetic hemodynamics <sup>176</sup> and to study pulmonary valve replacement with reduced FSI models <sup>177</sup>. Overall, research on right-sided valve FSI remains limited compared to the left-sided aortic and mitral valves.

# 4 Methods

This chapter presents the methods employed throughout the thesis, building on the theoretical foundations outlined in the previous chapter. It is divided into two main parts: "The simplified heart model" (Section 4.1), which encompasses Studies I–II, and "Patient-specific modeling" (Section 4.2), covering Studies III–V.

The first part describes the construction of the experimental phantom setup (Study I), developed to generate validation data for the FSI model applied to a simplified left heart geometry (Study II). The second part details the further development of the FSI model to simulate patient-specific mitral valves, validated first against *in vivo* data from healthy volunteers (Study III), and subsequently against data from patients with mitral regurgitation in pre- and postoperative conditions (Study IV). Finally, Study V presents a comparative analysis of pediatric healthy and regurgitant mitral valves, aiming to identify novel diagnostic parameters for valve disease.

## 4.1 The simplified heart model

A simplified left heart model was designed to assess the error margin of our FSI model under controlled conditions with well-defined boundary conditions and material parameters. This heart model was 3D printed for phantom experiments and simulated with FSI for validation. The validation allowed us to compare the error margins of the model to clinically acceptable values and thus served as the foundation for future steps toward patient-specific modeling.

## 4.1.1 In vitro phantom experiments (Study I)

Study I aimed to design a cardiac motivated *in vitro* test setup with a left heart phantom to create a highly controlled experimental environment, minimizing confounding factors, to measure and provide benchmarking data for the validation of FSI models. Pulsatile physiological-inspired waveforms were generated with a computer-controlled motor and pump assembly (Fig. 4.1). Catheter pressure measurements and medical imaging techniques were employed such that the pressure, velocity, and opening of the valve could be quantified and used for validating the FSI model. All *in vitro* measurements, including the geometry files of the phantom, are publicly available in the Zenodo Repository <sup>178</sup>.

#### The *in vitro* test setup

The *in vitro* test setup was constructed using a positive displacement pump <sup>179</sup> that enabled water to be pumped in and out of a membrane chamber via a piston (Fig. 4.1A). The setup offered a stroke volume of 0–130 ml in both forward- and backward flow, with adjustable stroke rates of 1–200 beats per minute. The pump was set up to simulate flow waveforms corresponding to cardiac output values of 2.9, 4.4, and 5.4 l/min at 60 beats per minute. A programmable motor (56B10A C type, Myostat Motion Control Inc., Newmarket, ON, Canada) powered the pump, and the two units were connected through a carbon fiber rod. The phantom was connected to the pump at the apex and mounted in a plastic reservoir containing 25 liters of room-temperature water, allowing water to flow in and out of the model.

## The phantom geometry and flow description

The phantom included a ventricle, atrium, mitral and aortic valves, and an apex with dimensions approximated by the adult human heart (Fig. 4.1B). The mitral valve leaflets were designed to open and close without chordae tendineae or papillary muscles, governed solely by water flow. This design succeeded in all cases but one. A simplified ball valve replaced a realistic aortic valve to reduce complexity while retaining functional opening and closing with each pumping cycle, thus minimizing potential malfunctions during testing.

Flow entered and exited through the apex: during inflow, the mitral valve closed, and the aortic valve opened; during outflow, the mitral valve opened, and the aortic valve closed, simulating diastolic and systolic valve configurations (Fig. 4.1A). Two static pressure probes were placed in the ventricle and atrium to allow catheter-based pressure measurements.

The rigid phantom was 3D-printed in Grey Pro Resin (Formlabs Inc., Somerville, USA) using a stereolithography 3D printing technique with a detachable atrium to allow silicone mitral valve replacement (Fig. 4.1C). The valves were cast in clear silicone (Agilus30, Stratasys Ltd.) with stiffness levels Shore A25, A40, and A60 (Dreve Biopor AB, Damvig A/S, Copenhagen, Denmark).

A) The motor and pump setup as assembled in the MRI-scanner

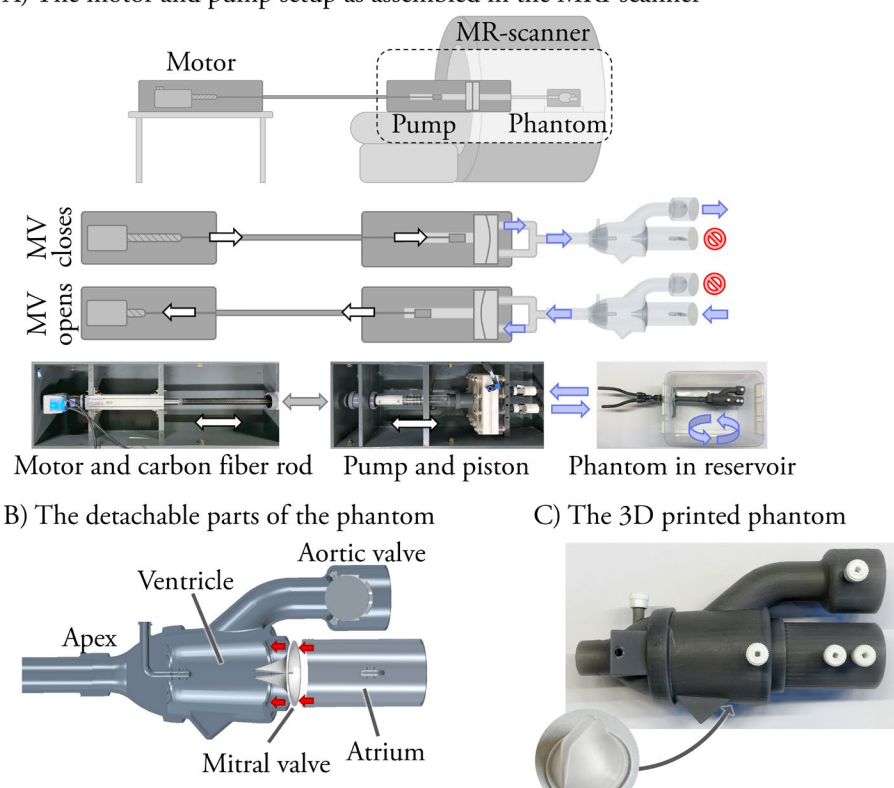


**Figure 4.1. Overview of the phantom setup in Study I.** A) The computer-controlled motor connects to a piston via a carbon fiber rod (grey arrow). The piston moves water in and out of the pump (white/black arrows), which governs the water in- and outflow in the phantom (blue arrows). The figure details the setup configurations for a closed and open mitral valve (MV). B) The phantom atrium can be detached from the ventricle so that the mitral valve can be changed. C) The final 3D-printed phantom used for *in vitro* experiments. The figure was reproduced and adapted from <sup>226</sup> according to the Creative Commons CC BY license.

### Measurements and analysis

Six different *in vitro* tests were investigated, where three different cardiac outputs were combined with three mitral valves of different stiffness, to imitate different physiological scenarios.

Catheters for pressure measurements were connected to the phantom pressure probes located in the ventricle and atrium. During 17 consecutive cycles, the pressure in the atrium and ventricle was simultaneously tracked and averaged to reduce noise and cycle-to-cycle variations.

With 2D and 4D MRI, the mass flow and bulk velocity were measured at the apex, aortic valve, and atrium on a 1.5 T MR clinical scanner (MAGNETOM Sola, Siemens Healthcare, Erlangen, Germany). The velocity profile in the ventricle was quantified, and the flow distribution was visualized with streamlines using the 4D MRI data. Based on cine MRI, the mitral valve opening was measured at peak flow.

Commercially available ultrasound systems EPIQ CVx (Philips Medical Systems, Andover, MA, USA) and Vivid E95 (GE Healthcare; Vingmed Ultrasound, Horten, Norway) were used for both 2D and 3D imaging. The mean and maximum velocity through the valve were quantified with continuous wave Doppler, and the corresponding mean and maximum pressure difference (referred to as the pressure gradient in the clinical setting) was manually calculated with the Bernoulli equation. The valve opening was measured on 2D 3-chamber-view and 3D images.

## 4.1.2 Validation of the FSI model (Study II)

Study II aimed to validate FSI simulations of a simplified left heart model, including the mitral valve under diastolic, physiologically inspired conditions, against *in vitro* experimental data obtained from Study I. The phantom geometry from the *in vitro* experiments was employed in the simulations. The mass flow measured by MRI at the apex of the phantom was used as boundary conditions to numerically imitate the investigated *in vitro* cases. The FSI model was evaluated based on the transmitral velocity, ventricular and atrial pressure, and the valve opening, and the error margin was compared to clinically acceptable standards.

The opening phase of the valve was the primary focus of this study. Therefore, the time frames corresponding to the open valve configuration in the *in vitro* data were chosen for simulation and validation.

#### The simulation model

During the simulations, the diastolic valve configuration was simulated (Fig. 4.2A), with the aortic valve boundary closed and the mitral valve boundary modeled as a free flow outlet, allowing flow to pass through the mitral valve. The overall flow in the domain was governed by mass flow boundary conditions applied at the apex of the phantom (Fig. 4.2B), which were obtained from MRI measurements from the *in vitro* tests. This ensured that the same flow conditions were obtained in the simulations as observed in the phantom experiments.

The water in the phantom was modeled as Newtonian, with a turbulence model, the elliptic blending k- $\epsilon$   $^{180,181}$ , employed. The silicone mitral valve was modeled as isotropic, linear elastic with Young's modulus based on values obtained from inhouse material tests on the silicone material used for 3D printing.

The CFD domain employed two meshes: a static background mesh accounting for the entire lumen and a smaller, morphing overset mesh resolving the valve

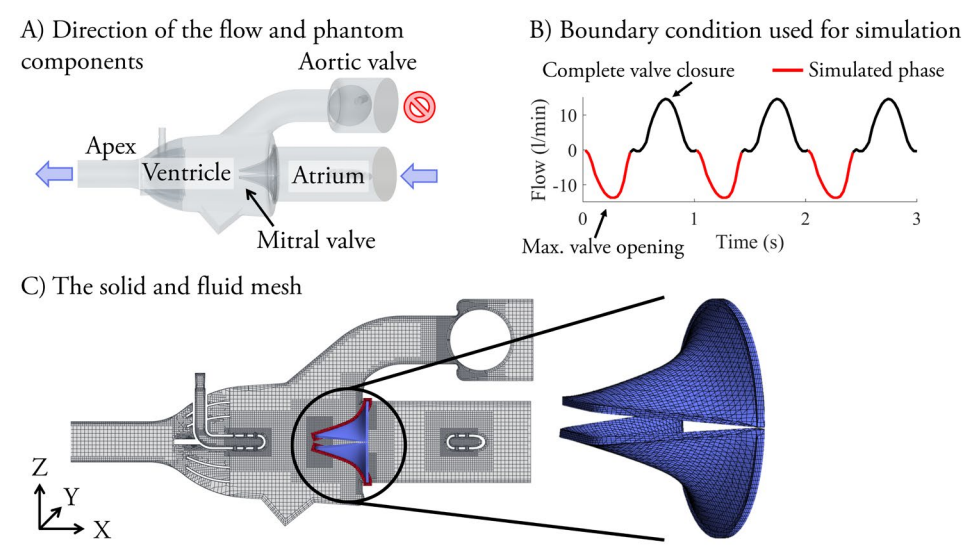


Figure 4.2: The FSI simulations of the phantom in Study II. Showing A) the flow direction employed to create the mitral valve's opening and the phantom components. B) The typical appearance of a volume flow measurement used at the inlet of the flow domain measured by MRI. The peak opening of the mitral valve was selected for simulation (red). C) The CFD mesh visualized in a cross-sectional plane through the domain, showing the background mesh (grey), the overset mesh (red) and the valve (blue). The image was reproduced and adapted from <sup>227</sup> according to the Creative Commons CC BY license.

deformations, according to the Chimera method <sup>182</sup>. This approach allowed for large structural deformation without requiring remeshing. Both fluid meshes were created with finite volume hexahedral cells, was based on a mesh independence study (Fig. 4.2C). The valve leaflets were meshed with finite solid first-order tetrahedral elements, with three element layers across the valve thickness, based on an FE-mesh independence study.

In the CFD solver, the convection terms and time were discretized to the first order, and the diffusive terms were discretized to the second order. An Arbitrary Lagrangian-Eulerian <sup>124</sup> approach was employed for solving the deformation of the overset mesh, and a B-spline mesh morpher was used to model smaller local deformations of the fluid mesh based on the deformations obtained from the structural solver.

The structural solver employed the Newton method, and the time step for the transient, implicit FSI simulation was set to 0.0015 s. This study used the commercial CFD and FEM software STAR-CCM+ (2021.1.1 build 16.02.009, Siemens Digital Industries Software, Plano, TX, USA) and Abaqus/Standard (v. 2017, Dassault Systèmes Simulia Corp., Johnston, RI, USA) to achieve FSI.

#### Model evaluation

For all five cases, the pressure difference across the valve, the velocity through the valve, and the valve opening were simulated and compared to the *in vitro* data. The velocity profile and streamlines derived from 4D MRI data qualitatively assessed the flow.

## 4.2 Patient-specific modeling

With the validated computational model from Study II as a foundation, the next step involved patient-specific modeling. The pipeline was adapted for patient-specific valve geometries, healthy as well as diseased, and flow conditions obtained from echocardiograms. To evaluate the performance of the model, comparisons to *in vivo* echocardiographic data were made.

## 4.2.1 Validation in healthy volunteers (Study III)

The aim of Study III was to propose a framework using standard clinical assessment data from 2D and 3D echocardiography to provide patient-specific mitral valve models using a semi-automated segmentation process simulated with FSI. The

framework was validated against *in vivo* echocardiographic data from ten healthy volunteers, and the echocardiographic data were compared with MRI data to evaluate the impact of the choice of modality on the simulation outcome (Fig. 4.3).

### Study population and patient-specific modeling

Ten healthy volunteers (median age 13 years, age range 1 to 37 years, 5 females) were included in the study. According to the Helsinki Declaration, they all gave written informed consent signed by themselves or a parent. All volunteers underwent an echocardiographic examination, and five also underwent an additional MRI scan. The echocardiographic examination included a 4-chamber view with and without color Doppler, 3D images of the mitral valve and the left ventricle, and transvalvular velocity measurements with continuous wave Doppler with an EPIQ CVx (Philips Medical Systems, Andover, MA, USA) ultrasound system with an X5-1 transducer. The cardiac MRI was performed on a 1.5 T clinical scanner (MAGNETOM Aera, Siemens Healthineers, Erlangen, Germany), including short- and long-axis cine sequences and a 4D flow research sequence covering the entire heart.

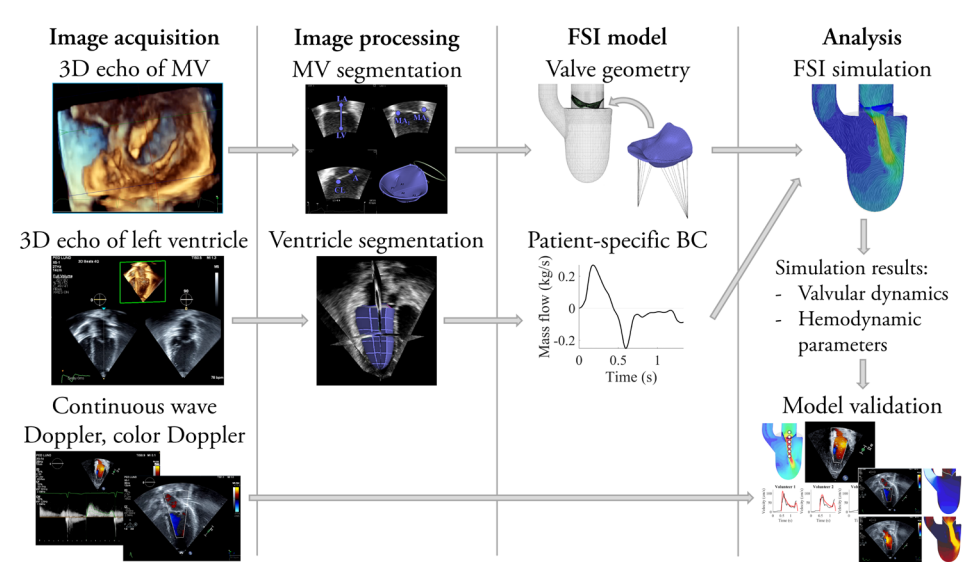


Figure 4.3: The pipeline for patient-specific healthy mitral valve simulations in Study III. From echocardiograms, patient-specific valve geometries and flow conditions were obtained, and thus, patient-specific simulation models. The simulation results were validated and compared against Doppler data. MV = mitral valve, echo = echocardiogram, FSI = fluid-structure interaction, BC = boundary conditions. The figure was reproduced from <sup>75</sup> according to the Creative Commons

The patient-specific mitral valve geometry was obtained via a semi-automated segmentation process from 3D images of the mitral valve (4D MV-assessment 2, TOMTEC Imaging Systems GmbH, Unterschleissheim, Germany). The patient-specific hemodynamics were modeled by deriving patient-specific mass flow boundary conditions from left ventricular volume measurements performed on 3D echocardiograms and MRI data. To construct the full mitral valve apparatus, 23 chordae tendineae were attached to the valve leaflets, originating from the two papillary muscle heads. The entire valve apparatus was then inserted into our simplified left heart model, including the left ventricle, left atrium, and the left ventricular outflow tract 75.

#### The simulation model

Building on the experimentally validated pipeline from Study II, developments required for the patient-specific mitral valves was performed. The mitral valve leaflet tissue was now modeled as a hyperelastic material with parameters based on curve fitting to biaxial experimental data of human mitral valves from the literature <sup>183</sup>. The contact between the leaflets was modeled with a penalty-based algorithm with a zero-penetration constraint.

The mitral valve apparatus was rigidly fastened along its circumferential edge onto the atrial wall of the domain, and the walls of the fluid domain were fixed in space. To model the contraction of the heart, the patient-specific mass flow boundary condition was applied at the apex of the ventricle. The boundary at the aortic valve was modeled as a zero-pressure outlet during systole and a wall during diastole, and the upstream boundary of the mitral valve was modeled as a zero-pressure outlet throughout the cardiac cycle.

The mitral valve leaflets were modeled using first-order hexahedral elements and the fluid domain was meshed using hexahedral volume elements, based on stand-alone mesh sensitivity analyses.

FSI was achieved with the commercial software Star-CCM+ (2022.1 build 17.02.007-R8, Siemens Digital Industries Software, Plano, TX, USA) and Abaqus/CAE (v. 2020, Dassault Systèmes Simulia Corp., Johnston, RI, USA). The convective terms in the fluid solver were now discretized with a second-order upwind scheme and a first-order temporal discretization.

#### Model evaluation

To validate and evaluate the FSI model, the hemodynamic velocity field was compared to color Doppler images, and the transvalvular velocity was compared to continuous wave Doppler measurements.

Cardiac MRI is the clinical standard for volume measurements; thus, the left ventricular measurements performed on 3D echocardiograms were compared against the respective measurements conducted on MRI data to evaluate the impact of modality choice.

## 4.2.2 Modeling mitral regurgitation (Study IV)

Study IV aimed to apply our patient-specific computational framework to pediatric mitral valve regurgitation in both the pre- and post-operative conditions, using standard echocardiographic data. The framework was evaluated against echocardiographic data from seven patients, before and after surgery, based on clinical parameters used for assessing and grading mitral valve disease (Fig. 4.4).

### Study population and patient-specific modeling

Pediatric patients with severe mitral regurgitation (N = 7) were recruited from the Hospital for Sick Children in Toronto, aged 2–17 years (median age: 6 years), of

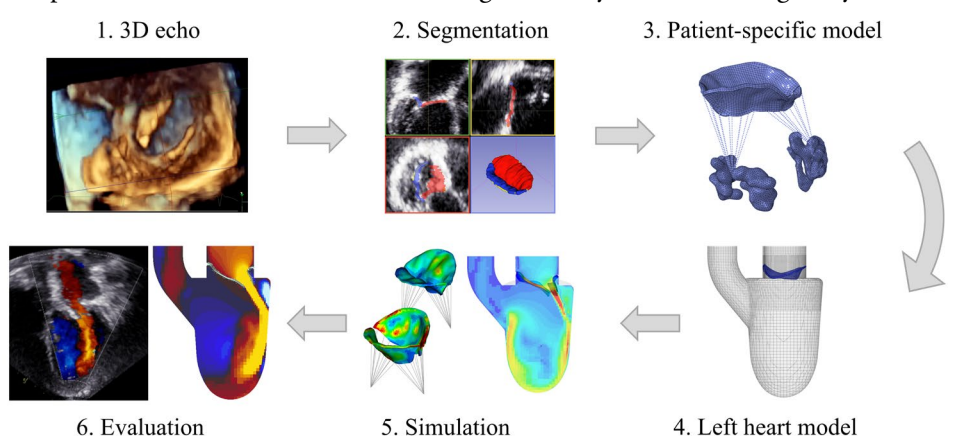


Figure 4.4: The pipeline for patient-specific mitral regurgitation simulations in Study IV. Patient-specific valve geometries and papillary muscle positions were manually segmented pre-and post-operatively from 3D echocardiography (echo) images. The valve apparatus was placed inside a left heart model, simulated using fluid-structure interaction (FSI), and evaluated against pre- and pots-operative echocardiography data.

whom 57% were female (Table 4.1). The study was approved by SickKids Research Ethics Board (REB: 81838) and the Swedish Ethical Review Board (2021-05978-02) and complies with the Helsinki Declaration.

Data were obtained from routine pre- and post-operative echocardiography using a Vivid E95 system (GE Healthcare, Vingmed Ultrasound, Horten, Norway). For model input, 3D echocardiography images of the mitral valve and 3D full-volume datasets of the left ventricle were acquired, alongside Doppler spectral curves of transvalvular flow for model evaluation. For verifying the valve dimensions and chordal structures, the 2-chamber, 4-chamber, and parasternal views were used.

**Table 4.1: Patient demographics.** An overview of the regurgitation grade pre- and post-operatively for all included patients, and a short description of their diagnosis.

Patient	Sex	Age (years)	Regurg. pre-op	Diagnosis	Regurg. post-op
1	М	11	Severe	Severe mitral regurgitation with pseudo cleft at PML	Mild
2	F	12	Severe	Severe mitral regurgitation due to rheumatic fever	Trivial
3	М	7	Moderate	Severe mitral regurgitation due to rheumatic fever	Mild
4	М	5	Moderate	Severe mitral regurgitation due to dysplastic MV with AML prolapse	Trivial
5	F	2	Moderate	Severe mitral regurgitation with AML prolapse	Trivial
6	F	2	Severe	Severe mitral regurgitation due to dilated cardio-myopathy	Moderate
7	F	17	Severe	Severe mitral regurgitation due to cleft in AML	Trivial

Patient-specific mitral valve geometries (as well as the position of the papillary muscles) were manually segmented (3D Slicer <sup>184</sup>), in their pre- and post-operative configurations. The dimensions of the final segmentations were cross-checked against 2D echocardiography measurements. Flow boundary conditions were

derived from left ventricular volume measurements (as in Study III), with endsystolic and end-diastolic volumes confirmed by the Simpson's method.

#### The simulation model

The simulation framework developed and validated in Study III was employed to evaluate pediatric regurgitant mitral valves. Now, pre- and post-operative flow conditions were applied separately based on echocardiographic data to model the difference in flow after surgery.

The simulations were implemented in Star-CCM+ (2022.1 build 17.02.007-R8, Siemens Digital Industries Software, Plano, TX, USA) and Abaqus/CAE (v. 2020, Dassault Systèmes Simulia Corp., Johnston, RI, USA) and run as transient cases with a 0.4 ms timestep.

#### Model evaluation

For the overall valvular function, the simulation model was compared against echocardiographic color Doppler images, where the valvular dynamics and the overall hemodynamics field were qualitatively compared.

The systolic valve function was evaluated based on the grade of (residual) regurgitation and the size of the coaptation defect, before and after surgery. The grading and location of regurgitation were visually assessed in both simulation results and echocardiography and binarily compared.

The diastolic valve function was evaluated based on the mean pressure gradient. The simulated mean gradient was compared against continuous wave Doppler measurements pre- and post-operatively and reported in terms of mean difference ± standard deviation and further assessed using a Bland-Altman analysis.

## 4.2.3 Valve strain and chordal forces (Study V)

The aim of Study V was to compare valve strain and chordal forces in healthy and regurgitant pediatric mitral valves using the previously developed patient-specific FSI model. The objective was to explore novel diagnostic parameters, which are not accessible through conventional imaging, that may capture pathological changes and provide deeper insights into valve dynamics and hemodynamics in both healthy and diseased configurations.

We used the echocardiographic data from the healthy cohort in Study III and the patient cohort in Study IV. However, for the healthy cohort, only participants

younger than 18 years were included in this study. The valve strain in healthy valves from Study III was compared with newly derived strain values from the regurgitant valves, which had not been previously analyzed. The chordal forces were assessed for both groups for the first time in Study V.

#### Model evaluation

The valve strain was assessed qualitatively by comparing maximum principal strain maps across the three configurations: healthy, pathological (pre-operative), and repaired (post-operative). For quantitative analysis, mean strain values compared for the entire valve, the atrial and ventricular surfaces, at both peak systolic and diastolic configurations between the groups. Full-width half-maximum (FWHM) analysis of the strain maps was performed to quantify strain variations.

The chordal forces were evaluated as the sum of the reaction forces from all individual chordae across the three groups. Comparisons were carried out both at the group level and for individual cases, considering the force over the full cardiac cycle as well as peak systolic and diastolic values.

Statistical analysis was conducted to test for differences in valve strain and chordal forces between groups. The non-parametric Kolmogorov-Smirnov test <sup>185</sup> was applied for unpaired comparisons (healthy vs. regurgitant valves), while the Wilcoxon signed-rank test <sup>186</sup> was used for paired comparisons (pre-operative vs. post-operative valves). These were selected as they are appropriate for small sample sizes and non-normally distributed data.

# 5 Results

This chapter presents the principal findings from the research conducted in this thesis. The results are organized into two main parts: "The simplified heart model", summarizing the outcomes of Studies I–II, and "Patient-specific modeling", which details the results and key insights obtained in Studies III–V.

## 5.1 The simplified left heart model

## 5.1.1 *In vitro* phantom experiments (Study I)

In Study I, an *in vitro* setup was designed for creating benchmarking data for validation purposes of heart valve FSI models. A phantom, mimicking the left heart, was 3D printed, where clinically relevant flow parameters and the mitral valve opening were tracked using pressure probes, MRI, and echocardiography.

Technical validation of the experimental setup was conducted to ensure reliable measurements. At the start and end of each MRI examination, 2D MRI measurements were taken at the aortic valve and atrium of the phantom, showing differences of 0.45 ± 0.35 l/min (3.5%) at the aortic valve and 0.86 ± 0.67 l/min (6.7%) at the atrium. Pressure measurements in the ventricle, recorded over 17 consecutive pump cycles, demonstrated a cycle-to-cycle variation of 0.5%. These low cycle-to-cycle variations demonstrate that the setup was reliable over time, with a steady pulsatile flow. The variation for the MRI measurements was higher than that obtained from the pressure measurements because they were taken approximately 30–45 minutes apart, compared to the pressure measurements that were conducted over 20 seconds.

The pressure measurements revealed higher ventricular pressure during systole than during diastole (Fig. 5.1) and a nearly zero relative pressure in the atrium throughout the pumping cycle.

MRI velocity measurements showed that the transmitral velocity increased with higher cardiac output and higher stiffness of the valve. Velocities measured by 4D flow MRI were underestimated compared to the corresponding 2D MRI measurements. Streamlines obtained from 4D flow MRI showed the velocity jet through the open mitral valve during diastole, and how the water exited through the aortic valve during systole (Fig. 5.1). Measurements of the valve opening showed a larger opening for higher cardiac output, and decreased valve stiffness.

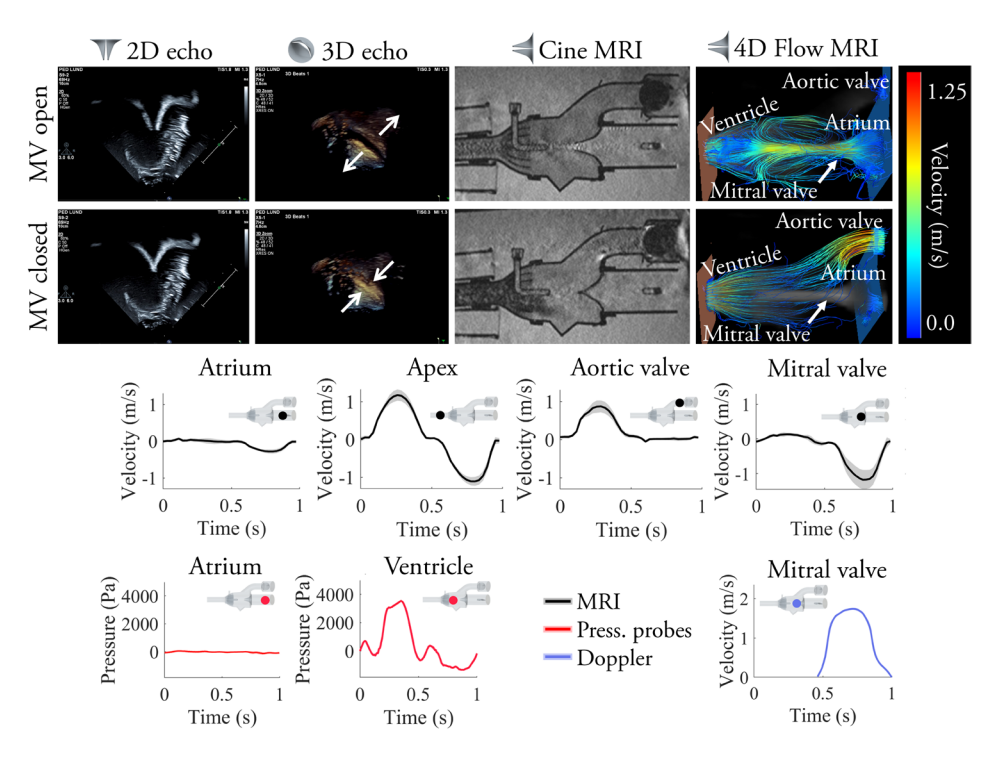


Figure 5.1: The main results from Study I. The top rows showed the phantom imaged with echocardiography (echo) and MRI for the open and closed mitral valve (MV) configurations. The graphs depict quantitative measurements of the water velocity using MRI (black) and Doppler (blue), and the pressure (red) in the domain. The small sketch of the phantom in each graph details where in the phantom the measurements were conducted. Results from all investigated flow cases can be seen in Paper I <sup>226</sup>. The figure was reproduced and adapted from <sup>226</sup> according to the Creative Commons CC BY license.

Doppler measurements of the transmitral velocity confirmed the findings of the MRI measurements; higher transmitral flow was obtained for higher cardiac output and increased valve stiffness. From the Doppler velocity measurements, the corresponding pressure difference across the valve was determined using the simplified Bernoulli equation, using the density of water. These were higher than the corresponding measurements from the pressure probes. The valve opening measurements were conducted on 2D and 3D echocardiograms showing an increased valve opening for increased cardiac output.

## 5.1.2 Validation of the FSI model (Study II)

In Study II, the FSI model of a simplified left heart was developed and validated against the *in vitro* data from Study I during diastolic physiological-inspired conditions, to quantify the simulation error for clinically relevant parameters and relate those to clinically acceptable standards.

Visual assessment, comparing the streamlines obtained from the simulations to the 4D flow MRI data, showed a high level of agreement. The simulations capture the recirculation zone in the ventricle downstream of the narrowest part of the mitral valve, where the flow was accelerated (Fig. 5.2).

The simulated pressure difference across the valve correlated well with the measurements by the catheter pressure probes. Simulations showed an underestimation of the maximum and mean pressure by  $78 \pm 37$  Pa (6.8 %) and  $80 \pm 59$  Pa (14 %) (Fig. 5.2). These errors (corresponding to approximately 0.6 mmHg) are much smaller compared to the limits set to grade mitral valve disease.

The valve opening was underestimated by the model compared to measurements performed on MRI and 2D echocardiograms by  $0.41 \pm 0.27$  mm (7.3 %) and  $0.41 \pm 0.50$  mm (6.7 %), respectively. The opening area deviated by  $0.33 \pm 0.015$  cm<sup>2</sup> (5.4 %) compared to measurements from 3D echocardiography.

The simulated transmitral velocity correlated well with continuous wave Doppler measurements, although it underestimated the mean velocity by  $0.07 \pm 0.04$  m/s (7.9 %) and the maximum velocity by  $0.14 \pm 0.07$  m/s (8.4 %). This underestimation aligns well with the observed underestimation of the pressure difference across the valve.

In the clinical environment, error margins within a range of up to 10 % to 15% are widely considered acceptable <sup>187</sup>. The error margins identified in this highly controlled validation amounted to 5.4–14 % for the investigated parameters, which

all fall within this range. This implies that the simulation model in its current state can predict clinically relevant parameters in a simplified left heart model, good enough for further development.

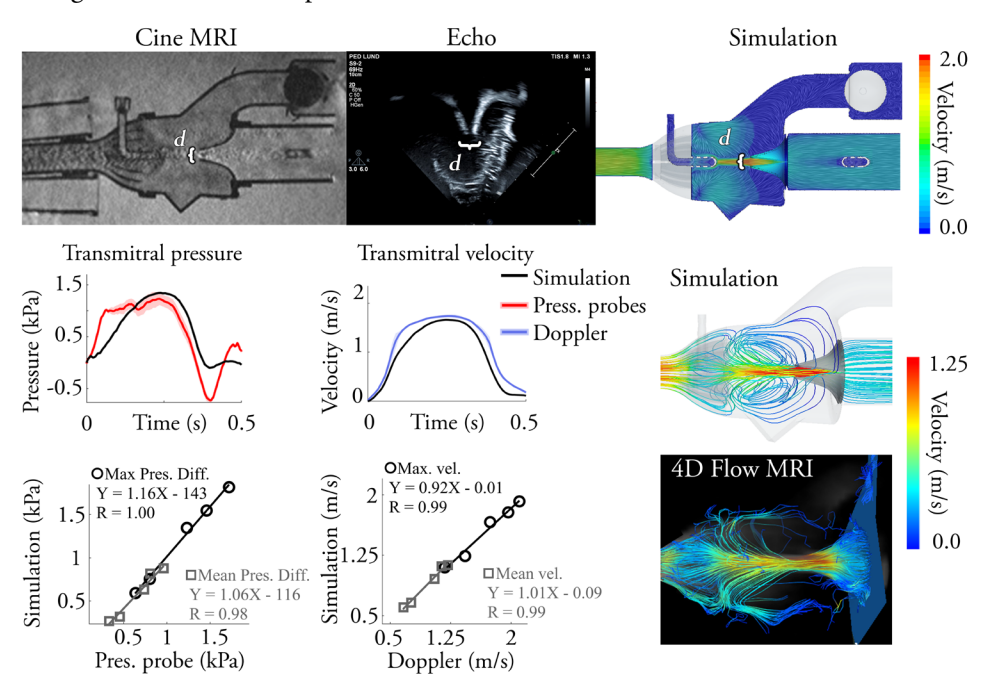


Figure 5.2: The main results from Study II. The top row shows the measurements of the valve opening (d) across modalities. Comparisons between simulation and *in vitro* measurements are shown during the opening phase of the pump cycle, with correlation plots showing the agreement between the simulation and *in vitro* measurements for the mean and maximum pressure and velocity. A qualitative analysis of the streamlines was conducted by comparing simulation results and 4D Flow MRI data. Results for all flow cases can be found in Paper II <sup>227</sup>. The image was reproduced and adapted from <sup>227</sup> according to the Creative Commons CC BY license.

## 5.2 Patient-specific modeling

## 5.2.1 Validation in healthy volunteers (Study III)

In Study III, an FSI model for patient-specific mitral valve simulations was developed based on standard echocardiographic assessment data and validated in ten healthy volunteers based on clinically relevant parameters.

The implemented framework required approximately 2 hours of preparation work per volunteer, including segmentation, meshing, and model setup. All simulations were run in parallel on 40 cores, on an AMD 7413 node, on a high-performance cluster, requiring a computational time of 15–86 h (median 40 h) per volunteer.

Compared to 4-chamber view color Doppler images, the FSI simulation predicted realistic global hemodynamic patterns and flow directionality (Fig. 5.3A). This was confirmed by the quantitative comparison of the transmitral velocity, showing an average difference in the max velocity of 4.52 cm/s (3.6  $\pm$  29%) and the mean velocity over the cardiac cycle by 4.58 cm/s (8.3  $\pm$  22%) compared to Doppler measurements (Fig. 5.3B). This error margin falls within clinically acceptable ranges of up to 10 to 15%  $^{187}$ .

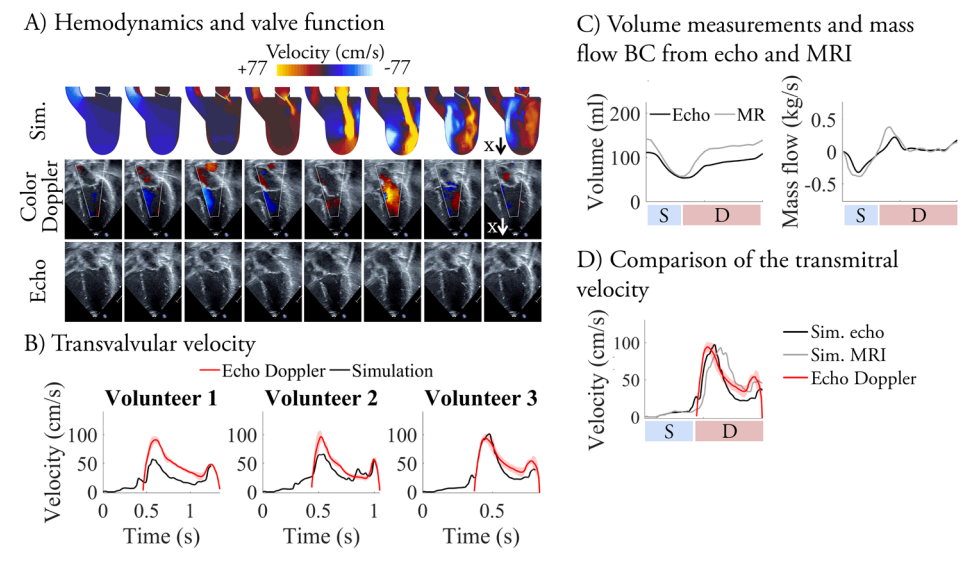


Figure 5.3: The main results from Study III. Showing A) the blood velocity distribution comparing simulation results to echocardiograms with and without color Doppler for Volunteer nr 4, B) the corresponding transvalvular velocity measurements from simulation and echocardiographic measurements for three of the volunteers. C) Left ventricular volumes measured on echocardiograms and MRI were compared, as well as the corresponding mass flow boundary conditions. D) The resulting transvalvular flow based on the different boundary conditions compared to Doppler measurements. Results for all volunteers are found in Paper III <sup>75</sup>. The figure was reproduced and adapted from <sup>75</sup> according to the Creative Commons CC-BY license.

Left ventricular volume measurements based on echocardiography and MRI were compared. The analysis showed that echocardiography underestimated the end-diastolic volume by  $19 \pm 3.8\%$  and the end-systolic volume by  $1.8 \pm 20\%$  compared to MRI (Fig. 5.3C). The mass flow derived from these volume measurements correlated with a  $31 \pm 16\%$  difference in maximum mass flow and a  $30 \pm 10\%$  difference in mean mass flow (Fig. 5.3C), reflecting the higher relative difference in end-diastolic compared to end-systolic volumes.

To quantify how the choice of modality affects simulation outcome, the transvalvular velocity from simulations based on echocardiography-derived mass flow and MRI-derived mass flow were compared (Fig. 5.3D). MRI-based simulations yielded a 24 ± 7% higher mean and 21 ± 14% higher maximum transvalvular velocities than echocardiography-based simulations, due to the higher mass flow from MRI data.

## 5.2.2 Modeling mitral regurgitation (Study IV)

In Study IV, our previously developed and validated framework was further developed to simulate patient-specific mitral valve regurgitation in children, both in its pathologic condition before surgery as well as after surgery. The model was evaluated against the corresponding echocardiographic data from seven patients based on clinical parameters used to grade mitral valve disease.

The model successfully reproduced key valvular dynamics and hemodynamics in both pre- and post-operative conditions (Fig. 5.4A). During systole, it consistently captured the regurgitant jet directed into the left atrium, as well as the angle of the jet, across all seven patients. In diastole, the valve opened appropriately, producing an inflow jet during ventricular filling that closely matched Doppler flow patterns. Two different ventricular flow patterns were observed: where the inflow jet caused the ventricular flow to rotate clockwise in the ventricle (in three patients), and where the inflow jet remained straight, dissipating into the ventricle (in four patients). Both ventricular flow behaviors were accurately reproduced by the model. Post-operatively, the residual regurgitant jet was captured in three of the four patients with residual regurgitation, while in the three others, the absence of regurgitation was reproduced correctly.

The simulated regurgitation grade matched the echocardiographic assessment in six of seven patients pre-operatively. Post-operatively, four of the seven mitral regurgitation grades were reproduced accurately, while in three patients the model predicted mild regurgitation compared with trivial regurgitation on

echocardiography. The location of the simulated coaptation defect agreed with echocardiographic findings in six of seven patients, both pre- and post-operatively (Fig. 5.4B).

The transvalvular velocity was compared with continuous-wave Doppler measurements to assess pressure gradients. The mean difference between simulated and Doppler-derived mean transmitral gradients was  $0.38 \pm 1.57$  mmHg preoperatively and  $-0.42 \pm 3.26$  mmHg post-operatively (Fig. 5.4C).

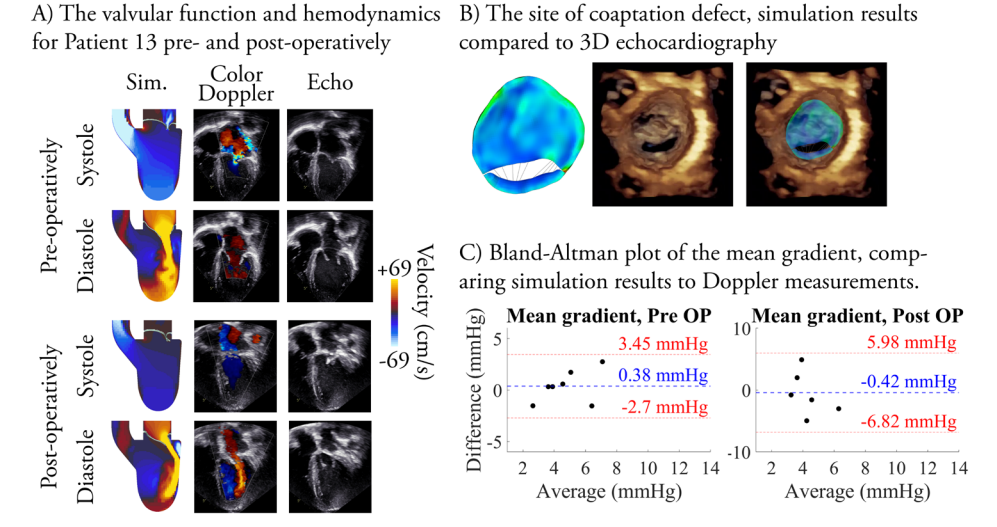


Figure 5.4: The main results from Study IV. A) The hemodynamics field pre- and post-operatively comparing simulation results to echocardiography with and without color Doppler. B) The site of regurgitation visualized at peak systole for the simulation results and the corresponding 3D echocardiography. C) the Bland-Altman analysis of the mean gradient, pre- and post-operatively. Here, the difference between the Doppler measurements and the simulated data is plotted against the average of all data points for the mean gradient. The limits indicate the mean value (blue, dotted line) and the 95% limits of agreement (red, dotted lines).

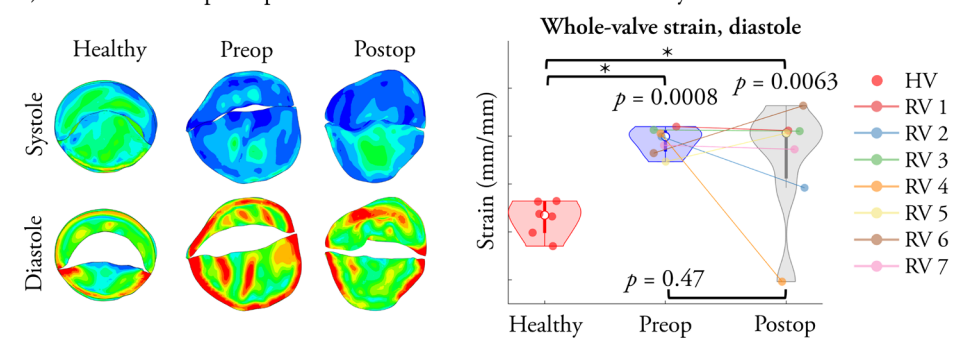
## 5.2.3 Valve strain and chordal forces (Study V)

In Study V, building on the healthy and patient cohorts from our previous studies, valve strain and chordal forces were evaluated and compared to investigate their potential as indicators of pathological changes in the mitral valve.

For the healthy valves, average strains were  $4.99 \pm 2.74\%$  in systole and  $6.56 \pm 0.68\%$  in diastole, with strain concentrations along the circumferential edges (where the valve was rigidly attached to the arterial wall) and at the commissures (Fig. 5.5A). A consistent difference in strain was observed between the atrial and ventricular surfaces of the valves.

In the pre-operative valves, average strain was reduced during systole (1.90  $\pm$  1.51%) but elevated during diastole (9.80  $\pm$  0.50%). The post-operative valves exhibited similar values (1.87  $\pm$  1.31% in systole, 9.01  $\pm$  2.29% in diastole). Strain concentrations appeared across the center of the anterior leaflet and along the circumferential edges (due to the boundary conditions). Both diseased conditions showed different strain patterns between the atrial and ventricular sides.

#### A) The maximum principal strain distribution and statistical analysis



#### B) Chordal forces over time for all three groups

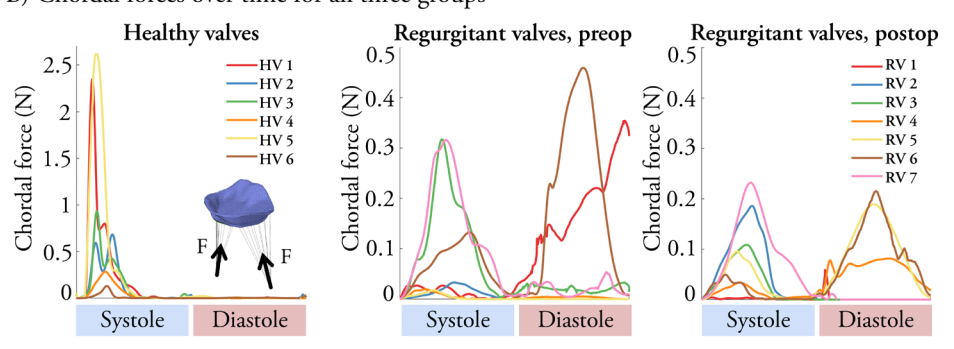


**Figure 5.5:** The main results from Study V. A) The maximum principal strain in the systolic and diastolic configurations in the three groups, accompanied by the statistical test performed on the average diastolic strain value of the entire valve. B) The chordal forces over time for the healthy, pre-operative and post-operative mitral valves. HV = healthy valve, RV = regurgitant valve.

Statistical analysis confirmed significant diastolic strain differences between healthy and diseased valves (pre- and post-operative; p < 0.05) (Fig. 5.5 A). FWHM analysis revealed significant systolic differences between healthy and post-operative valves, and diastolic differences between healthy and diseased valves. No significant differences were found between the pre- and post-operative conditions.

For the chordal forces, healthy valves displayed high systolic and negligible diastolic forces (Fig. 5.5B). In contrast, several regurgitant valves deviated from this pattern, with lower systolic forces and measurable diastolic forces. When comparing the preand post-operative conditions, systolic chordal forces decreased after surgery in nearly all patients. During diastole, most pathological valves exhibited low forces that further decreased post-operatively, except in two patients. Statistically, systolic chordal forces differed significantly between healthy and diseased valves (p < 0.05).

# 6 Discussion

This thesis has provided new insights into mitral valve function and left heart hemodynamics and illustrated how these complex interactions can be quantitatively captured using FSI modeling. This chapter synthesizes the main findings and reflects on the key challenges, limitations, and open questions that have emerged from the studies included in this thesis.

The discussion is structured in three main parts: "Developing the patient-specific model," (Section 6.1) which examines the construction of patient-specific valve geometries, left heart models, and hemodynamic boundary conditions; "Model validation," (Section 6.2) which evaluates how effectively the simulations reproduce mitral valve function and hemodynamics; and "Novel parameters with diagnostic potential" (Section 6.3), where the valve strain and chordal forces are discussed. The chapter is concluded by Section 6.4 with a reflection on future directions for advancing the presented research and translating it into clinical practice.

## 6.1 Developing the patient-specific model

## 6.1.1 Patient-specific valve geometries

## Segmentation

Previous FSI simulations of the mitral valve have used MRI data for valve segmentation <sup>47</sup>, however, this poses significant challenges in properly resolving the mitral valve leaflets. Others have instead relied on invasive transesophageal echocardiography to segment and construct their patient-specific models <sup>73</sup>. In this work, the resolution of our transthoracic echocardiography data proved sufficient for

proper valve segmentation, based on inter- and intraobserver variability analyses, circumventing the need for invasive echocardiographic imaging. Although manual segmentation is time-consuming, it remains the gold standard for accuracy and has been utilized in previous mitral valve reconstructions <sup>47,64</sup>. It also provides greater control over the delineation of complex anatomical structures, ensuring accurate representation of the mitral apparatus.

In Study III, the healthy mitral valve geometries were reconstructed using a semiautomated segmentation method and validated against 2D echocardiographic measurements, demonstrating good agreement and were consistent with anatomical dimensions reported in larger healthy cohorts <sup>188</sup>. In Study IV, the regurgitant valves were manually segmented, as it provided higher control over anatomical details, enabling precise delineation of pathological features.

Echocardiography served as the imaging modality for segmenting mitral valves in our research, as it remains the gold standard in heart valve assessment <sup>35,38</sup> and for its clinical accessibility and high temporal resolution.

### Material modeling of mitral valve tissue

Modeling the material behavior of the mitral valve remains a major challenge, as no consensus exists in literature regarding the most appropriate constitutive model. The limited experimental data available on human tissue shows substantial variability in mechanical responses 93,94, making it difficult to determine accurate material parameters. In this thesis, the mitral valve tissue was modeled as isotropic and hyperelastic, which is a reasonable assumption given current evidence 145,189. Previous studies have demonstrated that anisotropy has only a minor influence on large-scale deformations and valve function 145,189, supporting this simplification. While pediatric tissue is expected to be more compliant than adult tissue 183, no experimental data on pediatric mitral valves have been published to date. Consequently, the same material model was applied for the children and adult volunteers in Study III. Notably, no consistent error bias was observed between healthy pediatric and adult simulations, supporting this approach at the current stage of development. In Studies IV-V, the same material model was further used for diseased pediatric valves, although the effects of regurgitation on tissue mechanics remain unknown. This uncertainty represents one of the key challenges for the field: valve opening dynamics, leaflet strains, and stresses cannot be reliably quantified without a clearer understanding of pathological tissue behavior. However, acquiring sufficient pediatric diseased tissue for mechanical testing is inherently difficult, given the rarity of available samples, their small size, and the challenges associated with handling them <sup>183</sup>.

#### 6.1.2 The left heart model

Designing the human heart for FSI simulations is challenging, as simplifications must balance numerical feasibility with clinical relevance. Previous studies have ranged from simplified mitral valve geometries embedded within tubular domains <sup>52,147</sup> to more detailed models combining patient-specific ventricular geometries with idealized valves <sup>148,149</sup>. While these approaches provided insight into valve dynamics, stress distributions, and flow patterns, they lacked in vivo validation. Advanced efforts, such as those by Mao et al. 70 and Gao et al. 47, incorporated patient-specific geometries of ventricle and mitral valve, simulating hemodynamics under ventricular contraction. However, Mao et al. 70 still underpredicted peak transvalvular flow by 36%, illustrating that greater structural complexity does not necessarily improve accuracy. Similarly, the whole-heart model presented by Feng et al. 158 provides a powerful framework to study valve-ventricle interactions at the organ level, but the lack of patient-specific dimensions and in vivo validation limits its clinical applicability. These considerations support our strategy of modeling the left ventricle as a generic domain with fixed walls, while representing ventricular contraction with patient-specific mass flow boundary conditions, derived from left ventricular volume measurements over the cardiac cycle.

Despite inherent limitations in our model, such as neglecting annular and papillary muscle motion, our framework captures patient-specific velocity and pressure variations throughout the cardiac cycle, performing comparably to more complex models. This balance of accuracy and computational efficiency highlights its potential for clinical integration. While our approach showed strong agreement with healthy volunteer data <sup>75</sup>, its assumptions may be less appropriate in diseased valves, where chordal dynamics and valve-ventricle interactions play a larger role (as reflected in our simulated transvalvular velocities in Studies III and IV). Although it has been shown that the annular movement does not affect leaflet stress and chordal forces <sup>190</sup>, a physiologically contracting ventricle might make the model visually more accessible to the clinical staff. Sensitivity analyses that include papillary muscle and annular motion could help clarify their impact on valve function and hemodynamics. Ultimately, the key question is what value added complexity provides. Here, a simplified heart domain proved to be accurate enough, with errors under 15%, yet exploring contracting ventricles, moving annuli, and dynamic

papillary muscles could further define which effects must be resolved for clinically meaningful simulations and which can be approximated with simpler methods.

#### 6.1.3 Patient-specific hemodynamics

Previous studies have either applied normal pressure values obtained from the literature <sup>70</sup> or implemented a Windkessel model <sup>47,172</sup> to estimate the pressure at the domain boundaries. While these methods can approximate physiological conditions, they lack patient-specific information and require parameter estimation, thereby introducing additional unknowns and uncertainties into the model. To avoid this, patient-specific boundary conditions were defined in this thesis using patient-specific mass flow rates derived from left ventricular volume measurements obtained through echocardiography.

Since MRI remains the gold standard for volumetric assessments <sup>191</sup>, the echocardiography-derived boundary conditions were compared against MRI measurements to evaluate potential imaging-related differences in simulation outcome. The echocardiographic volumes correlated well with MRI data but showed a consistent overestimation of end-diastolic volumes, in agreement with previous findings <sup>187,192–194</sup>. Consequently, simulations based on echocardiography-derived volumes tended to underestimate the transvalvular velocities relative to MRI-based models. Nonetheless, echocardiography offers higher temporal resolution, which poses an advantage in pediatric patients with high resting heart rates (>100 bpm), as this provides higher temporal resolution in the boundary conditions.

#### 6.2 Model validation

Previous FSI studies of the mitral valve have commonly validated their models by comparing simulation results with earlier numerical work <sup>69,78,82,90</sup> or with clinical observations <sup>79,96</sup>. While such comparisons provide a basic consistency check, they remain limited, as accuracy is only judged relative to other models rather than to reality <sup>5</sup>. More recent work has incorporated patient imaging data from MRI <sup>95</sup>, CT <sup>69,70,153</sup> and echocardiography <sup>62,63,70</sup>, to compare flow vorticity, leaflet stress and strain, papillary muscle forces, and ventricular geometry. This represents an important step forward, particularly as hospitals already generate large amounts of imaging data that could support computational modeling. Yet, these validations were typically performed on single-patient cohorts, limiting generalizability.

In this thesis, we address this limitation by providing *in vivo* validation against cohorts of six to ten participants, covering healthy (Study III) and diseased (Study IV) mitral valves. Validation against patient data remains challenging, as measurements and image quality vary between observers, and the assessment of echocardiography or MRI data can be subjective. On the other hand, experimental validation poses further difficulties <sup>4</sup>, with only a few groups having developed dedicated setups <sup>5,195,196</sup>. As an example, geometric measurements in echocardiography are sensitive to the probe angle, as non-orthogonal imaging planes can distort dimensions. In contrast, 3D imaging enables offline manual adjustment of the measurement plane to improve accuracy <sup>197</sup>. Comparable geometric validations of FSI models against *in vitro* data reported 5–26% differences between simulated and experimental or imaging-based measurements <sup>70,198–200</sup>, whereas our model in Study II achieved relative simulation errors ≤7.5% for estimating the vale opening.

Other studies have compared simulations to *in vitro* tests using phantoms <sup>172,201–203</sup> or animal tissue <sup>153,204</sup>, though these primarily focused on mechanical parameters such as papillary muscle forces or local flow velocities. Critically, key clinical metrics such as the transvalvular velocity and pressure gradients have rarely been addressed. Many FSI studies on heart valve simulations either did not report transvalvular velocities <sup>95,126,160</sup> or lacked *in vivo* validation <sup>52,82,147,205</sup>. As velocity validation remains challenging <sup>206</sup>, comparisons have often been made only against previous simulations instead of experimental data <sup>207</sup>. This highlights the need for systematic validation against *in vivo* patient data across larger cohorts to ensure that FSI models are not only numerically consistent but also clinically reliable and relevant – a key objective of this work.

In Study III, the simulated velocities matched our Doppler measurements and healthy reference values  $^{208}$ , and reproduced the characteristic E and A waves corresponding to ventricular relaxation and atrial contraction. The deviations (0.6–6.4%) in Study III were lower than those reported in earlier studies (~10%) based on single-patient data  $^{70}$ . In Study IV, the regurgitant valves showed slightly larger deviations. However, the simulated transvalvular pressure gradient achieved a mean absolute error below 1 mmHg, well within clinical grading thresholds  $^{209-211}$ . This accuracy is noteworthy given that Doppler-derived and catheter-based gradients typically differ by 2.7  $\pm$  1.1 mmHg  $^{212}$ . Consequently, both the average error and variability of our simulations fall within the intrinsic uncertainty of the Doppler technique itself  $^{213}$ , confirming the robustness of our model observed already in Study II.

Most prior studies of diseased mitral valves focused solely on the pre-operative conditions <sup>63,81,96,118</sup> or excluded post-operative hemodynamics <sup>163,214</sup>. In contrast, Study IV reproduced the pre-operative regurgitation grade and captured the changes following valve repair. Post-operatively, minor discrepancies were observed between lower regurgitation grades (e.g., trivial vs. mild). However, these grades are both clinically considered as acceptable post-operative results. To the author's knowledge, this is one of the first studies to directly compare simulated and echocardiographic assessments of both regurgitation site and grade before and after surgery in a pediatric cohort.

Overall, our framework advances the field by validating healthy and regurgitant mitral valves across comparatively large pediatric cohorts, demonstrating clinical feasibility. Since many earlier FSI studies remain limited by insufficient validation, their clinical translation is still constrained. Rigorous validation, across larger cohorts and focusing on clinically relevant parameters routinely used by cardiologists and surgeons is therefore essential. Only through such systematic evaluation can computational models achieve generalizable and clinically meaningful predictive capability.

### 6.3 Novel parameters with diagnostic potential

#### The valve strain

The strain values obtained in the healthy valves in Study III were consistent with *in vivo* echocardiographic measurements (~8.5–10%) in healthy adult valves <sup>215,216</sup>. Although recent FE simulations reported higher strains (10–50%) under ventricular pressures of 100 mmHg <sup>217,218</sup>, the lower strains predicted by our model reflect the lower transvalvular load (~20 mmHg) that was applied.

Compared to the regurgitant cohort in Study IV, the difference in maximum principal strain was statistically significant, while no significant difference was found between the pre- and post-operative configurations. This suggests that surgical valve repair improves valve function but does not fully restore physiological strain. Previous studies have reported regurgitant systolic strains of ~19% <sup>96</sup>, which exceeds our values, likely due to differences in material modeling. In contrast, regurgitant *in vivo* human data have shown strains of 10–13% <sup>215</sup>, closely matching our results.

The strain distributions further distinguished the healthy and regurgitant valves. FWHM analysis showed similar systolic strain variation across all valves, though healthy valves had higher mean values. In diastole, healthy valves displayed lower

strain and smaller variation, while regurgitant valves exhibited broader distributions with higher average strain values. These localized high-strain zones, patterns previously observed in adults <sup>69</sup>, may potentially indicate residual biomechanical dysfunction. Strain predictions are inherently sensitive to the choice of material model and the inclusion of pre-strain <sup>80</sup>, underscoring the potential for improved accuracy through more advanced material formulations in future work. Elevated leaflet strain has been associated with pathology <sup>215</sup> and to disrupt cellular homeostasis and tissue remodeling <sup>48</sup>, supporting that leaflet strain may serve as an indicator of disease through its reflection of adverse hemodynamic loading.

#### The chordal forces

In the healthy valves, simulated chordal forces peaked during systole and were negligible during diastole, confirming that chordae provide support during closure without restricting valve opening <sup>219</sup>. Our results are consistent with prior work on healthy valves <sup>152,153,220</sup>. In the regurgitant valves, peak systolic forces were lower than in the healthy valves and decreased further after surgical repair, reflecting the overall reduction in mass flow associated with valve repair <sup>221</sup>. Interestingly, diastolic forces were observed in four regurgitant valves, which likely stemmed from the exclusion of movement and modeled positioning of the papillary muscle heads, restricting the leaflet motion. Despite this, the post-operative reduction in forces aligns with *in vitro* findings <sup>222</sup>, with computational studies reporting peak systolic forces of 2.6–3.5 N at 80–120 mmHg <sup>153,220</sup>, while *in vitro* testing of bovine and human valves yielded 1.6–5 N at 120 mmHg <sup>223,224</sup>. These values scale well with our results. In contrast, systolic forces in elderly regurgitant valves (4.5–9.41 N) were reported <sup>225</sup>, which are higher than our values, likely reflecting differences in valve anatomy, left-heart modeling strategies, and ventricular pressures.

Statistically significant differences in systolic chordal forces were observed between healthy and diseased valves. Although diastolic differences were not statistically significant, individual force-time curves provided valuable insight. Clinically, chordal forces offer insight into pathological loading conditions: elevated systolic forces may increase the risk of chordal rupture, while abnormal diastolic forces could indicate leaflet tethering and restricted leaflet motion. Further, chordal imbalance has been shown to impair leaflet coaptation <sup>225</sup>, contributing to regurgitation. Thus, chordal force analysis holds promise as a biomechanical marker of valve dysfunction.

### 6.4 Future perspectives

While this thesis has achieved several important outcomes in relation to its overarching aims, several aspects of the work remain to be explored, emphasizing the need for continued research. This section discusses the prospective options for model development in the near future and discusses the long-term trajectory towards clinical implementation.

#### 6.4.1 Next steps in the model development

The ideal continuation of this thesis would be to further develop and validate the computational model to address the remaining questions highlighted in the previous section above. Material testing of diseased mitral valves was beyond the scope of this work; however, exploring alternative constitutive models, such as those described in Section 3.3.1, would be valuable for assessing their impact on simulation outcomes. Another important step would be to incorporate patient-specific contracting ventricular geometries. This would allow for evaluation of how ventricular contraction influences our simulation results compared to our current model. This would enable investigations into valve-ventricle interactions in secondary mitral disease, where the valve appears incompetent due to ventricular dysfunction but could function normally if ventricular performance were restored. Modeling these interactions could help clinicians better understand the extent to which ventricular dysfunction affects mitral valve behavior: a relationship that remains challenging to assess in clinical practice. Furthermore, incorporating ventricular contraction may improve the visual and intuitive appeal of the model for clinical staff, which is an important factor for clinical translation.

Further validation is also required to better understand the model's accuracy and to identify where improvements are most needed. Given the large variability among pediatric mitral valve anatomies, blood flow, and pathologies, studies including larger patient cohorts are essential to achieve proper statistical rigor. Another promising direction would be to segment the mitral valve at multiple time points during the cardiac cycle and use image registration to compare simulations with *in vivo* data at multiple time points, providing a more quantitative assessment of valve behavior than was possible in this thesis. This would enable a better understanding of the simulated valve dynamics and whether another modeling approach is necessary.

Finally, expanding the scope of mitral regurgitation modeling would be of high clinical relevance. While this work successfully simulated repaired mitral regurgitations, it would be equally important to investigate unsuccessful repairs that ultimately required prosthetic valve replacement. Predicting post-operative valve dysfunction would be of great value to clinicians, as it could influence the choice and timing of repair strategy. A logical next step would be to perform blinded post-operative simulations of the already included regurgitant cases and compare predicted outcomes to actual surgical results. This would provide critical insight into the predictive capacity of the model and identify areas requiring improvement. Achieving this milestone would represent a key step toward true clinical implementation of patient-specific mitral valve simulations.

#### 6.4.2 Toward clinical implementation

Looking ahead, I envision two major long-term goals for this research: achieving clinical implementation and expanding the framework to simulate other regions of the heart, including more complex (congenital) heart diseases.

Returning to the central aim of this thesis – to improve surgical planning for children with heart disease and thereby increase the likelihood of better surgical outcomes - the ultimate milestone must be clinical implementation. Without reaching the clinic, the model cannot fulfill its intended purpose. To make this possible, extensive validation across larger patient cohorts is essential, as discussed earlier. Equally, pathways toward commercialization or streamlining the current pipeline to achieve a "plug-and-play" framework needs to be considered, particularly if our model is to be adopted beyond the University Hospital in Lund and integrated into broader clinical practice. Ensuring that the model is both scientifically robust and translatable to clinical practice will be key steps in bridging the gap between research and clinical care.

In parallel, expanding the model beyond the mitral valve and left ventricle presents an exciting opportunity. Incorporating the aortic valve, or extending the framework to the right side of the heart to study tricuspid and pulmonary valve pathologies (which are widely under-explored with FSI), would allow for a more comprehensive understanding of valvular disease. Ultimately, this progression could pave the way toward whole-heart models capable of simulating highly complex congenital defects, such as atrioventricular septal defects with a common atrioventricular valve, which is one of the most serious congenital defects. Such advancements would broaden the clinical applicability of the simulations and bring the field closer to a holistic, patient-

specific tool for supporting decision-making in pediatric cardiology and cardiac surgery, where it is needed the most.

# 7 Summary and conclusions

The overall aim of this thesis was to develop a computational framework for preoperative simulations using standard clinical assessment data from echocardiography for diseased mitral valves to predict the post-operative hemodynamics and valve function in children with heart disease.

Below, the main conclusions of each study (I–V) are summarized.

- I. To establish reliable benchmarking data, a controlled experimental setup was developed using a simplified left heart model containing a mitral valve. Phantom experiments were performed where the mitral valve dynamics and flow behavior were monitored with echocardiography, MRI, and pressure probes, generating a comprehensive multimodal dataset for future validation of cardiac-inspired simulation models.
- II. A left heart fluid-structure interaction model was presented, and multi-modal validation showed error margins small enough for clinical use. The validation of the model against phantom data demonstrated small error margins and showed that the model could reliably reproduce key diagnostic parameters such as pressure gradients, valve opening, and flow behavior under physiological conditions in a simplified model.
- III. Patient-specific mitral valve simulations, validated in ten healthy volunteers, showed errors small enough for clinical applicability. Fluid-structure interaction simulations in ten healthy volunteers, validated against in vivo echocardiographic data, captured clinically important parameters, including the valvular dynamics and the transvalvular velocity, with errors small enough for clinical use.
- IV. Patient-specific mitral regurgitation simulations were conducted pre- and postoperatively and evaluated against in vivo data. Based on 2D and 3D

- echocardiography, the FSI model was evaluated against *in vivo* data using clinical diagnostic parameters; overall valvular function, regurgitation grade, site of regurgitation, and transvalvular pressure gradient in children with mitral regurgitation, demonstrating its ability to capture disease-specific features and surgical outcomes
- V. Simulation results of healthy and regurgitant mitral valves were compared to identify potentially new diagnostic markers. A statistically significant difference was found in healthy and regurgitant mitral valves. The chordal forces in diastole were higher for the regurgitant valves than for the healthy valves, consistent with leaflet tethering. These biomechanical parameters may serve as complementary markers of mitral valve disease, as they capture pathological changes unattainable from medical imaging data alone.

## 8 References

- 1. Atlas Writing Group and European Society of Cardiology and others. European Society of Cardiology: cardiovascular disease statistics 2021. *Eur Heart J* 73, 716–799 (2022).
- 2. Baumgartner, H. *et al.* 2020 ESC Guidelines for the management of adult congenital heart disease. *Eur Heart J* **42**, 563–645 (2021).
- 3. Rabbah, J. P., Saikrishnan, N. & Yoganathan, A. P. A novel left heart simulator for the multi-modality characterization of native mitral valve geometry and fluid mechanics. *Ann Biomed Eng* 41, 305–315 (2013).
- 4. Marom, G. Numerical Methods for Fluid–Structure Interaction Models of Aortic Valves. *Archives of Computational Methods in Engineering* **22**, 595–620 (2015).
- 5. Schoenborn, S., Pirola, S., Woodruff, M. A. & Allenby, M. C. Fluid-Structure Interaction Within Models of Patient-Specific Arteries: Computational Simulations and Experimental Validations. *IEEE Rev Biomed Eng* 17, 280–296 (2022).
- Cohn, J. N., Ferrari, R. & Sharpe, N. Cardiac remodeling-concepts and clinical implications: A consensus paper from an International Forum on Cardiac Remodeling. J Am Coll Cardiol 35, 569–582 (2000).
- 7. Boron, W. & Boulpaep, E. *Medical Physiology*. (Elsevier health sciences, 2012).
- 8. Carlsson, M., Ugander, M., Mosén, H., Buhre, T. & Arheden, H. Atrioventricular plane displacement is the major contributor to left ventricular pumping in healthy adults, athletes, and patients with dilated cardiomyopathy. *Am J Physiol Heart Circ Physiol* **292**, 1452–1459 (2007).

- 9. Chung, C. S., Karamanoglu, M. & Kovács, S. J. Duration of diastole and its phases as a function of heart rate during supine bicycle exercise. *Am J Physiol Heart Circ Physiol* **287**, 2003–2008 (2004).
- Lam, J. H. C., Ranganathan, N., Wigle, E. D. & Silver, M. D. Morphology of the Human Mitral Valve I. Chordae Tendineae: A New Classification. *Circulation* 41, 449–458 (1970).
- 11. Levine, R. A. *et al.* Mitral valve disease-morphology and mechanisms. *Nat Rev Cardiol* 12, 689–710 (2015).
- 12. Lie-Venema, H. *et al.* Origin, fate, and function of epicardium-derived cells (EPCDs) in normal and abnormal cardiac development. *The Scientific World Journal* 7, 1777–1798 (2007).
- 13. Dal-Bianco, J. P. & Levine, R. A. Anatomy of the Mitral Valve Apparatus. Role of 2D and 3D Echocardiography. *Cardiol Clin* 31, 151–164 (2013).
- 14. O'Rourke, R. A. & Crawford, M. H. Mitral valve regurgitation. *Curr Probl Cardiol* 9, 1–52 (1984).
- 15. Nishimura, R. A., Vahanian, A., Eleid, M. F. & Mack, M. J. Mitral valve diseasecurrent management and future challenges. *The Lancet* **387**, (2016).
- 16. Banerjee, A., Kohl, T. & Silverman, N. H. Echocardiographic Evaluation of Congenital Mitral Valve Anomalies in Children. *Am J Cardiol* **76**, 1284–1291 (1995).
- 17. Wood, A. E. *et al.* Mitral valve reconstruction in a pediatric population: Late clinical results and predictors of long-term outcome. *Journal of Thoracic and Cardiovascular Surgery* **130**, 66–73 (2005).
- 18. Sacks, M. S., Merryman, W. D. & Schmidt, D. E. On the biomechanics of heart valve function. *J Biomech* 42, 1804–1824 (2009).
- 19. Vassileva, C. M. *et al.* Long-term survival of patients undergoing mitral valve repair and replacement: A longitudinal analysis of medicare fee-for-service beneficiaries. *Circulation* 127, 1870–1876 (2013).
- 20. Alsoufi, B. *et al.* Results after mitral valve replacement with mechanical prostheses in young children. *Journal of Thoracic and Cardiovascular Surgery* **139**, (2010).
- 21. Harb, S. C. & Griffin, B. P. Mitral Valve Disease: a Comprehensive Review. *Curr Cardiol Rep* 19, (2017).
- 22. Kutty, S., Colen, T. M. & Smallhorn, J. F. Three-dimensional echocardiography in the assessment of congenital mitral valve disease. *Journal of the American Society of Echocardiography* 27, 142–154 (2014).

- 23. Fishbein, G. A. & Fishbein, M. C. Mitral Valve Pathology. *Curr Cardiol Rep* 21, (2019).
- 24. Nishimura, R. *et al.* 2014 AHA/ACC guideline for the management of patients with valvular heart disease: a report of the American College of Cardiology/American Heart Association Task Force on Practice Guidelines. *Circulation* 129, e521–e643 (2014).
- 25. Espinola-Zavaleta, N. *et al.* Three-dimensional echocardiography in congenital malformations of the mitral valve. *Journal of the American Society of Echocardiography* 15, 468–472 (2002).
- 26. Hakim, F. A., Krishnaswamy, C. & Mookadam, F. Mitral arcade in adults A systematic overview. *Echocardiography* **30**, 354–359 (2013).
- Delmo Walter, E. M., Javier, M. & Hetzer, R. Repair of Parachute and Hammock Valve in Infants and Children: Early and Late Outcomes. *Semin Thorac Cardiovasc Surg* 28, 448–459 (2016).
- 28. Simpson, J. et al. Three-dimensional Echocardiography in Congenital Heart Disease: An Expert Consensus Document from the European Association of Cardiovascular Imaging and the American Society of Echocardiography. *Journal of the American Society of Echocardiography* 30, 1–27 (2017).
- 29. Ong, C. S. *et al.* Role of virtual reality in congenital heart disease. *Congenit Heart Dis* 13, 357–361 (2018).
- Xu, J. J. et al. Patient-specific three-dimensional printed heart models benefit preoperative planning for complex congenital heart disease. World Journal of Pediatrics 15, 246–254 (2019).
- 31. Edler, I. & Hertz, C. H. The use of ultrasonic reflectoscope for the continuous recording of the movements of heart walls. *Kungl Fysiogr sallsk i Lund forhandl* 24, 1–19 (1954).
- 32. Mohamed, A. A., Arifi, A. A. & Omran, A. The basics of echocardiography. *J Saudi Heart Assoc* 22, 71–76 (2010).
- 33. Anavekar, N. S. & Oh, J. K. Doppler echocardiography: A contemporary review. *J Cardiol* 54, 347–358 (2009).
- 34. Hatle, L., Brubakk, A., Tromsdal, A. & Angelsen, B. Noninvasive assessment of pressure drop in mitral stenosis by doppler ultrasound. *Br Heart J* **40**, 131–140 (1978).
- 35. Otto, C. M. *et al.* 2020 ACC/AHA Guideline for the Management of Patients With Valvular Heart Disease: A Report of the American College of Cardiology/American

- Heart Association Joint Committee on Clinical Practice Guidelines. *J Am Coll Cardiol* 77, e25–e197 (2021).
- 36. Ng, A. & Swanevelder, J. Resolution in ultrasound imaging. *Continuing Education in Anaesthesia, Critical Care and Pain* 11, 186–192 (2011).
- 37. Rumack, C. & Levine, D. *Diagnostic Ultrasound, 5th Edition*. (Elsevier Health Sciences, 2017).
- 38. Vahanian, A. *et al.* 2021 ESC/EACTS Guidelines for the management of valvular heart disease. *Eur Heart J* **43**, 561–632 (2022).
- 39. Brown, R. W., Cheng, Y. N., Haacke, E. M., Thompson, M. R. & Venkatesan, R. *Magnetic Resonance Imaging, 2nd Edition.* (John Wiley & Sons, 2014).
- 40. Lauterbur, P. C. Image Formation by Induced Local Interactions: Examples Employing Nuclear Magnetic Resonance. *Nature* 242, 190–191 (1973).
- 41. Mansfield, P. & Grannell, P. K. NMR 'diffraction' in solids? *Journal of Physics C: Solid State Physics* **6**, L422–L426 (1973).
- 42. Dyverfeldt, P. *et al.* 4D flow cardiovascular magnetic resonance consensus statement. *Journal of Cardiovascular Magnetic Resonance* 17, (2015).
- 43. Nayak, K. S. et al. Cardiovascular magnetic resonance phase contrast imaging. Journal of Cardiovascular Magnetic Resonance 17, (2015).
- 44. Guglielmo, M., Rovera, C., Rabbat, M. G. & Pontone, G. The Role of Cardiac Magnetic Resonance in Aortic Stenosis and Regurgitation. *J Cardiovasc Dev Dis* 9, (2022).
- 45. Guglielmo, M. & Pontone, G. Risk stratification in cardiomyopathies (dilated, hypertrophic, and arrhythmogenic cardiomyopathy) by cardiac magnetic resonance imaging. *European Heart Journal, Supplement* 23, E118–E122 (2021).
- 46. Malahfji, M. & Shah, D. Cardiac magnetic resonance in valvular heart disease: assessment of severity and myocardial remodeling. *Methodist Debakey Cardiovasc J* 16, 106 (2020).
- 47. Gao, H. *et al.* A coupled mitral valve—left ventricle model with fluid–structure interaction. *Med Eng Phys* 47, 128–136 (2017).
- 48. Rego, B. V, Wells, S. M., Lee, C.-H. & Sacks, M. S. Mitral valve leaflet remodelling during pregnancy: insights into cell-mediated recovery of tissue homeostasis. *J R Soc Interface* 13, 20160709 (2016).

- 49. Votta, E. *et al.* 3-D computational analysis of the stress distribution on the leaflets after edge-to-edge repair of mitral regurgitation. *Journal of Heart Valve Disease* 11, 810–822 (2002).
- 50. Kunzelman, K. S. *et al.* Finite element analysis of the mitral valve. *J Heart Valve Dis* 2, 326–340 (1993).
- 51. Prot, V. & Skallerud, B. Nonlinear solid finite element analysis of mitral valves with heterogeneous leaflet layers. *Comput Mech* **43**, 353–368 (2009).
- 52. Lau, K. D., Diaz, V., Scambler, P. & Burriesci, G. Mitral valve dynamics in structural and fluid-structure interaction models. *Med Eng Phys* **32**, 1057–1064 (2010).
- 53. de Oliveira, D. C. *et al.* A toolbox for generating scalable mitral valve morphometric models. *Comput Biol Med* **135**, 104628 (2021).
- 54. Park, J., Geirsson, A. & Bonde, P. N. Mathematical Blueprint of a Mitral Valve. *Semin Thorac Cardiovasc Surg* **31**, 399–411 (2019).
- 55. Warraich, H. J., Shahul, S., Matyal, R. & Mahmood, F. Bench to bedside: Dynamic mitral valve assessment. *J Cardiothorac Vasc Anesth* **25**, 863–866 (2011).
- 56. Pouch, M. A. *et al.* Development of a semi-automated method for mitral valve modeling with medial axis representation using 3D ultrasound. *Med Phys* **39**, 933–950 (2012).
- 57. Carnahan, P. *et al.* DeepMitral: Fully Automatic 3D Echocardiography Segmentation for Patient Specific Mitral Valve Modelling. in *MICCAI 2021: 24th International Conference* 459–468 (2021).
- 58. Andreassen, B. S., Veronesi, F., Gerard, O., Solberg, A. H. S. & Samset, E. Mitral Annulus Segmentation Using Deep Learning in 3-D Transesophageal Echocardiography. *IEEE J Biomed Health Inform* 24, 994–1003 (2020).
- 59. Costa, E. *et al.* Mitral Valve Leaflets Segmentation in Echocardiography using Convolutional Neural Networks. in *IEEE 6th Portuguese Meeting on Bioengineering* 1–4 (IEEE, 2019).
- 60. Cibis, M. *et al.* The effect of spatial and temporal resolution of cine phase contrast MRI on wall shear stress and oscillatory shear index assessment. *PLoS One* 11, (2016).
- 61. Su, B. *et al.* Cardiac MRI based numerical modeling of left ventricular fluid dynamics with mitral valve incorporated. *J Biomech* **49**, 1199–1205 (2016).
- 62. Fumagalli, I. *et al.* An image-based computational hemodynamics study of the Systolic Anterior Motion of the mitral valve. *Comput Biol Med* **123**, 103922 (2020).

- 63. Biffi, B. *et al.* A workflow for patient-specific fluid–structure interaction analysis of the mitral valve: A proof of concept on a mitral regurgitation case. *Med Eng Phys* 74, 153–161 (2019).
- 64. Ma, X., Gao, H., Griffith, B. E., Berry, C. & Luo, X. Image-based fluid-structure interaction model of the human mitral valve. *Comput Fluids* 71, 417–425 (2013).
- 65. Emendi, M. *et al.* Patient-Specific Bicuspid Aortic Valve Biomechanics: A Magnetic Resonance Imaging Integrated Fluid–Structure Interaction Approach. *Ann Biomed Eng* 49, 627–641 (2021).
- 66. Chen, C. et al. Deep Learning for Cardiac Image Segmentation: A Review. Front Cardiovasc Med 7, (2020).
- 67. Schneider, R. J. *et al.* Patient-specific mitral leaflet segmentation from 4D ultrasound. in *International Conference on Medical Image Computing and Computer- Assisted Intervention* vol. 6893 LNCS 520–527 (Springer, 2011).
- 68. Jolley, M. A., Ghelani, S. J., Adar, A. & Harrild, D. M. Three-Dimensional Mitral Valve Morphology and Age-Related Trends in Children and Young Adults with Structurally Normal Hearts Using Transthoracic Echocardiography. *Journal of the American Society of Echocardiography* 30, 561–571 (2017).
- 69. Feng, L. et al. On the chordae structure and dynamic behaviour of the mitral valve. IMA Journal of Applied Mathematics (Institute of Mathematics and Its Applications) 83, 1066–1091 (2018).
- 70. Mao, W., Caballero, A., McKay, R., Primiano, C. & Sun, W. Fully-coupled fluid-structure interaction simulation of the aortic and mitral valves in a realistic 3D left ventricle model. *PLoS One* **12**, 1–22 (2017).
- 71. Sacks, M. S. *et al.* On the Simulation of Mitral Valve Function in Health, Disease, and Treatment. *J Biomech Eng* 141, (2019).
- 72. Wu, W. *et al.* The effects of leaflet material properties on the simulated function of regurgitant mitral valves. *J Mech Behav Biomed Mater* **142**, (2023).
- 73. Liu, H. *et al.* A Computational Pipeline for Patient-Specific Prediction of the Postoperative Mitral Valve Functional State. *J Biomech Eng* 145, (2023).
- 74. Kong, F., Caballero, A., McKay, R. & Sun, W. Finite element analysis of MitraClip procedure on a patient-specific model with functional mitral regurgitation. *J Biomech* **104**, (2020).
- 75. Christierson, L. *et al.* Prediction of healthy mitral valve hemodynamics in children and adults: validation of fluid-structure interaction simulations against echocardiography and magnetic resonance imaging. *Comput Biol Med* **194**, (2025).

- 76. Panicheva, D., Villard, P. F., Hammer, P. E., Perrin, D. & Berger, M. O. Automatic extraction of the mitral valve chordae geometry for biomechanical simulation. *Int J Comput Assist Radiol Surg* **16**, 709–720 (2021).
- 77. Toma, M. *et al.* Fluid–structure interaction and structural analyses using a comprehensive mitral valve model with 3D chordal structure. *Int J Numer Method Biomed Eng* **33**, 1–12 (2017).
- 78. Collia, D., Zovatto, L. & Pedrizzetti, G. Analysis of mitral valve regurgitation by computational fluid dynamics. *APL Bioeng* **3**, 1–10 (2019).
- 79. Domenichini, F. & Pedrizzetti, G. Asymptotic Model of Fluid–Tissue Interaction for Mitral Valve Dynamics. *Cardiovasc Eng Technol* **6**, 95–104 (2015).
- 80. Rausch, M. K. *et al.* Mechanics of the mitral valve: A critical review, an in vivo parameter identification, and the effect of prestrain. *Biomech Model Mechanobiol* 12, 1053–1071 (2013).
- 81. Toma, M. *et al.* Fluid-Structure Interaction Analysis of Subject-Specific Mitral Valve Regurgitation Treatment with an Intra-Valvular Spacer. *Prosthesis* 2, 65–75 (2020).
- 82. Cai, L. *et al.* Some Effects of Different Constitutive Laws on FSI Simulation for the Mitral Valve. *Sci Rep* **9**, 1–15 (2019).
- 83. Zhang, W., Ayoub, S., Liao, J. & Sacks, M. S. A meso-scale layer-specific structural constitutive model of the mitral heart valve leaflets. *Acta Biomater* **32**, 238–255 (2016).
- 84. Ross, C., Laurence, D., Wu, Y. & Lee, C.-H. Biaxial Mechanical Characterizations of Atrioventricular Heart Valves. *Journal of Visualized Experiments* **6**, 1–19 (2021).
- 85. Jensen, A. S., Baandrup, U., Hasenkam, J. M., Kundu, T. & Jørgensen, C. S. Distribution of the microelastic properties within the human anterior mitral leaflet. *Ultrasound Med Biol* **32**, 1943–1948 (2006).
- 86. Gao, H. *et al.* Modelling mitral valvular dynamics–current trend and future directions. *Int J Numer Method Biomed Eng* **33**, 1–15 (2017).
- 87. Grashow, J. S., Yoganathan, A. P. & Sacks, M. S. Biaixal Stress–Stretch Behavior of the Mitral Valve Anterior Leaflet at Physiologic Strain Rates. *Ann Biomed Eng* 34, 315–325 (2006).
- 88. Grashow, J. S., Sacks, M. S., Liao, J. & Yoganathan, A. P. Planar Biaxial Creep and Stress Relaxation of the Mitral Valve Anterior Leaflet. *Ann Biomed Eng* **34**, 1509–1518 (2006).

- 89. Lee, C. H. *et al.* On the effects of leaflet microstructure and constitutive model on the closing behavior of the mitral valve. *Biomech Model Mechanobiol* 14, 1281–1302 (2015).
- 90. Xu, F. *et al.* Computational investigation of left ventricular hemodynamics following bioprosthetic aortic and mitral valve replacement. *Mech Res Commun* 112, 103604 (2021).
- 91. Amini, R. *et al.* On the in vivo deformation of the mitral valve anterior leaflet: Effects of annular geometry and referential configuration. *Ann Biomed Eng* **40**, 1455–1467 (2012).
- 92. Zhang, W., Rossini, G., Kamensky, D., Bui-Thanh, T. & Sacks, M. S. Isogeometric finite element-based simulation of the aortic heart valve: Integration of neural network structural material model and structural tensor fiber architecture representations. *Int J Numer Method Biomed Eng* 37, 1–28 (2021).
- 93. Ross, C. J. *et al.* An investigation of the glycosaminoglycan contribution to biaxial mechanical behaviours of porcine atrioventricular heart valve leaflets. *J R Soc Interface* 16, (2019).
- 94. Prot, V., Skallerud, B., Sommer, G. & Holzapfel, G. A. On modelling and analysis of healthy and pathological human mitral valves: Two case studies. *J Mech Behav Biomed Mater* 3, 167–177 (2010).
- 95. Gao, H. *et al.* A finite strain nonlinear human mitral valve model with fluid-structure interaction. *Int J Numer Method Biomed Eng* **30**, 1597–1613 (2014).
- 96. Feng, L., Gao, H., Griffith, B., Niederer, S. & Luo, X. Analysis of a coupled fluid-structure interaction model of the left atrium and mitral valve. *Int J Numer Method Biomed Eng* **35**, (2019).
- 97. Feng, L. *et al.* Fluid–structure interaction in a fully coupled three-dimensional mitral–atrium–pulmonary model. *Biomech Model Mechanobiol* **20**, 1267–1295 (2021).
- 98. Chandran, K. B. Role of Computational Simulations in Heart Valve Dynamics and Design of Valvular Prostheses. *Cardiovasc Eng Technol* 1, 18–38 (2010).
- 99. Luraghi, G., Migliavacca, F. & Rodriguez Matas, J. F. Study on the Accuracy of Structural and FSI Heart Valves Simulations. *Cardiovasc Eng Technol* **9**, 723–738 (2018).
- 100. Kheradvar, A. et al. Emerging Trends in Heart Valve Engineering: Part IV. Computational Modeling and Experimental Studies. Ann Biomed Eng 43, 2314–2333 (2015).

- 101. Alexy, T. *et al.* Physical Properties of Blood and their Relationship to Clinical Conditions. *Front Physiol* 13, (2022).
- 102. Chien, S. *et al.* Blood Viscosity: Influence of Erythrocyte Aggregation. *Science* (1979) 157, 829–831 (1967).
- 103. Abbas, S. S., Nasif, M. S. & Al-Waked, R. State-of-the-art numerical fluid–structure interaction methods for aortic and mitral heart valves simulations: A review. *Simulation* **98**, 3–34 (2021).
- 104. De Vita, F., de Tullio, M. D. & Verzicco, R. Numerical simulation of the non-Newtonian blood flow through a mechanical aortic valve: Non-Newtonian blood flow in the aortic root. *Theor Comput Fluid Dyn* 30, 129–138 (2016).
- 105. Abbas, S. S., Nasif, M. S., Said, M. A. M. & Al-Waked, R. Numerical simulation of the non-Newtonian blood flow through aortic Bileaflet mechanical heart valve using fluid-structure interaction approach. *AIP Conf Proc* 2035, 1–10 (2018).
- 106. Hanafizadeh, P., Mirkhani, N., Davoudi, M. R., Masouminia, M. & Sadeghy, K. Non-Newtonian Blood Flow Simulation of Diastolic Phase in Bileaflet Mechanical Heart Valve Implanted in a Realistic Aortic Root Containing Coronary Arteries. Artif Organs 40, E179–E191 (2016).
- 107. Al-Azawy, M. G., Turan, A. & Revell, A. Investigating the impact of non-Newtonian blood models within a heart pump. *Int J Numer Method Biomed Eng* **33**, (2017).
- 108. Khellaf, B. & Boussad, B. Computational hemodynamic investigation of a new bileaflet mechanical heart valve. *Simulation* **96**, 459–469 (2020).
- 109. Fiusco, F., Rorro, F., Broman, L. M. & Prahl Wittberg, L. Numerical and experimental investigation of a lighthouse tip drainage cannula used in extracorporeal membrane oxygenation. *Artif Organs* 47, 330–341 (2023).
- 110. Romano, E., Sousa, L., António, C., Castro, C. & Pinto, S. I. S. *Non-Linear or Quasi-Linear Viscoelastic Property of Blood for Hemodynamic Simulations*. (Springer, 2020).
- 111. Sequeira, A. & Janela, J. An overview of some mathematical models of blood rheology. *A Portrait of State-of-the-Art Research at the Technical University of Lisbon* 65–87 (2007).
- 112. Pope, S. *Turbulent Flows*. (Cambridge University Press, 2018).
- 113. Versteeg, H. K. & Malalasekera, W. An Introduction to Computational Fluid Dynamics: The Finite Volume Method. (Pearson Education Limited, 2007).

- 114. Ge, L., Jones, S. C., Sotiropoulos, F., Healy, T. M. & Yoganathan, A. P. Numerical Simulation of Flow in Mechanical Heart Valves: Grid Resolution and the Assumption of Flow Symmetry. *J Biomech Eng* 125, 709–718 (2003).
- 115. Chnafa, C., Mendez, S. & Nicoud, F. Image-based large-eddy simulation in a realistic left heart. *Comput Fluids* **94**, 173–187 (2014).
- 116. Sadipour, M., Hanafizadeh, P., Sadeghy, K. & Sattari, A. Effect of Aortic Wall Deformation with Healthy and Calcified Annulus on Hemodynamic Performance of Implanted On-X Valve. *Cardiovasc Eng Technol* 11, 141–161 (2020).
- Mirkhani, N., Davoudi, M. R., Hanafizadeh, P., Javidi, D. & Saffarian, N. On-X Heart Valve Prosthesis: Numerical Simulation of Hemodynamic Performance in Accelerating Systole. *Cardiovasc Eng Technol* 7, 223–237 (2016).
- 118. Halevi, R. *et al.* Fluid–structure interaction modeling of calcific aortic valve disease using patient-specific three-dimensional calcification scans. *Med Biol Eng Comput* 54, 1683–1694 (2016).
- 119. Al-Azawy, M. G., Turan, A. & Revell, A. Assessment of turbulence models for pulsatile flow inside a heart pump. *Comput Methods Biomech Biomed Engin* **19**, 271–285 (2016).
- 120. Wei, Z. A., Sonntag, S. J., Toma, M., Singh-Gryzbon, S. & Sun, W. Computational Fluid Dynamics Assessment Associated with Transcatheter Heart Valve Prostheses: A Position Paper of the ISO Working Group. *Cardiovasc Eng Technol* 9, 289–299 (2018).
- 121. Dedè, L., Menghini, F. & Quarteroni, A. Computational fluid dynamics of blood flow in an idealized left human heart. *Int J Numer Method Biomed Eng* 37, (2021).
- 122. Nobili, M. *et al.* Numerical simulation of the dynamics of a bileaflet prosthetic heart valve using a fluid-structure interaction approach. *J Biomech* 41, 2539–2550 (2008).
- 123. Frieberg, P. *et al.* Computational Fluid Dynamics Support for Fontan Planning in Minutes, Not Hours: The Next Step in Clinical Pre-Interventional Simulations. *J Cardiovasc Transl Res* **15**, 708–720 (2022).
- 124. Donea, J., Giuliani, S. & Halleux, J. P. An arbitrary Lagrangian-Eulerian finite element method for transient dynamic fluid-structure interactions. *Comput Methods Appl Mech Eng* 33, 689–723 (1982).
- 125. Dimasi, A. et al. Fluid-Structure Interaction and In Vitro Analysis of a Real Bileaflet Mitral Prosthetic Valve to Gain Insight Into Doppler-Silent Thrombosis. J Biomech Eng 141, 1–9 (2019).

- 126. Khodaei, S. *et al.* Personalized intervention cardiology with transcatheter aortic valve replacement made possible with a non-invasive monitoring and diagnostic framework. *Sci Rep* 11, 1–28 (2021).
- 127. Ge, L. Numerical Simulation of 3D, Complex, Turbulent Flows with Unsteady Coherent Structures: From Hydraulics to Cardiovascular Fluid Mechanics. *Thesis* 220 (2004).
- 128. Hadzic, H. Development and Application of a Finite Volume Method for the Computation of Flows Around Moving Bodies on Unstructured, Overlapping Grids. (Technische Universität Hamburg, 2006).
- 129. Ge, L., Leo, H. L., Sotiropoulos, F. & Yoganathan, A. P. Flow in a mechanical bileaflet heart valve at laminar and near-peak systole flow rates: CFD simulations and experiments. *J Biomech Eng* 127, 782–797 (2005).
- 130. Le, T. B. & Sotiropoulos, F. Fluid-structure interaction of an aortic heart valve prosthesis driven by an animated anatomic left ventricle. *J Comput Phys* **244**, 41–62 (2013).
- 131. Borazjani, I., Ge, L., Le, T. & Sotiropoulos, F. A parallel overset-curvilinear-immersed boundary framework for simulating complex 3D incompressible flows. *Comput Fluids* 77, 76–96 (2013).
- 132. Stijnen, J. M. A., de Hart, J., Bovendeerd, P. H. M. & van de Vosse, F. N. Evaluation of a fictitious domain method for predicting dynamic response of mechanical heart valves. *J Fluids Struct* 19, 835–850 (2004).
- 133. Peskin, C. Flow patterns around heart valves: a numerical method. *J Comput Phys* 10, 252–271 (1972).
- 134. Griffith, B. & Patankar, N. Immersed methods for fluid-structure interaction. *Annu Rev Fluid Mech* **52**, 412–448 (2020).
- 135. Van Loon, R., Anderson, P., De Hart, J. & Baaijens, F. A combined fictitious domain/adaptive meshing method for fluid-structure interaction in heart valves. *Int J Numer Methods Fluids* **46**, 533–544 (2004).
- 136. De Hart, J., Peters, G. W. M., Schreurs, P. J. G. & Baaijens, F. P. T. A three-dimensional computational analysis of fluid-structure interaction in the aortic valve. *J Biomech* 36, 103–112 (2003).
- 137. Van Loon, R., Anderson, P. & Van De Vosse, F. A fluid-structure interaction method with solid-rigid contact for heart valve dynamics. *J Comput Phys* 217, 806–823 (2006).

- 138. Glowinski, R., Pan, T.-W., Hesla, T. & Joseph, D. A distributed Lagrange multiplier/fictitious domain method for particulate flows. *International Journal of Multiphase Flow* 25, 755–794 (1999).
- 139. Baaijens, F. A fictitious domain/mortar element method for fluid-structure interaction. *Int J Numer Methods Fluids* **35**, 743–761 (2001).
- 140. Griffith, B. & Luo, X. Hybrid finite difference/finite element immersed boundary method. *Int J Numer Method Biomed Eng* **33**, e2888 (2017).
- 141. Hsu, M. C., Kamensky, D., Bazilevs, Y., Sacks, M. S. & Hughes, T. J. R. Fluid–structure interaction analysis of bioprosthetic heart valves: significance of arterial wall deformation. *Comput Mech* 54, 1055–1071 (2014).
- 142. Kamensky, D. *et al.* An immersogeometric variational framework for fluid-structure interaction: Application to bioprosthetic heart valves. *Comput Methods Appl Mech Eng* 284, 1005–1053 (2015).
- 143. Xu, F. *et al.* A framework for designing patient-specific bioprosthetic heart valves using immersogeometric fluid–structure interaction analysis. *Int J Numer Method Biomed Eng* 34, 1–25 (2018).
- 144. Hsu, M. C. *et al.* Dynamic and fluid–structure interaction simulations of bioprosthetic heart valves using parametric design with T-splines and Fung-type material models. *Comput Mech* 55, 1211–1225 (2015).
- 145. Wu, M. C. H. *et al.* An anisotropic constitutive model for immersogeometric fluid–structure interaction analysis of bioprosthetic heart valves. *J Biomech* 74, 23–31 (2018).
- 146. Terahara, T., Takizawa, K., Tezduyar, T. E., Bazilevs, Y. & Hsu, M. C. Heart valve isogeometric sequentially-coupled FSI analysis with the space–time topology change method. *Comput Mech* **65**, 1167–1187 (2020).
- 147. Khaledian, N., Villard, P. F. & Berger, M. O. Capturing contact in mitral valve dynamic closure with fluid-structure interaction simulation. *Int J Comput Assist Radiol Surg* 17, 1391–1398 (2022).
- 148. Khodaei, S., Fatouraee, N. & Nabaei, M. Numerical simulation of mitral valve prolapse considering the effect of left ventricle. *Math Biosci* **285**, 75–80 (2017).
- 149. Khalafvand, S. S., Xu, F., Westenberg, J., Gijsen, F. & Kenjeres, S. Intraventricular blood flow with a fully dynamic mitral valve model. *Comput Biol Med* **104**, 197–204 (2019).

- 150. Yin, M., Luo, X. Y., Wang, T. J. & Watton, P. N. Effects of flow vortex on a chorded mitral valve in the left ventricle. *Int J Numer Method Biomed Eng* **26**, 381–404 (2010).
- Einstein, D. R., Kunzelman, K. S., Reinhall, P. G., Nicosia, M. A. & Cochran, R.
   P. Nonlinear Fluid-Coupled Computational Model of the Mitral Valve Title: Fluid-structure model of mitral valve. *J Heart Valve Dis* 14, 376–385 (2005).
- 152. Kunzelman, K. S., Einstein, D. R. & Cochran, R. P. Fluid-structure interaction models of the mitral valve: Function in normal and pathological states. *Philosophical Transactions of the Royal Society B: Biological Sciences* **362**, 1393–1406 (2007).
- 153. Toma, M. *et al.* Fluid–Structure Interaction Analysis of Papillary Muscle Forces Using a Comprehensive Mitral Valve Model with 3D Chordal Structure. *Ann Biomed Eng* 44, 942–953 (2016).
- 154. Toma, M. *et al.* Fluid-Structure Interaction Analysis of Ruptured Mitral Chordae Tendineae. *Ann Biomed Eng* **45**, 619–631 (2017).
- 155. Toma, M. *et al.* Effect of edge-to-edge mitral valve repair on chordal strain: Fluid-structure interaction simulations. *Biology (Basel)* **9**, 1–12 (2020).
- 156. Gao, H. *et al.* Fluid-structure interaction model of human mitral valve within left ventricle. *International Conference on Functional Imaging and Modeling of the Heart* 330–337 (2015).
- 157. Cai, L., Zhao, T., Wang, Y., Luo, X. & Gao, H. Fluid–structure interaction simulation of pathological mitral valve dynamics in a coupled mitral valve-left ventricle model. *Intelligent Medicine* 3, 104–114 (2023).
- 158. Feng, L., Gao, H. & Luo, X. Whole-heart modelling with valves in a fluid–structure interaction framework. *Comput Methods Appl Mech Eng* **420**, (2024).
- Mao, W., Li, K., Caballero, A. & Sun, W. Fully-Coupled FSI Simulation of Bioprosthetic Heart Valve Using Smoothed Particle Hydrodynamics. *Cardiology* 134, 178 (2016).
- 160. Caballero, A. *et al.* New insights into mitral heart valve prolapse after chordae rupture through fluid–structure interaction computational modeling. *Sci Rep* 8, (2018).
- 161. Caballero, A., Mao, W., McKay, R. & Sun, W. Transapical mitral valve repair with neochordae implantation: FSI analysis of neochordae number and complexity of leaflet prolapse. *Int J Numer Method Biomed Eng* 36, e3297 (2020).

- 162. Mao, W., Caballero, A., Hahn, R. T. & Sun, W. Comparative quantification of primary mitral regurgitation by computer modeling and simulated echocardiography. *Am J Physiol Heart Circ Physiol* 318, 547–557 (2020).
- 163. Caballero, A., Mao, W., McKay, R., Hahn, R. T. & Sun, W. A Comprehensive Engineering Analysis of Left Heart Dynamics After MitraClip in a Functional Mitral Regurgitation Patient. *Front Physiol* 11, (2020).
- 164. Bavo, A. M. et al. Fluid-Structure Interaction Simulation of Prosthetic Aortic Valves: Comparison between Immersed Boundary and Arbitrary Lagrangian-Eulerian Techniques for the Mesh Representation. PLoS One 11, (2016).
- 165. De Vita, F., De Tullio, M. & Verzicco, R. Numerical simulation of the non-Newtonian blood flow through a mechanical aortic valve: Non-Newtonian blood flow in the aortic root. *Theor Comput Fluid Dyn* **30**, 129–138 (2016).
- 166. Griffith, B. E. Immersed boundary model of aortic heart valve dynamics with physiological driving and loading conditions. *Int J Numer Method Biomed Eng* **28**, 317–345 (2012).
- 167. Spühler, J. H., Jansson, J., Jansson, N. & Hoffman, J. 3D fluid-structure interaction simulation of aortic valves using a unified continuum ALE FEM model. *Front Physiol* **9**, 1–16 (2018).
- 168. Mohammadi, H., Cartier, R. & Mongrain, R. The impact of the aortic valve impairment on the distant coronary arteries hemodynamics: a fluid–structure interaction study. *Med Biol Eng Comput* 55, 1859–1872 (2017).
- 169. Marom, G., Kim, H. S., Rosenfeld, M., Raanani, E. & Haj-Ali, R. Fully coupled fluid-structure interaction model of congenital bicuspid aortic valves: Effect of asymmetry on hemodynamics. *Med Biol Eng Comput* 51, 839–848 (2013).
- 170. de Oliveira, D. M., Abdullah, N., Green, N. C. & Espino, D. M. Biomechanical assessment of bicuspid aortic valve phenotypes: a fluid-structure interaction modelling approach. *Cardiovasc Eng Technol* 11, 431–447 (2020).
- 171. Yan, W., Li, J., Wang, W., Wei, L. & Wang, S. A fluid-structure interaction study of different bicuspid aortic valve phenotypes throughout the cardiac cycle. *Front Physiol* 12, 716015 (2021).
- 172. Lee, J. H. *et al.* Fluid–Structure Interaction Models of Bioprosthetic Heart Valve Dynamics in an Experimental Pulse Duplicator. *Ann Biomed Eng* **48**, 1475–1490 (2020).
- 173. Wu, W. *et al.* Fluid–Structure Interaction Model of a Percutaneous Aortic Valve: Comparison with an In Vitro Test and Feasibility Study in a Patient-Specific Case. *Ann Biomed Eng* 44, 590–603 (2016).

- 174. Singh-Gryzbon, S. *et al.* Development of a Computational Method for Simulating Tricuspid Valve Dynamics. *Ann Biomed Eng* 47, 1422–1434 (2019).
- 175. Dabiri, Y., Yao, J., Sack, K. L., Kassab, G. S. & Guccione, J. M. Tricuspid valve regurgitation decreases after mitraclip implantation: Fluid structure interaction simulation. *Mech Res Commun* 97, 96–100 (2019).
- 176. Ko, K. B., Seo, J.-H., Doshi, A., Sen, D. G. & Mittal, R. Computational Study on the Effects of Valve Orientation on the Hemodynamics and Leaflet Dynamics of Bioprosthetic Pulmonary Valves. *J Biomech Eng* 146, 121002 (2024).
- 177. Criseo, E., Fumagalli, I., Quarteroni, A., Marianeschi, S. M. & Vergara, C. Computational haemodynamics for pulmonary valve replacement by means of a reduced fluid-structure interaction model. *Int J Numer Method Biomed Eng* 40, e3846 (2024).
- 178. Christierson, L. *et al.* Multi-modal phantom experiments, mimicking flow through the mitral heart valve [Data set]. *Zenodo* https://doi.org/10.5281/zenodo.10117609 (2023).
- 179. Töger, J. *et al.* Independent validation of four-dimensional flow MR velocities and vortex ring volume using particle imaging velocimetry and planar laser-Induced fluorescence. *Magn Reson Med* 75, 1064–1075 (2016).
- 180. Manceau, R. & Hanjalić, K. Elliptic blending model: A new near-wall Reynolds-stress turbulence closure. *Physics of Fluids* 14, 744–754 (2002).
- 181. Billard, F. & Laurence, D. A robust k-ε-vZ/k elliptic blending turbulence model applied to near-wall, separated and buoyant flows. *Int J Heat Fluid Flow* 33, 45–58 (2012).
- 182. Steger, J., Dougherty, C. & Benek, J. A Chimera grid scheme. in *ASME/ASCE Mechanics Conference* (1983).
- 183. Pham, T., Sulejmani, F., Shin, E., Wang, D. & Sun, W. Quantification and comparison of the mechanical properties of four human cardiac valves. *Acta Biomater* 54, 345–355 (2017).
- 184. Pinter, C., Lasso, A. & Fichtinger, G. Polymorph segmentation representation for medical image computing. *Comput Methods Programs Biomed* 171, 19–26 (2019).
- 185. Massey, F. J. The Kolmogorov-Smirnov Test for Goodness of Fit. *Source: Journal of the American Statistical Association* **46**, 68–78 (1951).
- 186. Wilcoxon, F. Individual Comparisons by Ranking Methods. *Bulletin* 1, 80–83 (1945).

- 187. Mor-Avi, V. et al. Real-Time 3-Dimensional Echocardiographic Quantification of Left Ventricular Volumes Multicenter Study for Validation With Magnetic Resonance Imaging and Investigation of Sources of Error. JACC: Cardiovascular Imaging vol. 1 413–423 (2008).
- 188. Oliveira, D. *et al.* Geometric description for the anatomy of the mitral valve: A review. *J Anat* 237, 209–224 (2020).
- 189. Laurence, D. *et al.* An investigation of regional variations in the biaxial mechanical properties and stress relaxation behaviors of porcine atrioventricular heart valve leaflets. *J Biomech* 83, 16–27 (2019).
- 190. Prot, V., Haaverstad, R. & Skallerud, B. Finite element analysis of the mitral apparatus: Annulus shape effect and chordal force distribution. *Biomech Model Mechanobiol* **8**, 43–55 (2009).
- 191. Von Knobelsdorff-Brenkenhoff, F. & Schulz-Menger, J. Role of cardiovascular magnetic resonance in the guidelines of the European Society of Cardiology. *Journal of Cardiovascular Magnetic Resonance* 18, (2016).
- 192. Krell, K. et al. Real-Time Three-Dimensional Echocardiography of the Left Ventricle—Pediatric Percentiles and Head-to-Head Comparison of Different Contour-Finding Algorithms: A Multicenter Study. *Journal of the American Society of Echocardiography* 31, 702-711.e13 (2018).
- 193. Ylänen, K., Eerola, A., Vettenranta, K. & Poutanen, T. Three-dimensional echocardiography and cardiac magnetic resonance imaging in the screening of long-term survivors of childhood cancer after cardiotoxic therapy. *American Journal of Cardiology* 113, 1886–1892 (2014).
- 194. Miller, C. A. *et al.* Comparison of real-time three-dimensional echocardiography with cardiovascular magnetic resonance for left ventricular volumetric assessment in unselected patients. *Eur Heart J Cardiovasc Imaging* 13, 187–195 (2012).
- 195. Hessenthaler, A. *et al.* Experiment for validation of fluid-structure interaction models and algorithms. *Int J Numer Method Biomed Eng* **33**, (2017).
- 196. Kalmbach, A. & Breuer, M. Experimental PIV/V3V measurements of vortex-induced fluid-structure interaction in turbulent flow-A new benchmark FSI-PfS-2a. *J Fluids Struct* **42**, 369–387 (2013).
- 197. Gok, G. *et al.* Comparison of 2D vena contracta area with 3D planimetric mitral valve area in rheumatoid mitral valve disease. *International Journal of Cardiovascular Imaging* **36**, 2115–2120 (2020).

- 198. Zarrinchang, P., Ashrafizaadeh, M. & Jamshidi, N. Simulation of the female pelvic mobility and vesical pressure changes employing fluid-structure interaction method. *Int Urogynecol J* 34, 571–580 (2023).
- 199. Rong, L. Q. *et al.* A pairwise meta-analytic comparison of aortic valve area determined by planimetric versus hemodynamic methods in aortic stenosis. *Int J Cardiol* 322, 77–85 (2021).
- 200. Luraghi, G. *et al.* Evaluation of an aortic valve prosthesis: Fluid-structure interaction or structural simulation? *J Biomech* **58**, 45–51 (2017).
- Quaini, A. et al. A Three-Dimensional Computational Fluid Dynamics Model of Regurgitant Mitral Valve Flow: Validation Against In Vitro Standards and 3D Color Doppler Methods. Cardiovasc Eng Technol 2, 77–89 (2011).
- 202. Redaelli, A. *et al.* 3-D Simulation of the St. Jude Medical Bileaflet Valve Opening Process: Fluid-Structure Interaction Study and Experimental Validation. *Journal of Heart Valve Disease* 13, 804–813 (2004).
- 203. Hussein, N. *et al.* Simulation of semilunar valve function: computer-aided design, 3D printing and flow assessment with MR. *3D Print Med* **6**, (2020).
- 204. Toma, M. *et al.* High-resolution subject-specific mitral valve imaging and modeling: experimental and computational methods. *Biomech Model Mechanobiol* 15, 1619–1630 (2016).
- 205. Alharbi, Y. *et al.* Fluid structure computational model of simulating mitral valve motion in a contracting left ventricle. *Comput Biol Med* 148, (2022).
- 206. Kemp, I. *et al.* Experimental validation of the fluid-structure interaction simulation of a bioprosthetic aortic heart valve. *Australas Phys Eng Sci Med* **36**, 363–373 (2013).
- Amindari, A., Saltik, L., Kirkkopru, K., Yacoub, M. & Yalcin, H. C. Assessment of calcified aortic valve leaflet deformations and blood flow dynamics using fluidstructure interaction modeling. *Inform Med Unlocked* 9, 191–199 (2017).
- 208. Miyoshi, T. et al. Left Ventricular Diastolic Function in Healthy Adult Individuals: Results of the World Alliance Societies of Echocardiography Normal Values Study. Journal of the American Society of Echocardiography 33, 1223–1233 (2020).
- 209. Baumgartner, H. et al. Echocardiographic Assessment of Valve Stenosis: EAE/ASE Recommendations for Clinical Practice. *Journal of the American Society of Echocardiography* 22, 1–23 (2009).
- 210. Banerjee, A., Kohl, T. & Silverman, N. H. Echocardiographic evaluation of congenital mitral valve anomalies in children. *Am J Cardiol* 76, 1284–1291 (1995).

- Collins-Nakai, R. L., Rosenthal, A., Castaneda, A. R., Bernhard, W. F. & Nadas, A.
   S. Congenital Mitral Stenosis A Review of 20 Years' Experience. *Circulation* 56, 1039–1047 (1997).
- Voelker, W. et al. Validation of continuous-wave Doppler measurements of mitral valve gradients during exercise-a simultaneous Doppler-catheter study. Eur Heart J 10, 737–746 (1989).
- 213. Vernick, W. J., Ochroch, E. A., Horak, J., Hammond, M. & Hargrove, W. C. Validation study of doppler-derived transmitral valve gradients compared to near simultaneously obtained directly measured catheter gradients immediately after mitral valve repair surgery. *J Card Surg* 28, 329–335 (2013).
- 214. Rim, Y., Choi, A., McPherson, D. D. & Kim, H. Personalized computational modeling of mitral valve prolapse: Virtual leaflet resection. *PLoS One* **10**, (2015).
- El-Tallawi, K. C. et al. Valve Strain Quantitation in Normal Mitral Valves and Mitral Prolapse With Variable Degrees of Regurgitation. JACC Cardiovasc Imaging 14, 1099–1109 (2021).
- 216. Ben Zekry, S. *et al.* Patient-specific quantitation of mitral valve strain by computer analysis of three-dimensional echocardiography: A pilot study. *Circ Cardiovasc Imaging* **9**, (2016).
- 217. Wu, W. *et al.* A Computational Framework for Atrioventricular Valve Modeling Using Open-Source Software. *J Biomech Eng* 144, (2022).
- 218. Narang, H. *et al.* Pre-surgical Prediction of Ischemic Mitral Regurgitation Recurrence Using In Vivo Mitral Valve Leaflet Strains. *Ann Biomed Eng* **49**, 3711–3723 (2021).
- 219. Espino, D. M., Shepherd, D., Hukins, D. & Buchan, K. G. The role of Chordae tendineae in mitral valve competence. *J Heart Valve Dis* 14, 603–609 (2005).
- 220. Votta, E. et al. Mitral valve finite-element modelling from ultrasound data: A pilot study for a new approach to understand mitral function and clinical scenarios. Philosophical Transactions of the Royal Society A: Mathematical, Physical and Engineering Sciences 366, 3411–3434 (2008).
- 221. Arunamata, A., Tierney, E. S. S., Tacy, T. A. & Punn, R. Echocardiographic measures associated with early postsurgical myocardial dysfunction in pediatric patients with mitral valve regurgitation. *Journal of the American Society of Echocardiography* 28, 284–293 (2015).
- 222. Ostli, B. *et al.* In Vitro System for Measuring Chordal Force Changes Following Mitral Valve Patch Repair. *Cardiovasc Eng Technol* **3**, 263–268 (2012).

- 223. Jimenez, J. H., Soerensen, D. D., He, Z., Ritchie, J. & Yoganathan, A. P. Mitral valve function and chordal force distribution using a flexible annulus model: An in vitro study. *Ann Biomed Eng* 33, 557–566 (2005).
- 224. Rego, B. V. *et al.* A noninvasive method for the determination of in vivo mitral valve leaflet strains. *Int J Numer Method Biomed Eng* **34**, (2018).
- 225. Pham, T. *et al.* Finite Element Analysis of Patient-Specific Mitral Valve with Mitral Regurgitation. *Cardiovasc Eng Technol* **8**, 3–16 (2017).
- 226. Christierson, L. *et al.* Multi-Modal in Vitro Experiments Mimicking the Flow Through a Mitral Heart Valve Phantom. *Cardiovasc Eng Technol* 15, 572–583 (2024).
- 227. Christierson, L. *et al.* Validation of fluid-structure interaction simulations of the opening phase of phantom mitral heart valves under physiologically inspired conditions. *Comput Biol Med* 171, (2024).

## 9 Appended papers

- I. L. Christierson, P. Frieberg, T. Lala, J. Töger, P. Liuba, J. Revstedt, H. Isaksson, and N. Hakacova. Multi-Modal in Vitro Experiments Mimicking the Flow Through a Mitral Heart Valve Phantom. Cardiovascular Engineering and Technology, 2024, 1-12
  Reproduced with permission from Springer Nature.
- II. L. Christierson, P. Frieberg, T. Lala, J. Töger, P. Liuba, J. Revstedt, H. Isaksson, and N. Hakacova. Validation of fluid-structure interaction simulations of the opening phase of phantom mitral heart valves under physiologically inspired conditions. Computers in Biology and Medicine, 2024, 171: 108033

Reproduced under the Creative Commons CC-BY license.

- III. L. Christierson, P. Frieberg, P. Liuba, E. Hedström, J. Revstedt, H. Isaksson, and N. Hakacova. Prediction of healthy mitral valve hemodynamics in children and adults: validation of fluid-structure interaction simulations to echocardiography and magnetic resonance imaging. Computers in Biology and Medicine, 2025, 194:110455
  Reproduced under the Creative Commons CC-BY license.
- IV. L. Christierson, J. Revstedt, A. Pozza, A. Dragulescu, C. Morgan, O. Honjo, L. Mertens, H. Isaksson, and N. Hakacova. Toward Precision in Prediction of Pediatric Mitral Valve Repair Using Patient-Specific Fluid-Structure Interaction Modeling. (Submitted)

V. L. Christierson, J. Revstedt, L. Mertens, A. Dragulescu, M. Karlsson, H. Isaksson, and N. Hakacova. Mitral valve strain and chordal forces as potential diagnostic parameters in pediatric mitral valve disease. *Manuscript under preparation (to be submitted in 2025)*